Constitutive Modeling of Cu-Al-Ni Shape Memory Alloys

by

Srikanth Vedantam

B.Tech., Mechanical Engineering (1993)
Indian Institute of Technology, Madras

M.S., Mechanical Engineering (1995)
Pennsylvania State University

Submitted to the Department of Mechanical Engineering
in partial fulfillment of the requirements for the degree of

DOCTOR OF SCIENCE

at the

MASSACHUSETTS INSTITUTE OF TECHNOLOGY

September 2000

Author .....
Department of Mechanical Engineering
August 30, 2000

Certified by .....
Rohan Abeyaratne
Professor of Mechanical Engineering
Thesis Supervisor

Accepted by .....
Ain Sonin
Professor of Mechanical Engineering
Chairman, Department Committee on Graduate Students

Constitutive Modeling of Cu-Al-Ni Shape Memory Alloys

by

Srikanth Vedantam

Submitted to the Department of Mechanical Engineering
on August 30, 2000, in partial fulfillment of the
requirements for the degree of
DOCTOR OF SCIENCE

Abstract

Certain alloys can exist in multiple phases, which, in the context of solids, essentially mean multiple crystallographic structures. For example, at certain compositions, a Cu-Al-Ni alloy can exist as a cubic lattice (austenite), an orthorhombic lattice (γ_1'-martensite) or a monoclinic lattice (β_1'-martensite). The material changes from one phase to another under various conditions of thermal and/or mechanical loading. Under certain loads, multiple phases can coexist and when this happens, a sharp interface separates any two phases. As the stress or temperature changes, the interface propagates through the material and particles transform from one phase to the other as they cross the moving phase boundary. (A martensitic phase can exist in the form of many "variants", and an interface between co-existing variants is a twin boundary.)

The constitutive modeling of such materials is made difficult by the inherent anisotropic nature of such materials and by the nonmonotonicity of the stress-strain curves. We develop a systematic method by which we can calculate the free–energy of such a material based on its symmetry.

The velocity with which interfaces propagates controls the rate of phase transformations (i.e. the "kinetics"). It is well known that classical balance laws are insufficient for a complete description of the behavior of materials undergoing phase transformations. The classical continuum theory describes the bulk regions (regions away from the interfaces) in a satisfactory manner but leaves a gap in the information concerning the interface. This lacuna has been filled by either including nucleation and kinetic criteria that are consistent with the second law of thermodynamics, or by regularizing the continuum theory in some consistent manner. The above treatments seek to provide information on the boundaries between the phases. However, they suffer from the drawback that even though they are meant to be continuum scale descriptions of microscale phenomena which take place on the transformation front they do not model the physics of the transformations.

A more natural way of obtaining the relevant information would be to directly study the transformation process at a microscale and then perform an appropriate homogenization so that the resulting law is applicable at a continuum scale. Such an approach would facilitate a deeper understanding of the transformation process as well as enable the continuum theory to reflect the micromechanical processes that govern the transformation. We develop a lattice model of twin and phase boundaries that accounts for microstructural effects. The model incorporates the effect of ledges in the interface. A quasicontinuum model is obtained by approximating the resulting difference-differential equation of motion of the ledge, but retaining leading discreteness effects. The quasicontinuum model now models the interface at a continuum scale but incorporates lattice effects. The kinetic relation obtained from

such a model explains the experimentally observed difference in the stress required for moving boundaries between different variants of martensite. The kinetic relation obtained for phase boundaries has the feature that the hysteresis loops do not decrease in size to zero for vanishing loading rates.

Thesis Supervisor: Rohan Abeyaratne
Title: Professor of Mechanical Engineering

Acknowledgments

I would like to gratefully acknowledge the excellent guidance of Professor Rohan Abeyaratne. I have no doubt that the diverse things that he has taught me, in my intellectual endeavors as well as in the more mundane, will stand me in good stead throughout my career. I am deeply appreciative of the chance I have been given to complete my thesis with him.

I would also like to thank Professors David Parks and Nicolas Hadjiconstantinou for consenting to serve on my committee. I enjoyed all my interactions with them including being their Teaching Assistant in the past.

I have had several excellent office–mates and colleagues Dr. Alfred Pettinger, Dr. Yu-Hsuan Su, Dr. Muralidhar Ravuri, Vitaly Napadow, and numerous others who made my stay at this institute all the more pleasurable. My gratitude also goes to Ms. Debra Blanchard for all the help and enjoyable moments she provided during my stay at MIT. My parents Bharati Devi and Prof. V.M.K. Sastri, my wife Aparna, and the rest of my family deserve special thanks for the support and encouragement they have given me over the years.

Contents

List of Figures

List of Tables

Chapter 1

Introduction

Recently, a lot of interest has been focussed on *Shape memory alloys*. These are usually alloys such as CuAlNi, NiTi, InTl, AgCd, CuZnNi, etc. which are capable of recovering from large apparently permanent deformations. The recovery from such large deformations is accomplished by means of a solid-solid phase transformation that occurs under applied thermal or mechanical loading. The phase transformation that is responsible for the shape memory effect is diffusionless and involves a change in crystallographic structure. These materials have been well–studied experimentally but there have been few fully three–dimensional constitutive models. Such constitutive models become more important for understanding and optimizing applications of these materials in Micro–Electro–Mechanical Systems, for example (see Bhattacharya and James [14]). In this thesis, we develop a constitutive model for shape memory alloys undergoing cubic–orthorhombic transitions, focusing in particular on CuAlNi.

There have been several one-dimensional constitutive models for shape memory alloys (Bekker et al [12] and Liang and Rogers [45] and references contained therein). However, there are far fewer three–dimensional constitutive models of shape memory alloys since they pose several challenges. The phenomena exhibited by these materials involve nonlinearities in the geometry as well as the material behavior. The material is anisotropic due to the low symmetry exhibited by one or more of the phases. The different phases of the material exchange stability depending on the temperature and stress state. Finally, the phases are capable of coexisting and are separated by mobile interfaces. The kinetics of these interfaces must also be constitutively specified in order to model the material behavior fully.

We develop a systematic procedure by which the constitutive model for homogeneous single crystals of the phase transforming material can be fully specified. The free–energy of the material is specified to have the requisite properties of material symmetry and temperature dependence. The kinetics of the interface are supplied by studying micromechanical models.

Interface kinetics have been studied in detail from a continuum viewpoint by several authors (Abeyaratne and Knowles [2]–[6], Truskinovsky [76]). Using continuum theory, one may propose restrictions on the kinetic relation. However, the form of the kinetic relation cannot be determined from continuum mechanics alone. In fact, the interface mobility has been experimentally found to be strongly dependent on the microstructure of the material (Ichinose et al [38], Chu [17]). So far there have been no models of the phase boundary kinetics which have explicitly incorporated the microstructure of the body. Our goal is to develop micromechanical models for the various kinds of interfaces which are applicable at the continuum level but retain microstructural information.

Our constitutive model is applicable in a small range of temperature around the transformation temperature (the temperature at which both phases are equally stable). We assume that the material exhibits *constrained behavior* as described by Ball and James [11] and assume that the deformation gradients are on the energy wells even under applied stresses.

1.1 Material behavior

Material scientists distinguish between two phenomena that may contribute to the large recoverable deformations of Shape memory alloys (SMAs). The first one is the process of *deformation twinning* and the second is a *phase transformation.*

The alloys that exhibit the shape memory effect usually exist in several different crystallographic structures at different temperatures and stresses. At higher temperatures the atoms of the alloy arrange themselves in a lattice of high symmetry, being preponderantly cubic. The material in such a state is said to be in the *austenite phase.* At lower temperatures, the atoms tend to arrange themselves in lower symmetry lattice structures such as tetragonal, orthorhombic and monoclinic. The material in this state is said to be in the *martensitic phase.* Additionally, since the martensite phase is one of low symmetry, there exist several *variants* of martensite. The different variants of martensite are related

to each other through the renaming of lattice vectors. The lattice parameters of the different phases are different and deformation is accommodated through the substitution of one lattice structure with another. Under applied mechanical and thermal loads the material changes between the austenite and martensite phases. This transformation between phases usually occurs through a moving *phase boundary* across which the material changes phase. As a phase boundary sweeps through the material, the material transforms from one phase to another. Similarly, when the body is solely in the martensite phase, under the application of stress, the body may transform between the different variants of martensite. The interface between the several variants is termed as a *twin boundary* and the variants are described as being twin related.

The free–energy of the material has local minima associated with each of these phases. However, the global minimum varies with temperature. Above a certain temperature, θ_T, *the transformation temperature*, the global minimum of the free energy is at the austenite phase. Whereas below the transformation temperature, the martensite phase has wells corresponding to the global minimum of the free–energy. At the transformation temperature, both the austenite and martensite phases have wells corresponding to the global minimum of the free–energy. Thus, a stress free specimen of this material changes phase as the temperature is raised and lowered above and below the transformation temperature. This phenomenon is known as a *temperature induced transformation.* Note that the transformation is a heterogeneous one; a second phase nucleates and grows at the expense of the parent phase by means of propagating interfaces.

The martensite phase can also be stress induced above the transformation temperature. A specimen in the austenite phase above the transformation temperature transforms to martensite upon loading. This transformation is again a heterogeneous one. Phase boundaries nucleate and propagate through the specimen upon loading converting the austenite phase to martensite. Unloading reverses the transformation and phase boundaries again propagate through the body reconverting martensite to austenite. This process of the forward change causes the specimen to deform by a large amount (up to 10% in certain alloys) and the reverse transformation recovers the strain completely. This phenomenon is known as the *pseudoelastic effect.*

A third phenomenon displayed by SMAs is the *shape memory effect.* It is a combination of the temperature induced transformation and the pseudoelastic effect. The material

is now deformed from a twinned martensite state below the transformation temperature. Since martensite is of low symmetry, it can form microstructure in which some regions are symmetry related with others. This is known as twinned crystal and under the application of stress, one region can grow at the expense of the other. This is a process known as detwinning. Detwinning accommodates deformation and when the stress is released the material remains in the detwinned martensitic form. However, raising the temperature above the transformation temperature transforms the material to austenite and cooling converts the austenite to original state of twinned martensite. The cycle is then complete and the shape is completely recovered. This phenomenon involves both temperature and stress-cycling. Pettinger [59] and Shaw and Kyriakides [68] provide detailed descriptions of the three phenomena described above.

1.2 Continuum models

SMAs involve coexistent phases and the various physical phenomena exhibited are due to the motion of the interfaces between these phases. The continuum description of these problems involves the statement of the global conservation principles of linear and angular momentum and energy in conjunction with constitutive laws which are consistent with the second law of thermodynamics. The classical treatment of phase transformations views phase boundaries as sharp interfaces across which continuum fields suffer jump discontinuities. The global balance laws then localize to partial differential equations appropriate to each phase in regions where the interfaces are absent and to jump conditions across phase boundaries. The constitutive model must therefore be capable of supplying information about the behavior of each phase away from interfaces and about the kinetics of the interfaces.

The continuum information away from interfaces is provided by specifying a free–energy function which, provided the material is thermoelastic, is sufficient for a complete description of the material excepting the heat transfer characteristics. The form of the free-energy has been studied by Ericksen [25] for crystals undergoing cubic–tetragonal transitions. Crystals undergoing other kinds of transitions such as cubic–monoclinic or cubic–orthorhombic have been studied using a modified Landau theory approach by Koyoma and Nittono [43], Nittono and Koyoma [46] and Falk and Konopka [27]. Group theory is used to guarantee the correct symmetry required of the free–energy.

While the free–energy function describes the single phase homogeneous material, further information needs to be supplied about the formation and mobility of the interfaces. The physical conditions corresponding to these are *nucleation*, where a secondary phase is born inside the parent phase, and *growth*, where the secondary phase expands consuming the parent according to some kinetic law. Providing nucleation and kinetic conditions leads to a well–posed theory that is able to describe the dynamic process of phase transformation. Abeyaratne and Knowles [2]–[5] describe these ideas in detail.

The dynamic process of phase transformation being generally a non–equilibrium process, the entropy production is non zero. One may rewrite the entropy production inequality as a product of a thermodynamic driving force f and the interface normal speed V_n (Abeyaratne and Knowles [3]). The kinetic law for the interface is then provided by assuming that the thermodynamic driving force is some function of the normal interface speed: $f = \varphi(V_n)$. To be consistent with the second law of thermodynamics the function $\varphi(V_n)$ is restricted by the inequality $\varphi(V_n)V_n > 0$. Details are provided in the next Chapter. Continuum theory is able to supply just this amount of detail. For further information about the form of the kinetic relation we must take recourse to a mircromechanical model of the interface.

1.3 Micromechanical models

The kinetic relation purports to import microstructural information about the phase boundary into the continuum theory. However, the kinetic relations obtained from various theories in the literature on phase transformations have so far not explicitly considered means of doing so. In this thesis, one of our fundamental goals is to derive appropriate micromechanical models in such a manner as to contribute microstructural information at the continuum level.

We are motivated in this by the Frenkel–Kontorova [29] (FK) model for a dislocation. The model illustrated in Figure 1-1 consists of a chain of atoms on a periodic substrate and with the nearest neighbor atoms connected by linear springs. A constant horizontal force f acts on each of the atoms. If, in the model, each of the wells were occupied by a single atom, the force required to translate the chain of atoms by a distance equal to the period of the substrate would equal the theoretical shear strength (or resistance to slip) of a defect free crystal. The chain of atoms represent the atoms on the slip plane and the substrate

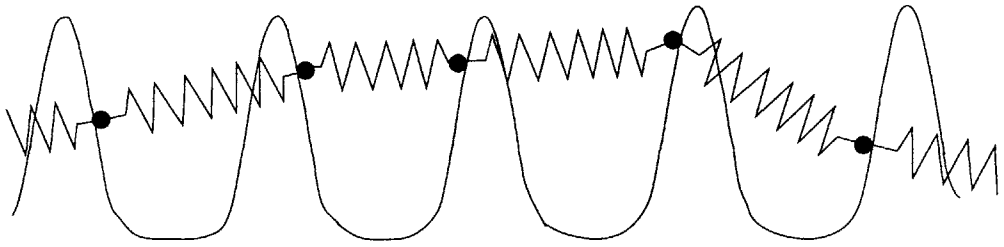

Figure 1-1: The Frenkel–Kontorova model of a dislocation.

potential is due to the atoms above and below the slip plane. The spring forces model the forces due to the adjacent atoms on the slip plane.

Most crystal lattices possess dislocations and the FK model incorporates these defects by considering a situation where all atoms to the left of a particular atom have already displaced into the adjacent well on their right whereas the remaining atoms remain in their original wells. Such a configuration of atoms has a particular well in which two atoms simultaneously reside and which represents the dislocation in the crystal. Now the application of a much smaller force than the theoretical shear strength of the crystal propagates atoms to their adjacent wells one at a time causing the "dislocation" to move.

The motion of this dislocation in a modified model—in which the substrate potential consists of piecewise parabolas—has been analyzed by several authors. For example, Atkinson and Cabrera [10] studied steady motion of a kink along the chain. Other authors (Weiner and co–authors [23, 58, 80], Partom [56], Combs and Yip [19]) have studied the problem numerically at zero Kelvin and for more general substrates. The equations of motion arising from this model especially with a sinusoidal substrate—known as the discrete sine-Gordon equations—are common in other fields of physics such as friction models, planar domain walls in ferroelectrics and ferromagnets, non–linear spin waves, and crack propagation.

One of the main interesting features of the solution of the discrete problem described above is the dissipation of energy due to non–decaying waves. The kink or dislocation moving in the discrete lattice emits waves thus experiencing a continuous loss of energy. Thus a minimum amount of external work needs to be done on the crystal to maintain the motion. In other words, below a critical force on the atoms, no dislocation motion is possible. This phenomenon is also referred to as lattice trapping in the literature. This feature is observable in the lattice theories but not in simplistic continuum approximations of the lattice models (Abeyaratne and Vedantam [7]).

The results of the micromechanical model by itself are not suitable for use in the continuum theories. Therefore a continuum approximation is required, which retains the discrete lattice effects at the continuum scale. Abeyaratne and Vedantam [7] proposed such an improved continuum model by retaining a higher order term in the Taylor's series expansion of the discrete term. Pouget [64, 65] proposed an equivalent alternative formulation in which he approximates the dispersion relation of the discrete equation up to the second order.

Many modifications to the FK model have been proposed for greater accuracy. The substrate potential has been calculated using molecular statics simulations by Abeyaratne and Vedantam [8]. Currie et al [20] and Peyrard and Remoissenet [60] have studied a modification of the model in which the substrate was assumed to be deformable. The FK model at finite temperature has been studied by Landau [44], Weiner and co–authors [81, 82], Rönnpagel et al [22] and others.

1.4 Outline of thesis

Chapter 2 reviews the crystallography of this material. We describe the lattice structure of austenite and the *variants* of martensite. Coherency of the interface imposes a compatibility condition. The compatibility condition requires that the deformation gradient on either side of the interface be *rank–one* connected and leads to specific interface planes, *the habit planes*, between the variants. The compatibility equation can be solved for the habit planes given the deformation gradients on either side of the interface. In the case of a phase boundary, the austenite can only form a weakly coherent interface with twinned martensite and the compatibility condition is satisfied on an average. This leads again to specific habit planes between austenite and martensite phases. Finally, we describe the generalization of the basic continuum mechanics principles to bodies with propagating interfaces across which fields may suffer jump discontinuities. We obtain partial differential equations in regions where the fields are smooth and jump conditions across interfaces.

In Chapter 3 we describe a systematic procedure by which the free–energy of a material undergoing cubic–orthorhombic transitions can be constructed. We incorporate the material symmetry of the austenite phase. The free–energy is non–convex and has wells at the austenite and martensite phases. As described in Section 1.1, the well height corresponding to the austenite phase is lower (higher) than the wells corresponding to martensite phase

above (below) the transformation temperature. All the wells have the same height at the transformation temperature. Imposing the symmetry of the cubic austenite phase allows us to represent the free energy as a function of *irreducible polynomial invariants* of the strain tensor. We impose a constraint on the strain tensor following Ericksen [25] who uses an argument based on the ratio of linear elastic moduli at the transformation temperature. We expand the free–energy as a quartic of the components of strain tensor using the irreducible polynomial invariants. The temperature dependent coefficients of the free-energy expansion are determined using: (1) the transformation strain of martensite, (2) the linear elastic moduli of austenite and martensite, (3) the transformation temperature, and (4) the latent heat. We also assume that the transformation strains are independent of temperature in the range of validity of the free–energy expansion. The stress–strain relations can then be calculated from the free–energy function.

Following Abeyaratne and Knowles [3], the second law of thermodynamics is recast into a convenient form in Chapter 4 from which a *driving traction* is readily identified. The driving traction is assumed to depend on the normal speed of the interface as in other internal variable theories [66]. This dependence of the driving traction on the normal speed of the interface cannot be determined from continuum theory alone. We need to take recourse to a micromechanical model. We therefore motivate a discrete mechanical analog of twin boundary motion. The mechanical analog is similar to a FK model for dislocations and yields a kinetic relation. However since our goal is to obtain a kinetic relation suitable for continuum theory we attempt to homogenize the discrete FK model. We describe how the obvious homogenization fails and an improved model needs to be constructed. The improved continuum model provides a kinetic relation that displays stick–slip condition.

In Chapter 5 we study the kinetics of twin boundary propagation. We start with a homogeneous continuum motion that describes the propagation of a twin boundary and generalize it to a inhomogeneous motion which describes a transverse ledge propagation along the twin boundary. We derive the equation of motion corresponding to the inhomogeneous motion and find it inadequate to obtain a kinetic relation for the twin boundary. We then motivate a modified equation of motion by looking at a lattice picture of the twin boundary propagation. The modified equation can be solved to obtain the twin boundary kinetics. The kinetic laws for compound and type I twins are then calculated.

In Chapter 6 we compare the energy of a continuum body undergoing a shear deforma-

tion in directions and on planes specified by the different twin solutions (compound, type I and type II) with a corresponding calculation based on molecular statics for atoms undergoing the same deformation. The energy of the continuum body is calculated using the polynomial free–energy obtained in Chapter 3. The molecular statics calculation is based on Lenard–Jones interatomic potential where the Lenard–Jones parameters are fitted to the lattice spacing and the linear elastic moduli in the direction and on the plane of shear.

In Chapter 7 phase boundaries are treated in a manner analogous to twin boundaries. Phase boundaries in CuAlNi form between austenite and twinned martensite. The compatibility condition matches the deformations of the austenite and twinned martensite in an average sense. We consider an inhomogeneous motion in a layer as a model for a ledge propagating transversely along a phase boundary. Using the modified equation of motion in this case leads to the kinetics of phase boundaries. The kinetics of different kinds of phase boundaries are compared.

Finally, in Chapter 8, we present conclusions and a discussion of the models and results. We then conclude by presenting open problems requiring future work.

In Appendix A, we detail the symmetry transformations for the cubic group as well as the group theoretic results used to obtain the irreducible polynomial invariants of the strain energy function. In Appendix B, we derive the formulas for the elastic moduli of austenite and the martensite phases.

1.5 Notation

In this thesis, boldface lower–case letters stand for vectors and upper–case boldface letters stand for tensors. Superscripts T and -1 represent the transpose and inverse of a tensor respectively. The tensor product of two vectors $\boldsymbol{a}$ and $\boldsymbol{b}$ is represented by $\boldsymbol{a} \otimes \boldsymbol{b}$ and the inner and outer products by $\boldsymbol{a} \cdot \boldsymbol{b}$ and $\boldsymbol{a} \times \boldsymbol{b}$ respectively. The unit vector in the direction of a vector $\boldsymbol{a}$ is represented with a superposed caret $\hat{\boldsymbol{a}}$. The identity tensor and the null tensor are represented by $\mathbf{1}$ and $\mathbf{0}$ respectively.

Chapter 2

Crystallography and continuum theory

2.1 Introduction

In this thesis we focus on the cubic (β_1) $\rightarrow$ orthorhombic (γ_1' with 2H structure) transformations occurring in the shape memory alloy CuAlNi. We adopt the Cauchy–Born hypothesis and this allows us to connect the continuum deformation gradients to the lattice level atomic rearrangements. In this chapter we describe the crystal structure of the different phases as well as a continuum description in terms of the deformation gradients. Thus in Section 2.2, we describe the lattice structure of the austenite and martensite phases and the variants of martensite, and the deformation gradients which would allow us to describe these phases in a continuum setting.

In addition to the change in crystalline structure during phase transformations, restrictions on the orientation of the parent and product phases arise as a result of compatibility of deformations at interfaces. Compatibility at interfaces leads to the requirement that the deformation gradients on either side be *rank-one* connected. Rank one connection of deformation gradients and the condition arising from it are described in the following sections.

We study *deformation twins* in this thesis as well as phase transformations. Deformation twins form when a portion of the crystal (usually of low symmetry) undergoes a large deformation relative to the original crystal. The deformed region and the original crystal are separated by a sharp coherent interface. Rank one connection between the deformed

and original crystals requires that the relative deformation be a simple shear. Depending on the interface plane and the shear direction three modes of twinning may be identified. They are known as Type I, Type II and Compound twins. Geometric and mathematical descriptions of twinning are given in Section 2.3. More details may be found in Jaswon and Dove [41], Klassen-Neklyudova [42], Christian [16] and James [39].

Martensitic transformations are described by Bowles and Mackenzie [15] and Wayman [79]. Compatibility of phase boundary also restricts the possible orientations of the phase boundary and 96 types of interfaces may be identified. Shield [69] describes them in detail. We outline the crystallography of phase boundaries in Section 2.4.

In our work, we assume that all the interfaces between the various phases and variants of the body are sharp across which some or all the fields suffer jump discontinuities. Then the global balance laws localize to PDEs away from interfaces and jump conditions across interfaces. We describe the derivation of such a formulation in Section 2.5.

2.2 Cubic-orthorhombic phase transitions

The specific type of martensite that we are considering is called γ_1'-martensite. It has an orthorhombic crystal structure and it is obtained from the cubic (austenite) phase in the following manner: let $\{\boldsymbol{c}_1, \boldsymbol{c}_2, \boldsymbol{c}_3\}$ be the three orthonormal vectors which are parallel to the edges of the austenite unit cube. Stretch this cube by the stretch ratio β in the direction $\boldsymbol{c}_3$, and by the stretch ratios α and γ along the two diagonals of the face perpendicular to $\boldsymbol{c}_3$. This carries the cube into a prism with a rhombic base; it corresponds to one of the variants of martensite. There are six such variants corresponding to stretching parallel to the three different cube edges and the two associated cube-face diagonals. The matrices of components (in the cubic basis) of the six associated stretch tensors $\boldsymbol{U}_i$, $i = 1, 2, \ldots, 6$, are

$$\boldsymbol{U}_1 = \begin{pmatrix} \frac{\alpha+\gamma}{2} & \frac{\alpha-\gamma}{2} & 0 \\ \frac{\alpha-\gamma}{2} & \frac{\alpha+\gamma}{2} & 0 \\ 0 & 0 & \beta \end{pmatrix}, \quad \boldsymbol{U}_2 = \begin{pmatrix} \frac{\alpha+\gamma}{2} & \frac{\gamma-\alpha}{2} & 0 \\ \frac{\gamma-\alpha}{2} & \frac{\alpha+\gamma}{2} & 0 \\ 0 & 0 & \beta \end{pmatrix}, \quad \boldsymbol{U}_3 = \begin{pmatrix} \frac{\alpha+\gamma}{2} & 0 & \frac{\alpha-\gamma}{2} \\ 0 & \beta & 0 \\ \frac{\alpha-\gamma}{2} & 0 & \frac{\alpha+\gamma}{2} \end{pmatrix} \tag{2.1}$$

and so on. The values of the lattice stretches α, β and γ for the alloy Cu-14.2wt% Al-4.3wt% Ni at its transformation temperature were measured by Otsuka and Shimuzu [52] and found

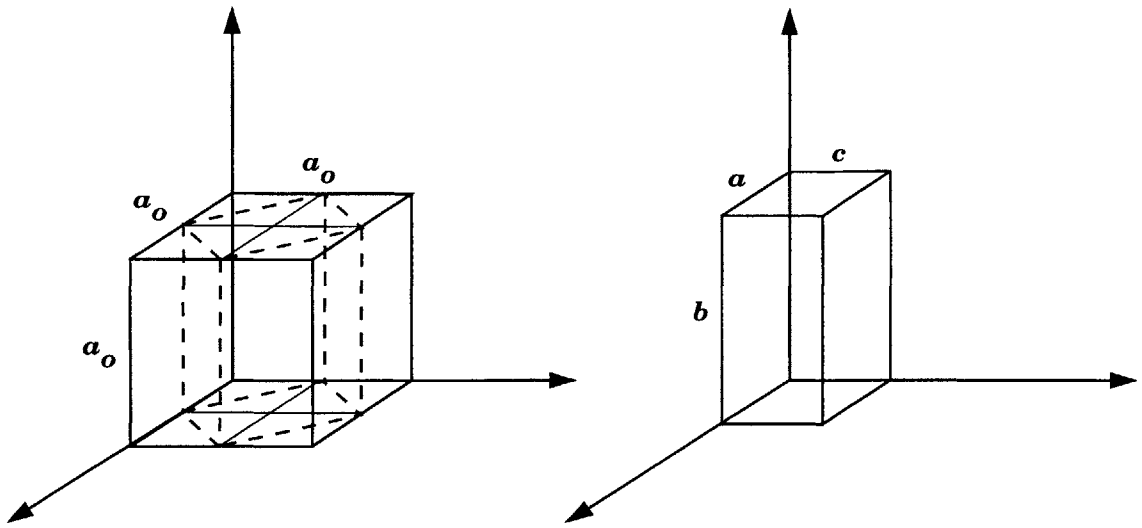

Figure 2-1: Cubic lattice and Orthorhombic lattice

to be

$$\alpha = 1.0619, \quad \beta = 0.9178, \quad \gamma = 1.0231. \tag{2.2}$$

The number of distinct stretch tensors that take austenite to martensite is alternatively given by the ratio of the order of the point group of austenite to the order of the point group of martensite (see, for example, van Tandeloo and Amelinckx [77], Bhattacharya [13]). The *point group* of a crystal lattice is the set of all rotations that map the lattice back into itself. The point group of a cubic lattice is the set of 24 rotations (namely, three rotations about each of the three distinct cube edges, two rotations about each of the four main diagonals, one rotation about the six distinct face diagonals and the identity transformation) that leave the orientation of the cube unchanged. The point group of the orthorhombic lattice is the set of 4 rotations (namely the three 180° rotations about the independent axes of the orthorhombic lattice and the identity transformation). The Lagrangian finite strain tensors $\boldsymbol{E}_i = \frac{1}{2}(\boldsymbol{U}_i^2 - \mathbf{1})$, $i = 1, 2, \ldots, 6$ corresponding the variants of martensite take the form (in the basis of cubic austenite):

$$\boldsymbol{E}_1 = \begin{pmatrix} p & q & 0 \\ q & p & 0 \\ 0 & 0 & r \end{pmatrix}, \quad \boldsymbol{E}_2 = \begin{pmatrix} p & -q & 0 \\ -q & p & 0 \\ 0 & 0 & r \end{pmatrix},$$

$$\boldsymbol{E}_3 = \begin{pmatrix} p & 0 & q \\ 0 & r & 0 \\ q & 0 & p \end{pmatrix}, \quad \boldsymbol{E}_4 = \begin{pmatrix} p & 0 & -q \\ 0 & r & 0 \\ -q & 0 & p \end{pmatrix}, \tag{2.3}$$

$$\boldsymbol{E}_5 = \begin{pmatrix} r & 0 & 0 \\ 0 & p & q \\ 0 & q & p \end{pmatrix}, \quad \boldsymbol{E}_6 = \begin{pmatrix} r & 0 & 0 \\ 0 & p & -q \\ 0 & -q & p \end{pmatrix}.$$

where

$$p = \frac{1}{2}\left(\frac{\alpha^2+\gamma^2}{2} - 1\right), \; q = \frac{1}{2}\left(\frac{\alpha^2-\gamma^2}{2}\right), \; r = \frac{1}{2}\left(\beta^2 - 1\right). \tag{2.4}$$

2.3 Crystallographic theory of martensite twins

Twinning is a process by which certain regions of a crystal take up a new orientation having a symmetry relation to the rest of the crystal; the lattice is reoriented in a regular fashion. It is prevalent in low symmetry materials such as the orthorhombic martensite phase of CuAlNi.

The twinned region of the crystal is usually a mirror image of the rest of the crystal and the plane separating the two regions is a mirror plane. It is assumed that the atoms are displaced parallel to the mirror plane; and the displacement is a fraction of the lattice translation vector in that direction, so the process is one of simple shear. All the atoms of the twinned region are moved through distances proportional to the distances from the mirror plane. The mirror plane is called the *twin plane* and the direction of displacement is called the *twin direction*.

It may be noted that twinning can occur in one direction only. If the lattice is sheared in the direction opposite to that in which twinning can occur, the lattice slips. Furthermore, if the lattice is sheared further in the direction of twinning, the lattice once again slips.

From the point of view of material science, twin types are classified according to the rotations that take one lattice into another. If the lattice on one side can be obtained by rotating the lattice on the other side by 180° about the twin plane normal the twin is referred to as *Type I*; if the two lattices are related by a 180° rotation about a vector in the twin plane the twin is referred to as being *Type II*; and finally, if the lattices are related through both rotations the twins are *compound twins*. Crystallographic theory defines compound twins as having both the twin plane normal and the shear directions *rational*; Type I as having the plane normal rational and shear direction *irrational*[1]; and Type II twins as having a rational shear direction and irrational twin plane normal.

Consider the general case of a body $\mathcal{B}$ divided into regions $\overset{+}{\mathcal{B}}$ and $\overset{-}{\mathcal{B}}$ by a plane Σ. Let the deformation gradient in the body be piecewise constant $\boldsymbol{F}_I$ and $\boldsymbol{F}_J$ in the regions $\overset{+}{\mathcal{B}}$ and $\overset{-}{\mathcal{B}}$ respectively (Figure 2-2). Then the deformation of the body is

$$\boldsymbol{y}(\boldsymbol{x}) = \begin{cases} \boldsymbol{F}_I \boldsymbol{x}, & \boldsymbol{x} \in \overset{+}{\mathcal{B}}, \\ \boldsymbol{F}_J \boldsymbol{x}, & \boldsymbol{x} \in \overset{-}{\mathcal{B}}. \end{cases} \tag{2.5}$$

Continuity of the deformation across Σ requires that

$$\boldsymbol{F}_I - \boldsymbol{F}_J = \boldsymbol{s} \otimes \hat{\boldsymbol{n}}, \tag{2.6}$$

which is the condition that $\boldsymbol{F}_I$ and $\boldsymbol{F}_J$ are rank-one connected. Here $\hat{\boldsymbol{\nu}}$ is the unit normal to Σ and $\boldsymbol{s}$ is a nonzero vector.

The compatibility equation (2.6) can be solved by applying a theorem of Ball and James [11]. We state the result in the particular case of twinning. To represent the solutions it is more convenient to rewrite (2.6) in the form

$$\boldsymbol{Q}\boldsymbol{U}_I - \boldsymbol{U}_J = \boldsymbol{1} + \boldsymbol{a} \otimes \hat{\boldsymbol{n}}. \tag{2.7}$$

Here $\boldsymbol{U}_I$ and $\boldsymbol{U}_J$ are the stretch tensors from the polar decomposition of $\boldsymbol{F}_I$ and $\boldsymbol{F}_J$ and

[1]Irrational planes and directions are those having Miller indices as irrational numbers or large integers. The irrational values are obtained when the plane does not pass through the Bravais lattice. Experimentally, irrational lines and planes are identified by large Miller indices.

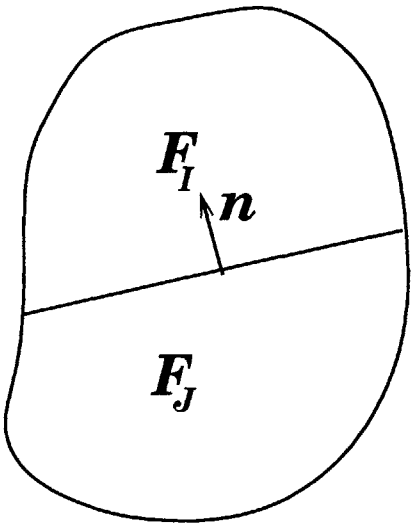

Figure 2-2: A piecewise homogeneous deformation separated by an interface Σ.

have the representations (2.1) in the cubic basis. For these variants it is possible to write

$$\boldsymbol{U}_I = \boldsymbol{R}\boldsymbol{U}_J\boldsymbol{R}^T, \tag{2.8}$$

where $\boldsymbol{R} = \mathbf{1} - 2\boldsymbol{e} \otimes \boldsymbol{e}$ is a 180° rotation about an axis $\boldsymbol{e}$. Note that det $\boldsymbol{U}_I$=det $\boldsymbol{U}_J$ and (2.7) implies by a straightforward calculation that $\boldsymbol{a}\cdot\hat{\boldsymbol{n}} = 0$. Thus the twinning deformation is a simple shear on the plane with normal $\hat{\boldsymbol{n}}$ and shear direction $\boldsymbol{a}$.

The solutions to the twinning equation (2.7) are

$$\hat{\boldsymbol{n}} = \boldsymbol{e} \qquad \boldsymbol{a} = 2\left(\frac{\boldsymbol{U}_J{}^{-1}\boldsymbol{e}}{|\boldsymbol{U}_J^{-1}\boldsymbol{e}|^2} - \boldsymbol{U}_J\boldsymbol{e}\right) \tag{2.9}$$

or

$$\hat{\boldsymbol{n}} = \frac{2}{\rho}\left(\boldsymbol{e} - \frac{\boldsymbol{U}_J^2\boldsymbol{e}}{|\boldsymbol{U}_J\boldsymbol{e}|^2}\right) \qquad \boldsymbol{a} = \rho\boldsymbol{U}_J\boldsymbol{e}, \tag{2.10}$$

where $\rho = |2\left(\boldsymbol{e} - \frac{\boldsymbol{U}_J^2\boldsymbol{e}}{|\boldsymbol{U}_J\boldsymbol{e}|^2}\right)|$ so that $\hat{\boldsymbol{n}}$ is a unit vector.

2.4 Crystallographic theory of phase boundaries

Phase boundaries separate austenite phase from martensite phase. For austenite to form a compatible interface with a single variant of martensite the lattice parameters of martensite must take up special values (Hane and Shield [35]). In fact, CuAlNi alloys cannot form

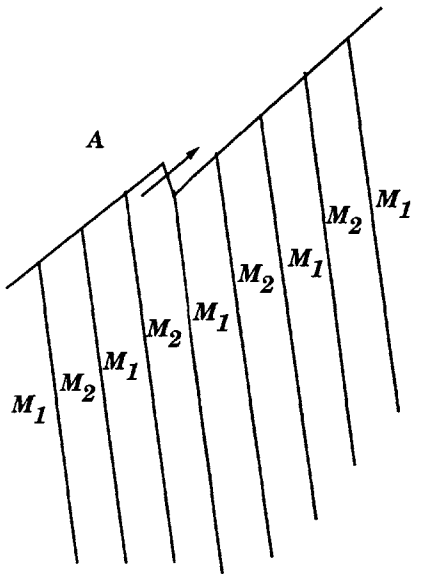

Figure 2-3: A body composed austenite and twinned martensite separated by a phase boundary.

austenite single variant martensite interfaces (Bhattacharya [13]). However, austenite forms *weakly compatible* interfaces with *twinned martensite*. The notion of a weakly compatible interface is described below.

Let $\boldsymbol{x}$ denote the position of a material point in the undeformed body (consisting of unstressed austenite). A deformation $\boldsymbol{y}(\boldsymbol{x})$ maps the point $\boldsymbol{x}$ into a point in the deformed body. We consider deformations in which $\boldsymbol{y}$ is continuous and piecewise differentiable. The gradient of the deformation is denoted by $\boldsymbol{F} = \nabla \boldsymbol{y}$ and takes a value of $\boldsymbol{F}_a$ in austenite and alternates between $\boldsymbol{F}_I$ and $\boldsymbol{F}_J$ in the martensite region, where I and J denote specific variants.

Continuity of deformation across any one of the interfaces between variants of martensite is given by the twinning equation (2.7). The atomic positions of the two variants of martensite match perfectly on the twin boundary and the twin variants are said to be *strongly compatible* (cf. Chu [17]). The atomic positions of austenite and of the twinned martensite variants match only in an average sense and the phases are said to be *weakly compatible*. Thus the continuity requirement across a phase boundary is of the form

$$(\lambda \boldsymbol{F}_J + (1-\lambda)\boldsymbol{F}_I) - \boldsymbol{F}_a = \boldsymbol{s} \otimes \hat{\boldsymbol{\nu}} \tag{2.11}$$

where $\lambda \in (0,1)$ represents the volume fraction variant-J in martensite.

The solutions to the twinning equation and the austenite-martensite phase boundary equation are well-known for the cubic to tetragonal transformation of interest to us (cf. Ball and James [1987], Bhattacharya [1992]). Since the solutions are used later, we summarize them here following Bhattacharya [1992] closely.

We first the phase boundary equation using the twinning equation (2.7) in the form

$$\boldsymbol{Q}_0\{\boldsymbol{U}_J + \lambda \boldsymbol{a} \otimes \hat{\boldsymbol{n}}\} = \boldsymbol{I} + \boldsymbol{s} \otimes \hat{\boldsymbol{\nu}}. \tag{2.12}$$

For a particular pair $\boldsymbol{a}$ and $\boldsymbol{n}$ obtained by solving (2.7), one can obtain the solution $\boldsymbol{Q}_0, \boldsymbol{s}, \hat{\boldsymbol{\nu}}$ and λ of equation (2.12). We outline the solution algorithm following Bhattacharya [13].

1. Evaluate the quantities $\delta = \boldsymbol{a} \cdot \boldsymbol{U}_J(\boldsymbol{U}_J^2 - \boldsymbol{1})^{-1}\hat{\boldsymbol{n}}$ and $\eta = \mathrm{Tr}(\boldsymbol{U}_J^2) - \mathrm{Det}(\boldsymbol{U}_J^2) + (|\boldsymbol{a}|^2/2\delta)$. The equation (2.12) is solvable if and only if $\delta \leq -2$ and $\eta \geq 2$.

2. The volume fraction of the martensite variant $\boldsymbol{U}_J$ is obtained from the formula

$$\lambda = \frac{1}{2}\left(1 - \sqrt{1 + \frac{2}{\delta}}\right). \tag{2.13}$$

3. If we label the eigenvalues of $\boldsymbol{C} = \{\boldsymbol{U}_J + \lambda \hat{\boldsymbol{n}} \otimes \boldsymbol{a}\}\{\boldsymbol{U}_J + \lambda \boldsymbol{a} \otimes \hat{\boldsymbol{n}}\}$, $\lambda_1 \leq \lambda_2 \leq \lambda_3$ and the corresponding eigenvectors as $\hat{\boldsymbol{e}}_1, \hat{\boldsymbol{e}}_2$ and $\hat{\boldsymbol{e}}_3$, then the solution to the phase boundary compatibility equation is given by

$$\begin{aligned} \boldsymbol{s} &= \rho\left(\sqrt{\frac{\lambda_3(1-\lambda_1)}{\lambda_3 - \lambda_1}}\hat{\boldsymbol{e}}_1 + \chi\sqrt{\frac{\lambda_1(\lambda_3 - 1)}{\lambda_3 - \lambda_1}}\hat{\boldsymbol{e}}_3\right) \\ \hat{\boldsymbol{\nu}} &= \frac{1}{\rho}\left(\sqrt{\frac{\lambda_3 - \sqrt{\lambda_1}}{\lambda_3 - \lambda_1}}\right)(-\sqrt{1-\lambda_1}\hat{\boldsymbol{e}}_1 + \chi\sqrt{\lambda_3 - 1}\hat{\boldsymbol{e}}_3) \end{aligned} \tag{2.14}$$

   where ρ is chosen to make $\hat{\boldsymbol{\nu}}$ a unit vector.

4. If $\lambda \neq \frac{1}{2}$, then another solution is obtained by replacing λ with $1 - \lambda$.

2.5 Sharp interface theory

Consider a homogeneous body $\mathcal{B}$ occupying a region R of three dimensional Euclidean space in the reference configuration. A *motion* of the body is described by a mapping $\boldsymbol{y}$ of material

points $\boldsymbol{x}$ and times t into points $\boldsymbol{y}(\boldsymbol{x},t)$ in space. That is, during the time interval T of interest

$$\boldsymbol{y} = \boldsymbol{y}(\boldsymbol{x},t) = \boldsymbol{x} + \boldsymbol{u}(\boldsymbol{x},t) \quad \forall \boldsymbol{x} \in R,\ t \in T. \tag{2.15}$$

We assume that the deformation $\boldsymbol{y}$ is at least twice continuously differentiable on $R \times T$, excepting on a collection of smooth surfaces S contained in R. On these surfaces S, the deformation may suffer jump discontinuities. These surfaces represent interfaces between variants or phases depending on the relationship between the lattice structure on either side. We adopt the Cauchy-Born hypothesis [24] and assume that the deformation gradient in the continuum is a macroscopic manifestation of the deformation of lattice vectors associated with the arrangement of atoms in the material. We write

$$\boldsymbol{F} = \nabla \boldsymbol{y} = \mathbf{1} + \nabla \boldsymbol{u}, \quad \forall \boldsymbol{x} \in R \backslash S, \tag{2.16}$$

for the deformation gradient and require that $\det \boldsymbol{F} > 0$. The particle velocity is denoted at points $(\boldsymbol{x},t)$, where it exits, by

$$\boldsymbol{v} = \boldsymbol{v}(\boldsymbol{x},t) = \frac{\partial \boldsymbol{u}(\boldsymbol{x},t)}{\partial t} \quad \forall \boldsymbol{x} \in R \backslash S. \tag{2.17}$$

We denote the *first Piola-Kirchoff stress* by $\boldsymbol{\sigma}$ and the *body force (density)* by $\boldsymbol{s}$. The balance laws of linear and angular momentum state that for every subregion $\mathcal{P}$ of $\mathcal{B}$, the following hold:

$$\int_{\partial \mathcal{P}} \boldsymbol{\sigma n}\ da + \int_{\mathcal{P}} \boldsymbol{b}\ dv = \frac{d}{dt} \int_{\mathcal{P}} \rho \boldsymbol{v}\ dv, \tag{2.18}$$

$$\int_{\partial \mathcal{P}} \boldsymbol{y} \times \boldsymbol{\sigma n}\ da + \int_{\mathcal{P}} \boldsymbol{y} \times \boldsymbol{b}\ dv = \frac{d}{dt} \int_{\mathcal{P}} \boldsymbol{y} \times \rho \boldsymbol{v}\ dv, \tag{2.19}$$

where $\boldsymbol{n}$ is the outward normal to $\partial \mathcal{P}$. We also denote the internal energy per unit mass by $\varepsilon(\boldsymbol{x},t)$ and the entropy per unit mass by $\eta(\boldsymbol{x},t)$. We assume that $\varepsilon(\boldsymbol{x},t)$ and $\eta(\boldsymbol{x},t)$ are piecewise continuous with piecewise continuous gradients on $R \times T$. We also assume that the temperature $\theta(\boldsymbol{x},t)$ is continuous with piecewise continuous first derivatives. The energy balance and the second law of thermodynamics state that, for every subregion $\mathcal{P}$ of $\mathcal{B}$,

$$\int_{\partial \mathcal{P}} \boldsymbol{\sigma n} \cdot \boldsymbol{v}\ da + \int_{\partial \mathcal{P}} \boldsymbol{q} \cdot \boldsymbol{n}\ da = \frac{d}{dt} \int_{\mathcal{P}} \rho\ \varepsilon\ dv + \frac{d}{dt} \int_{\mathcal{P}} \frac{1}{2} \rho \boldsymbol{v} \cdot \boldsymbol{v}\ dv, \tag{2.20}$$

$$\Gamma(\mathcal{P},t) \equiv \frac{d}{dt}\int_{\mathcal{P}} \rho\eta \; dv - \int_{\partial\mathcal{P}} \frac{\boldsymbol{q}\cdot\boldsymbol{n}}{\theta} \; da \geq 0. \tag{2.21}$$

Equivalently, upon localizing, the global balance laws (2.18–2.20) yield at a point in $\mathcal{B}\backslash S$ at a fixed time instant $t \in T$, the local balance laws:

$$\text{Div } \boldsymbol{\sigma} = \rho \; \dot{\boldsymbol{v}}, \tag{2.22}$$

$$\boldsymbol{\sigma}\boldsymbol{F}^T = \boldsymbol{F}\boldsymbol{\sigma}^T, \tag{2.23}$$

$$\dot{\boldsymbol{\sigma}}\cdot\boldsymbol{F} + \text{Div}\boldsymbol{q} = \rho \; \dot{\varepsilon}, \tag{2.24}$$

and (2.21) yields the local version of the second law:

$$\text{Div}\left(\frac{\boldsymbol{q}}{\theta}\right) \geq \rho \; \dot{\eta}. \tag{2.25}$$

In addition, the following jump conditions must necessarily hold for $\boldsymbol{x} \in S$:

$$[\![\boldsymbol{\sigma}\boldsymbol{n}_S]\!] + \rho[\![\boldsymbol{v}]\!]V_n = \boldsymbol{0}, \tag{2.26}$$

$$[\![\boldsymbol{\sigma}\boldsymbol{n}_S\cdot\boldsymbol{v}]\!] + [\![\rho(\varepsilon + \frac{1}{2}\boldsymbol{v}\cdot\boldsymbol{v}]\!]V_n + [\![\boldsymbol{q}\cdot\boldsymbol{n}_S]\!] = 0, \tag{2.27}$$

$$[\![\rho \; \eta]\!]V_n + [\![\frac{\boldsymbol{q}\cdot\boldsymbol{n}_S}{\theta}]\!] \leq 0. \tag{2.28}$$

Here the notation $[\![g]\!]$ of a generic function g denotes

$$[\![g]\!] = \overset{+}{g}\;(\boldsymbol{x},t) - \overset{-}{g}\;(\boldsymbol{x},t), \tag{2.29}$$

where $\overset{+}{g}\;(\boldsymbol{x},t)$ and $\overset{-}{g}\;(\boldsymbol{x},t)$ stand for the limiting values of g as the interface is approached from the positive and negative sides respectively, and the scalar V_n denotes the normal speed of the surface $S(t)$. The normal vector $\boldsymbol{n}_S$ is chosen such that the normal velocity $\boldsymbol{V}$ (and hence $\boldsymbol{n}$) is positive when the interface progresses into the positive region $\overset{+}{\mathcal{P}}$. Kinematics yields the following conditions for $\boldsymbol{x} \in S$:

$$[\![\boldsymbol{F}]\!]\boldsymbol{l} = \boldsymbol{0}, \tag{2.30}$$

$$[\![\boldsymbol{v}]\!] + V_n[\![\boldsymbol{F}]\!]\boldsymbol{n}_S = \boldsymbol{0}, \tag{2.31}$$

where $\boldsymbol{l}$ is any vector tangent to $S(t)$.

2.6 Constitutive theory

In order to describe specific material behavior, the following constitutive equations need to be specified

$$\begin{aligned} \psi &= \hat{\psi}(\boldsymbol{F}, \theta, \text{Grad}\theta), \\ \boldsymbol{S} &= \hat{\boldsymbol{S}}(\boldsymbol{F}, \theta, \text{Grad}\theta), \\ \boldsymbol{q} &= \hat{\boldsymbol{q}}(\boldsymbol{F}, \theta, \text{Grad}\theta), \\ \eta &= \hat{\eta}(\boldsymbol{F}, \theta, \text{Grad}\theta), \end{aligned} \tag{2.32}$$

and

$$f = \hat{f}(V_n). \tag{2.33}$$

Assuming that the material is thermoelastic and using the second law of thermodynamics and the requirements of material symmetry, we can see that the full constitutive response of the material can be given by specifying

$$\begin{aligned} \psi &= \hat{\psi}(\boldsymbol{E}, \theta), \\ \boldsymbol{q} &= \hat{\boldsymbol{q}}(\boldsymbol{E}, \theta), \end{aligned} \tag{2.34}$$

along with the kinetic relation (2.33). Here $\boldsymbol{E} = \frac{1}{2}(\boldsymbol{F}^T\boldsymbol{F} - \boldsymbol{1})$ is the Lagrangian strain tensor. The remainder of the thesis is dedicated to obtaining these constitutive functions for the phase transforming material CuAlNi.

Chapter 3

Constitutive Theory for CuAlNi

3.1 Introduction

The austenite-martensite phase transformation occurring in alloys such as CuAlNi, NiTi, InTl among others has been the subject of considerable attention recently due to its role in the shape memory effect exhibited by these alloys. The shape memory effect and related phenomena occurring in such materials arise from their capacity to fully recover from large, apparently permanent deformations under various conditions of thermal and/or mechanical loading. While several different alloys exhibit the shape memory effect, the cubic to orthorhombic transition occurring in several Copper-based alloys and the cubic to monoclinic transition in NiTi have been of particular interest in industry.

The behavior of CuAlNi has been well studied experimentally (Otsuka, Shimuzu and coworkers [51]-[71], Chu [17], Abeyaratne et al [1]). However there have been few theoretical and numerical studies due to the absence of a suitable constitutive model. The free-energy for such materials is non-convex and has multiple local minima at finite deformation gradients. A free-energy for cubic-tetragonal alloys has been developed by Ericksen [25] with parameters fitted for InTl by James (the full potential is presented in Collins and Levine [18]). Koyama and Nittono [43] and Nittono and Koyama [46] have studied cubic-orthorhombic and cubic-tetragonal transitions in Indium based alloys such as InTl, InCd, InPb and InSn. Falk and Konopka [27] have studied CuAlNi but they considered a transition from cubic austenite to twinned monoclinic martensite with the twins consisting of fine orthorhombic layers. However, experimental studies of Chu [17], and Abeyaratne et al [1] and theoretical studies of Abeyaratne and Vedantam [8] demonstrate the necessity of

a constitutive model describing cubic to orthorhombic transition in CuAlNi. This chapter is dedicated to a systematic development of the same.

We develop our free-energy function using the polynomial basis of irreducible invariants of the group of transformations describing the symmetry properties of the austenite parent phase. The polynomial bases were first enumerated by Smith and Rivlin [73] for several crystal classes and shown to be irreducible by Smith [72]. Moreover, Pipkin and Wineman [61] and Wineman and Pipkin [84] have shown that these polynomial bases are valid even for material whose constitutive equations cannot be expressed in terms of polynomials. A summary for the 32 crystallographic point groups is given in Green and Adkins [33]. Our free-energy is a fourth order polynomial function of an appropriate subset of the irreducible basis.

In Section 3.2, we construct a Helmholtz free energy appropriate for such materials. In Section 3.3, we fit the Helmholtz free energy function to relevant physical properties of CuAlNi alloys. In Section 3.4, the features of the free energy function are described.

3.2 Helmholtz free energy

3.2.1 Constitutive assumptions

We assume that the Helmholtz free energy per unit reference volume $\psi(\boldsymbol{F}, \theta)$ is a function of the deformation gradient $\boldsymbol{F} = \nabla \boldsymbol{y}(\boldsymbol{x})$ and the temperature θ. We require, as is standard, that the Helmholtz free energy be frame indifferent. This is a statement that for all rotations $\boldsymbol{Q}$,

$$\psi(\boldsymbol{F}, \theta) = \psi(\boldsymbol{Q}\boldsymbol{F}, \theta). \tag{3.1}$$

Using the polar decomposition theorem, the above statement reduces to

$$\psi(\boldsymbol{F}, \theta) = \psi(\boldsymbol{U}, \theta). \tag{3.2}$$

where $\boldsymbol{U} = \sqrt{(\boldsymbol{F}^T \boldsymbol{F})}$ is the right stretch tensor. In our calculations, we find it convenient to express the Helmholtz free energy as a function of the Lagrangian Green strain tensor $\boldsymbol{E} = \frac{1}{2}(\boldsymbol{U}^2 - \boldsymbol{1})$,

$$\psi(\boldsymbol{U}, \theta) = \hat{\psi}(\boldsymbol{E}, \theta). \tag{3.3}$$

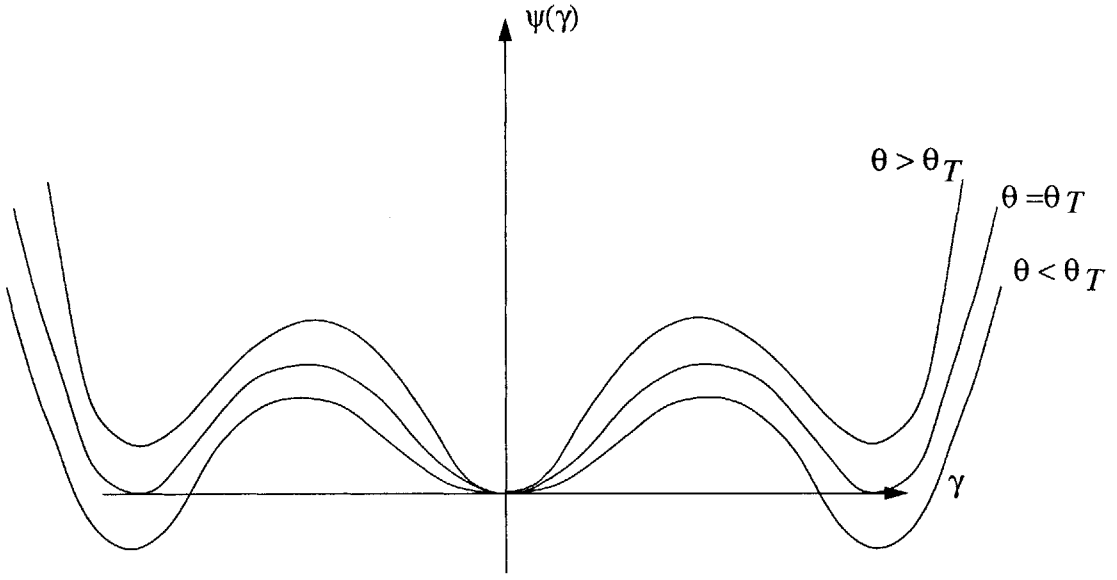

Figure 3-1: The dependence of free energy on strain at various temperatures.

Next, the free energy function is required to reflect the symmetry of the material. This requirement is expressed as

$$\hat{\psi}(\boldsymbol{R}^T \boldsymbol{E} \boldsymbol{R}, \theta) = \hat{\psi}(\boldsymbol{E}, \theta), \tag{3.4}$$

where $\boldsymbol{R}$ are orthogonal transformations belonging to the *point group* of the reference configuration $\mathcal{G}_{ref}$ (see Truesdell and Noll [75]).

Finally, we require some additional properties of the Helmholtz free-energy function to reflect the fact that the materials we are interested in exist in several metastable phases. To each metastable phase corresponds a local minimum of the free energy. Above a certain temperature θ_T (known as the *transformation temperature*), stress-free austenite phase is stable, whereas below the transformation temperature, martensite is the stable phase.

If unstressed austenite is taken as the reference, the above idea is the statement that $\boldsymbol{E} = \boldsymbol{0}$ minimizes the free energy above the transformation temperature (Figure 3-1)

$$\hat{\psi}(\boldsymbol{0}, \theta) < \hat{\psi}(\boldsymbol{E}, \theta), \quad \theta > \theta_T, \tag{3.5}$$

for all $\boldsymbol{E} \in \mathcal{E}^{sp} \neq \boldsymbol{0}$. Here we have used the shorthand notation

$$\mathcal{E}^{sp} = \{\boldsymbol{E} : 2\boldsymbol{E} + \boldsymbol{1} \text{ is symmetric and positive definite}\}. \tag{3.6}$$

Then, since we want martensite to be the stable phase below the transformation temperature (Figure 3-1),

$$\hat{\psi}(\boldsymbol{E}_i, \theta) < \hat{\psi}(\boldsymbol{E}, \theta), \quad \theta < \theta_T, \tag{3.7}$$

for all $\boldsymbol{E} \in \mathcal{E}^{sp} \neq \boldsymbol{E}_i,\ i = 1, \ldots, 6$. The $\boldsymbol{E}_i,\ i = 1, \ldots, 6.$ correspond to the strain tensors of the six variants of martensite listed in (2.3).

At the transformation temperature, we require the energies corresponding to the austenite and martensite minima to be equal (Figure 3-1):

$$\hat{\psi}(\boldsymbol{0}, \theta_T) = \hat{\psi}(\boldsymbol{E}_i, \theta_T) < \hat{\psi}(\boldsymbol{E}, \theta_T), \tag{3.8}$$

for all $\boldsymbol{E} \in \mathcal{E}^{sp} \neq \boldsymbol{0},\ \boldsymbol{E}_i,\ i = 1, \ldots, 6$.

3.2.2 Polynomial invariants

The CuAlNi austenite phase is cubic with the point group of $4/m\ \bar{3}\ 2/m$ [78]. Applying the symmetry transformations for a cubic material, it has been shown by Smith and Rivlin [73] that the free energy function $\hat{\psi}(\boldsymbol{E}, \theta) = \hat{\Psi}(E_{11}, E_{22}, E_{33}, E_{12}, E_{23}, E_{13}, \theta)$ is required to be a function of the nine polynomial irreducible invariants for this symmetry (see Appendix A for details):

$$\begin{aligned}
P_1 &= E_{11} + E_{22} + E_{33}, \\
P_2 &= E_{11}E_{22} + E_{22}E_{33} + E_{33}E_{11}, \\
P_3 &= E_{11}E_{22}E_{33}, \\
P_4 &= E_{12}E_{23}E_{13}, \\
P_5 &= E_{12}^2 + E_{23}^2 + E_{13}^2, \\
P_6 &= (E_{11} + E_{22})E_{12}^2 + (E_{22} + E_{33})E_{23}^2 + (E_{33} + E_{11})E_{13}^2, \\
P_7 &= E_{12}^2E_{23}^2 + E_{23}^2E_{13}^2 + E_{13}^2E_{12}^2, \\
P_8 &= E_{11}E_{12}^2E_{23}^2 + E_{22}E_{13}^2E_{12}^2 + E_{33}E_{23}^2E_{13}^2, \\
P_9 &= E_{12}^2E_{11}E_{22} + E_{23}^2E_{11}E_{33} + E_{13}^2E_{22}E_{33}.
\end{aligned} \tag{3.9}$$

Thus, if we want the free energy to reflect the symmetry of the parent phase it is necessary and sufficient to consider a free energy that is a function of the polynomials

$P_1, \ldots, P_9$:

$$\hat{\Psi}(E_{11}, E_{22}, E_{33}, E_{12}, E_{23}, E_{13}, \theta) = \tilde{\Psi}(P_1, \ldots, P_9, \theta). \tag{3.10}$$

Our aim is to develop the simplest form of the free energy which would have all the properties of interest. In particular, for the free energy to have the austenite and martensite wells, it is necessary to consider at least quartics. For simplicity, we restrict ourselves to a quartic polynomial function of $P_1, \ldots, P_9$.

3.2.3 Constraints

In crystals undergoing structural phase transitions, a precursor to the transition is a so-called "soft mode" of the crystal lattice. Near the transformation temperature it is experimentally observed that some ratios of the elastic constants tend to become small. Traditionally, such a feature has led to constraints such as incompressibility on materials. Such softening of elastic constants has been observed (Gobin and Guenin [32]) in crystals undergoing cubic-orthorhombic phase transitions. Ericksen [25] has inferred constraints on cubic-tetragonal crystals based on the softening of elastic constants. Here we adapt those constraints to a cubic-orthorhombic crystal.

In particular, the ratios of elastic moduli of the cubic phase near the transformation temperature

$$(C_{11} - C_{12})/(C_{11} + 2C_{12}) \text{ and } (C_{11} - C_{12})/C_{44} \tag{3.11}$$

have been observed to become small near the transformation temperature in the case of cubic-tetragonal crystals. Ericksen [25] proposed that the trace of the strain tensor and the shear strains vanish in such a case.

In the case of a cubic-orthorhombic CuAlNi, however, it has been observed that while the ratio $(C_{11} - C_{12})/(C_{11} + 2C_{12})$ becomes small, $(C_{11} - C_{12})/C_{44}$ is an order of magnitude larger near the transformation temperature. Due to this observation we retain Ericksen's first constraint and set the trace of the strain tensor to zero but we do not retain the second constraint. A second reason for the second constraint to be inappropriate is that the strain tensors of the orthorhombic variants contain shear terms. It will not be possible to constrain the shear strains to vanish and yet fit a well at the orthorhombic variants to the energy. In

terms of the irreducible polynomial invariants this condition reduces to

$$P_1 = E_{11} + E_{22} + E_{33} = 0. \tag{3.12}$$

With this constraint acting, the most general quartic polynomial expansion of the free energy takes the form

$$\begin{aligned}\tilde{\Psi}(P_1,\ldots,P_9,\theta) = a_1(\theta) \quad &+ \quad a_2(\theta)P_2 + a_3(\theta)P_3 + a_4(\theta){P_2}^2 + a_5(\theta)P_5 + a_6(\theta){P_5}^2 \\ &+ \quad a_7(\theta)P_6 + a_8(\theta)P_9 + a_9(\theta)P_2P_5 + a_{10}(\theta)P_7. \end{aligned} \tag{3.13}$$

In order to solve general problems with arbitrary deformations we may wish to relax the constraint. In this case the energy may be written as

$$\begin{aligned}\tilde{\Psi}(P_1,\ldots,P_9,\theta) \quad &= \quad a_1(\theta) + a_2(\theta)P_2 + a_3(\theta)P_3 + a_4(\theta){P_2}^2 + a_5(\theta)P_5 + a_6(\theta){P_5}^2 \\ &+ \quad a_7(\theta)P_6 + a_8(\theta)P_9 + a_9(\theta)P_2P_5 + a_{10}(\theta)P_7 + a_{11}(\theta){P_1}^2. \end{aligned} \tag{3.14}$$

The coefficients $a_1,\ldots,a_{11}$ are functions of temperature in general. We do not consider $a_1(\theta)$ further since it does not affect the mechanical properties of the material.

3.3 Coefficients for CuAlNi

In this section we calculate the coefficients of the free-energy (3.14) using experimental values for the transformation strains, elastic moduli and latent heat of transformation reported in the literature. The transformation strains have been calculated by Chu [17] and elastic moduli have been reported by Suezawa and Sumino [74] and Yasunaga et al [85, 86]. Latent heat values have been reported by Otsuka et al [54]. The experimental values are listed in Tables 3.1 and 3.2 using the Voigt notation and referred to the orthorhombic axes. The transformation temperature is highly sensitive to the composition of the alloy and a wide range of temperatures have been reported in literature.

From the polynomial free energy, the austenite elastic moduli are

$$C^a_{ijkl} = \left.\frac{\partial^2\tilde{\Psi}}{\partial E_{ij}\partial E_{kl}}\right|_{\boldsymbol{E}=\boldsymbol{0}}, \tag{3.15}$$

C_{11}	C_{12}	C_{44}
141	124	97

Table 3.1: Measured moduli for the cubic phase (Yasunaga et al [85, 86]) in GPa

C_{11}	C_{22}	C_{33}	C_{44}	C_{55}	C_{66}	C_{12}	C_{13}	C_{23}
205	189	141	62.6	54.9	19.7	45.5	115	124

Table 3.2: Measured moduli for the orthorhombic phase (Yasunaga et al [85, 86]) in GPa

and the martensitic elastic moduli are (see Appendix B)

$$C^m_{ijkl} = \left.\frac{\partial^2 \tilde{\Psi}}{\partial E_{ab} \partial E_{cd}}\right|_{\boldsymbol{E}=\boldsymbol{E}_m} U_{ai} U_{bj} U_{ck} U_{dl}. \tag{3.16}$$

The latent heat of transformation may be calculated using the formula

$$\lambda_T = \theta \left(\left.\frac{\partial \tilde{\Psi}}{\partial \theta}\right|_{\boldsymbol{E}=\boldsymbol{0}} - \left.\frac{\partial \tilde{\Psi}}{\partial \theta}\right|_{\boldsymbol{E}=\boldsymbol{E}_m} \right)\Bigg|_{\theta=\theta_T}. \tag{3.17}$$

For simplicity we assume that the coefficients $a_2, \ldots, a_{11}$ are linearly dependent on temperature. That is,

$$\begin{aligned} a_2(\theta) &= a_2^0 + a_2^T(\theta - \theta_{\mathrm{r}}) \\ &\cdot \\ &\cdot \\ &\cdot \\ a_{11}(\theta) &= a_{11}^0 + a_{11}^T(\theta - \theta_{\mathrm{r}}). \end{aligned} \tag{3.18}$$

Here, we have assumed that the elastic moduli were measured by Yasunaga et al at a room temperature of $\theta_{\mathrm{r}} = 300K$.

First we fit the elastic moduli at room temperature to the experimentally measured values. There are a total of three transformation strains, three austenite moduli and nine orthorhombic moduli. We fit the ten temperature independent constants $a_2^0, \ldots, a_{11}^0$ to the fifteen parameters using the method of least squares. Since the free energy coefficients are not fitted to all the elastic moduli exactly, we have to check the resulting free energy for convexity. We do this by evaluating that the determinants of the leading minors of the elastic moduli matrix in the Voigt notation at the austenite and martensite strains. Provided all

the determinants of the principal minors are positive, the free energy is a positive definite function. That is, we determine the elastic constants using equations (3.15) and (3.16) we evaluate the matrices for the austenite and martensite wells:

$$\begin{pmatrix} C_{1111} & C_{1122} & C_{1133} & C_{1123} & C_{1113} & C_{1112} \\ C_{2211} & C_{2222} & C_{2233} & C_{2223} & C_{2213} & C_{2212} \\ C_{3311} & C_{3322} & C_{3333} & C_{3323} & C_{3313} & C_{3312} \\ C_{2311} & C_{2322} & C_{2333} & C_{2323} & C_{2313} & C_{2312} \\ C_{1311} & C_{1322} & C_{1333} & C_{1323} & C_{1313} & C_{1312} \\ C_{1211} & C_{1222} & C_{1233} & C_{1223} & C_{1213} & C_{1212} \end{pmatrix}. \tag{3.19}$$

The energy is convex at the two wells if and only if the leading minors are all positive. That is,

$$
\begin{vmatrix}
C_{1111} & C_{1122} & C_{1133} & C_{1123} & C_{1113} & C_{1112} \\
C_{2211} & C_{2222} & C_{2233} & C_{2223} & C_{2213} & C_{2212} \\
C_{3311} & C_{3322} & C_{3333} & C_{3323} & C_{3313} & C_{3312} \\
C_{2311} & C_{2322} & C_{2333} & C_{2323} & C_{2313} & C_{2312} \\
C_{1311} & C_{1322} & C_{1333} & C_{1323} & C_{1313} & C_{1312} \\
C_{1211} & C_{1222} & C_{1233} & C_{1223} & C_{1213} & C_{1212}
\end{vmatrix} > 0,
$$

$$
\begin{vmatrix}
C_{1111} & C_{1122} & C_{1133} & C_{1123} & C_{1113} \\
C_{2211} & C_{2222} & C_{2233} & C_{2223} & C_{2213} \\
C_{3311} & C_{3322} & C_{3333} & C_{3323} & C_{3313} \\
C_{2311} & C_{2322} & C_{2333} & C_{2323} & C_{2313} \\
C_{1311} & C_{1322} & C_{1333} & C_{1323} & C_{1313}
\end{vmatrix} > 0, \tag{3.20}
$$

$$
\begin{vmatrix}
C_{1111} & C_{1122} & C_{1133} & C_{1123} \\
C_{2211} & C_{2222} & C_{2233} & C_{2223} \\
C_{3311} & C_{3322} & C_{3333} & C_{3323} \\
C_{2311} & C_{2322} & C_{2333} & C_{2323}
\end{vmatrix} > 0,
$$

$$
\begin{vmatrix}
C_{1111} & C_{1122} & C_{1133} \\
C_{2211} & C_{2222} & C_{2233} \\
C_{3311} & C_{3322} & C_{3333}
\end{vmatrix} > 0,
$$

$$
\begin{vmatrix}
C_{1111} & C_{1122} \\
C_{2211} & C_{2222}
\end{vmatrix} > 0,
$$

$$
C_{1111} > 0.
$$

Next, in order to determine the temperature-dependent coefficients $a_2^T, \ldots, a_{11}^T$ we use the data for latent heat of transformation reported by Otsuka et al [54]. They report a latent heat of transformation of $-48.3 MJm^{-3}$ at $300K$. We allow only the coefficients of the

quartic terms to depend on temperature. This implies that only $a_4^T, a_5^T, a_8^T, a_9^T, a_{10}^T$ are non-zero and the rest of the temperature coefficients vanish. Since the transformation strain of the material depends solely on the lattice parameters of the cubic and orthorhombic phases, and the lattice parameters may be assumed to be independent of temperature in the range of temperature under consideration, we assume that the transformation strains are independent of temperature. This condition and the condition on the heat of transformation give us four equations for the temperature coefficients. We also observe that since the coefficient a_{10}^T is multiplied by a products of the squares of off-diagonal strain terms and our conditions are on the value and the extrema of the energy, the coefficient a_{10}^T does not appear in our equations. We therefore set $a_{10}^T = 0$. Solving the four equations gives the following approximate coefficients of the free energy listed in (3.21). The coefficients a_i^0 are in GPa and the coefficients a_i^T are in GPa/K.

$$\begin{aligned} &a_2 = -4.265,\ a_3 = 566.5,\ a_4 = 2156.5,\ a_5 = 48.2, \\ &a_6 = 18933.1 + 962.3(\theta - 300),\ a_7 = 12378.9,\ a_8 = 21638.4,\ a_9 = 671.2, \\ &a_{10} = 68.2,\ a_{11} = -1164.2. \end{aligned} \tag{3.21}$$

3.4 Features of the constitutive model

3.4.1 Free energy

The free energy function determined in the previous section has the required minima at the austenite and martensite wells. We now locate these wells using various parameterizations of the free energy functions.

First we list the elastic moduli calculated from the free energy function (3.14) in Tables 3 and 4. The elastic moduli of the free energy function can be seen to closely match the experimentally measured moduli. The fitting of the coefficients was such that the latent heat of transformation at equilibrium matches the experimental value exactly. The transformation strains are also fitted exactly. The transformation temperature (the temperature at which the heights of the wells of the austenite and martensite phases are equal) is calculated from the free energy to be $\theta_T = 360K$. A wide range of values for the transformation temperature have been reported for several different compositions in the literature.

The temperature dependence of the free energy function is easily seen in a one dimensional slice of the free energy which passes through the austenite well and two of the

C_{11}	C_{12}	C_{44}
137	132	97

Table 3.3: Calculated moduli for the cubic phase in GPa

C_{11}	C_{22}	C_{33}	C_{44}	C_{55}	C_{66}	C_{12}	C_{13}	C_{23}
211	195	120	61	57	36	58	106	119

Table 3.4: Calculated moduli for the orthorhombic phase in GPa

martensite variants. Thus we consider the strain tensor as a function of a single variable κ as

$$\boldsymbol{E}(\kappa) = \begin{pmatrix} p(\kappa/q)^2 & \kappa & 0 \\ \kappa & p(\kappa/q)^2 & 0 \\ 0 & 0 & r(\kappa/q)^2 \end{pmatrix}. \tag{3.22}$$

A plot of $\psi(\kappa, \theta) = \tilde{\Psi}(\boldsymbol{E}(\kappa), \theta)$ is shown in Figure 3-2.

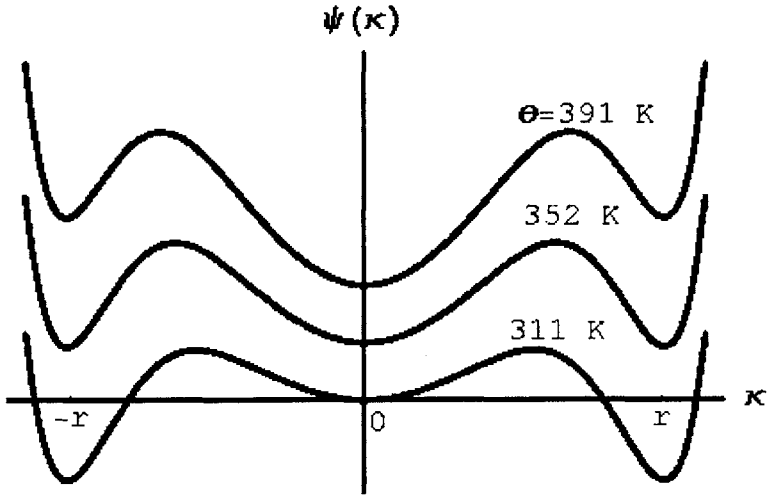

Figure 3-2: Temperature dependence of the free energy.

We can now consider other slices of the free energy to show more wells. Consider a

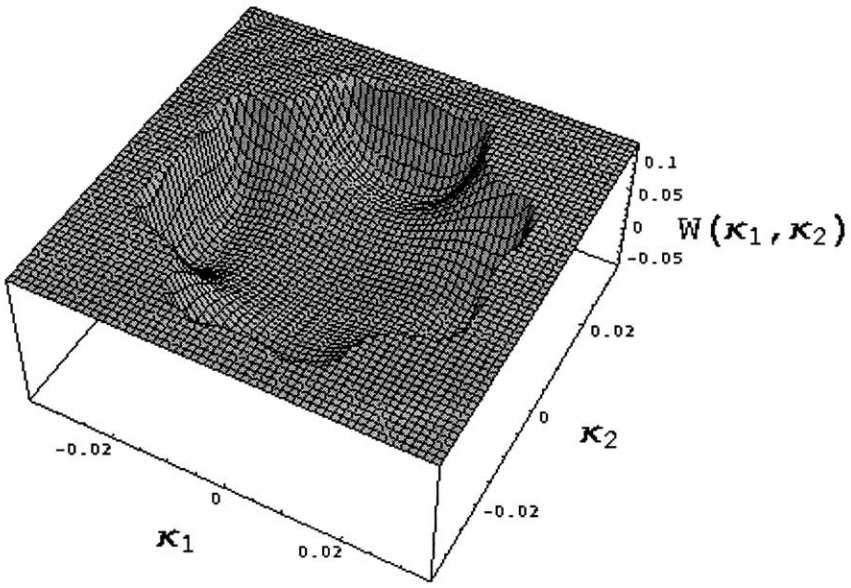

Figure 3-3: A slice of the free energy showing four variants.

parameterization of the free energy with κ_1, κ_2 as follows

$$\boldsymbol{E}(\kappa_1, \kappa_2) = \begin{pmatrix} p(\kappa_1/q)^2 + p(\kappa_2/q)^2 & \kappa_1 & \kappa_2 \\ \kappa_1 & p(\kappa_1/q)^2 + r(\kappa_2/q)^2 & 0 \\ \kappa_2 & 0 & r(\kappa_1/q)^2 + p(\kappa_2/q)^2 \end{pmatrix}. \tag{3.23}$$

The four variants of martensite designated by the strain tensors are $\boldsymbol{E}_1, \boldsymbol{E}_2, \boldsymbol{E}_3, \boldsymbol{E}_4$ in Section 2 are spanned by this parameterization when $(\kappa_1, \kappa_2) \in [-q, q] \times [-q, q]$. A plot of the energy $W(\kappa_1, \kappa_2) = \tilde{\Psi}(\boldsymbol{E}(\kappa_1, \kappa_2), \theta_T)$ is shown in Figure 3-3.

Finally, we parametrize the free energy function to show the austenite well and the six wells corresponding to the variants of martensite. A plot of the free energy in this case is shown in Figure 3-4. The austenite well is located at the origin and the six wells of martensite are located at a radial distance of $u = 1$ and angular positions of $t = \pi/3$.

3.4.2 Stress strain relation

We now calculate the stress-strain curves for this material under several loadings. First we consider shearing of a block of material in the austenite phase. The stress-strain curve is

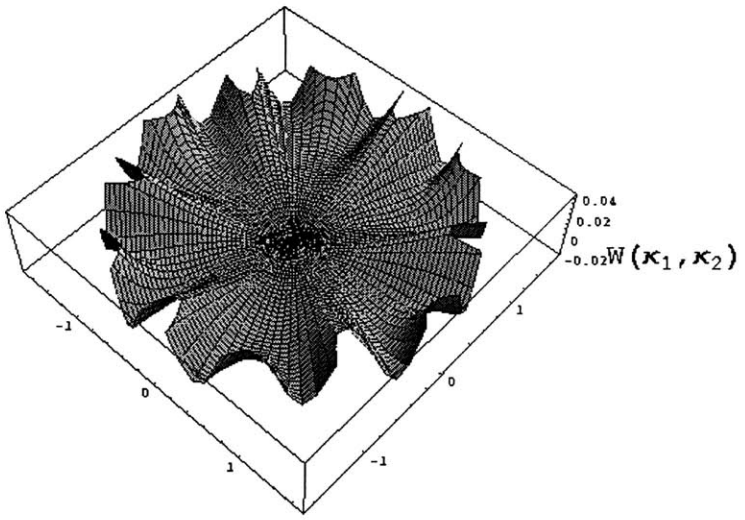

Figure 3-4: A slice of the free energy showing all six variants.

plotted in Figure 3-5. Since a single variant of martensite does not form a compatible interface with austenite, martensite cannot form from austenite by simple shearing. However, a single variant of martensite can transform to another single variant of martensite by simple shear. Depending on the initial and final variants of martensite there exist three types of solutions. We have plotted the energy and stress-strain curves for this deformation.

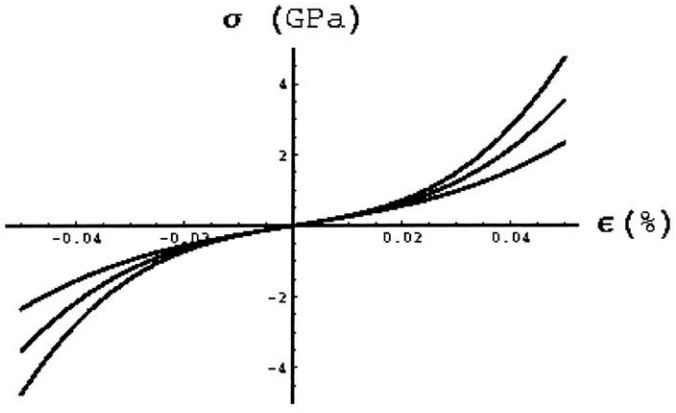

Figure 3-5: Shear stress vs. shear strain

3.5 Discussion

The free energy we obtained in Section 3.2.3 has the necessary properties of frame indifference and temperature dependent minima. Considering a quartic equation has the advantage that the free energy only has minima at the austenite phase and all the variants of the martensite phase.

Constraints were considered following Ericksen [25] which allowed us to obtain a highly tractable form of the free energy function. Finally, the free energy was constructed by fitting the transformation strains, elastic moduli and the heat of transformation. The elastic moduli calculated from the free energy match the measured moduli closely.

Stress strain curves obtained for this material show characteristic non–monotonicity when sheared on particular planes and in particular directions (obtained from the solution of the twinning equation) from the martensite phase. Similar non–monotonicity is not seen in shear from the austenite phase since a simple shear deformation does not connect austenite to martensite.

Chapter 4

Kink motion

4.1 Introduction

Many bodies accommodate macroscopic deformation through twinning and phase transformations. Twin and phase boundaries are particular kinds of interfaces in solids across which the crystalline lattice has either different orientations or structure respectively. Across these interfaces kinematic and thermodynamic quantities such as the deformation gradient, stress, internal energy, etc. may suffer jump discontinuities. A discontinuity in the deformation gradient leads to a breakdown of strong ellipticity in the nonlinear elasticity theory and results in non-uniqueness of the solutions of these problems. This lack of uniqueness has been circumvented using several different approaches (see Pettinger [59] for a detailed discussion). One approach has been to introduce an additional constitutive relation (cf. Abeyaratne and Knowles [2]–[6], [76]) called the *kinetic law or kinetic relation* which is valid on the interface. This is the approach we follow in this thesis.

Typically, the interfaces under consideration propagate in a direction normal to themselves at a speed, which in continuum theory, is specified by the kinetic law. The kinetic law is viewed as providing a continuum-scale description of the micromechanical processes underlying the front motion. In this chapter, we study these micromechanical processes in detail to obtain the form of this law for propagating sharp interfaces. For this we use a simple mechanical analog to illustrate how the kinetic law can be calculated by modeling the microscale mechanisms.

In many cases, the propagation of the interface in the apparently normal direction is in fact achieved by the rapid sideways propagation, at the micro-scale, of a "kink" (or step

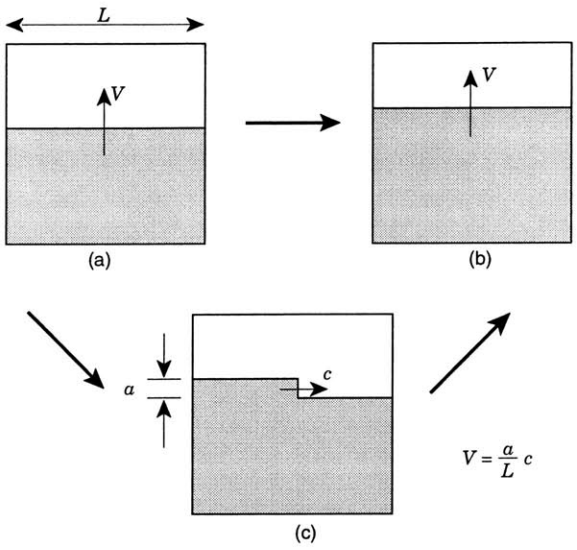

Figure 4-1: The apparently forward motion of the interface from (a) to (b) is achieved by the sideways propagation of a kink as shown in (c).

or ledge) along the front in a transverse direction (Figure 4-1), see for example Section 8.5 of [37]. A *mechanical analog* of this phenomenon is provided by the motion of an infinite chain of inter-connected particles on a corrugated surface. In some reference state, all of the particles lie within the same corrugation. The motion occurs because of forces that are applied on the particles in a direction normal to the corrugations. In the motion of interest, the chain of particles moves forward, from one corrugation to the next, but it does this one particle at a time. Thus, at some generic instant, all of the particles to the left of some particular one have advanced to the next corrugation whereas those to its right are still in the original corrugation. We are interested in calculating the velocity with which this pattern propagates along the chain (thereby determining the associated kinetic law).

In Section 2.5 we describe the sharp interface theory from a continuum viewpoint. In Section 4.2 we describe a thermodynamic quantity known as the driving traction and a standard postulate of the form of the kinetic relation. In Section 4.3 we describe twin boundary motion briefly from an atomic level perspective and describe how the features of twinning may be translated into an equivalent mechanical model. In Section 4.4 we describe the mechanical analog in greater detail and obtain the kinetic relation in that setting.

4.2 Driving traction and kinetic relation

Starting with Eshelby [26], several authors [3, 30] have calculated a thermodynamic quantity, the *driving traction* on the interface S. The driving traction has been viewed as a "conjugate force" to the "internal variable" phase boundary velocity. As mentioned earlier, in this thesis we restrict our consideration to isothermal processes and hence derive the driving traction in this case.

In an isothermal setting, the total dissipation rate for every subregion $\mathcal{P}$ is

$$\Gamma(\mathcal{P},t) \equiv \int_{\partial\mathcal{P}} \boldsymbol{\sigma}\boldsymbol{n}\cdot\boldsymbol{v}\ da - \frac{d}{dt}\int_{\mathcal{P}} \left(\psi(\boldsymbol{x},t) + \frac{1}{2}\rho\boldsymbol{v}\cdot\boldsymbol{v}\right)\ dv, \tag{4.1}$$

where $\psi(\boldsymbol{x},t)$ is the Helmholtz free-energy

$$\psi(\boldsymbol{x},t) = \varepsilon(\boldsymbol{x},t) - \theta\eta(\boldsymbol{x},t) \quad \forall \boldsymbol{x} \in R,\ t \in T. \tag{4.2}$$

This can be recast, following Abeyaratne and Knowles [3], in the form

$$\Gamma(\mathcal{P},t) = \int_{\mathcal{P}\cap\mathcal{S}} f(\boldsymbol{x},t)V_n(\boldsymbol{x},t)\ da, \tag{4.3}$$

where the *driving traction* $f(\boldsymbol{x},t)$ is defined on the surface $S(t)$ by

$$f(\boldsymbol{x},t) = \rho[\![\psi(\boldsymbol{x},t)]\!] - \frac{1}{2}\{\overset{+}{\boldsymbol{\sigma}}(\boldsymbol{x},t) + \overset{-}{\boldsymbol{\sigma}}(\boldsymbol{x},t)\}\cdot[\![\boldsymbol{F}(\boldsymbol{x},t)]\!] \quad \forall \boldsymbol{x} \in S,\ t \in T. \tag{4.4}$$

The dissipation rate (4.3) is required to be non-negative by the Clausius- Duhem version of the second law of thermodynamics. Localization of (4.3) and imposition of the second law leads to

$$f(\boldsymbol{x},t)V_n(\boldsymbol{x},t) \geq 0 \quad \boldsymbol{x} \in S,\ t \in T. \tag{4.5}$$

This inequality restricts the possible direction of motion of the interface. As mentioned above, the driving traction has been viewed as a "conjugate force" to the "internal variable" phase boundary velocity. This has led Abeyaratne and Knowles [2, 3] to postulate a *kinetic relation* of the form

$$f(\boldsymbol{x},t) = \varphi(V_n(\boldsymbol{x},t)) \quad \boldsymbol{x} \in S(t). \tag{4.6}$$

The function $\varphi(V_n(\boldsymbol{x},t))$ depends on the material and to be consistent with the dissipation

inequality (4.5) must be such that

$$\varphi(V_n(\boldsymbol{x},t))V_n(\boldsymbol{x},t) \geq 0 \tag{4.7}$$

for all possible values of V_n.

Continuum theory only takes us this far and the actual form of the kinetic relation $f(\boldsymbol{x},t) = \varphi(V_n(\boldsymbol{x},t))$ is still unknown. Since role of the kinetic relation is to incorporate the microstructural effects it seems natural to briefly abandon the continuum theory and examine the material at a microscale to obtain the kinetic relation. In the next section, we motivate a mechanical model that seems appropriate for twin boundary propagation.

4.3 Features of twin boundary motion and their mechanical analogs

In this section we describe a one dimensional mechanical analog of twin boundary motion. Twinning is described in greater detail in Chapter 2. We have used twin boundary motion to draw our analogy since twin boundaries appear to have regularity up to the atomic level (see the HRTEM picture in Figure 4-2). Our mechanical analog is based on the supposed motion of atoms as twins propagate. The displacements of the atoms are assumed to follow the continuum description of twinning motion (see Section 5.2). At very low temperatures, for which we created our model, this seems a reasonable supposition. In Chapter 7, we retain elements of this model for ledges in phase boundaries.

Figure 4-2 shows a High Resolution Transmission Electron Microscopy (HRTEM) picture of a NiAl alloy. In Figure 4-3 some features of the HRTEM picture are schematically redrawn in an exaggerated fashion to identify the configuration of the lattice in a twinned material. In the HRTEM picture we observe regions of different crystal orientations. The regions of differing crystal orientations are said to be twin related and the interface between such regions are called twin boundaries. These boundaries are sharp at atomic scales. However, there may be regions where there is distortion on more than one plane due to dislocations on the twin boundary. It is believed that the normal motion of twin boundaries is due to lateral motion of these dislocations along the twin boundary (Klassen-Neklyudova [42]). It can be seen from Figure 4-3 that for a twin boundary to move from its initial location at

$\mathcal{T}$ to the final location $\mathcal{P}$, all atoms on the plane $\mathcal{P}$ and above must translate by a fraction of the lattice parameter d. If this were to occur by a rigid translation of all atoms on and above plane $\mathcal{P}$, it can be shown that the shear stress required for this process will be several orders of magnitude above the Ultimate Shear Strength of the crystal. Instead dislocations as shown in Figure 4-4 are believed to propagate along the twin boundary. The stress required to move the dislocation is much smaller than that required move the entire plane of atoms. We incorporate this aspect in our mechanical model.

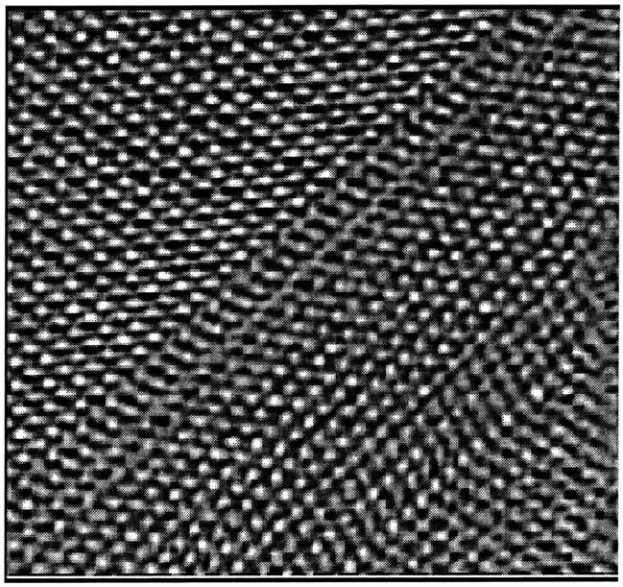

Figure 4-2: A HRTEM picture of Ni-Al alloy (courtesy Schryvers (1998)).

The atoms in the crystal are modeled by point masses with an pairwise interaction potential between atoms. The effect of the external stress acting on the crystal on the atoms in the plane $\mathcal{P}$ is modeled by a constant force on each point mass. The full three-dimensional problem is reduced to a two-dimensional one by considering the plane perpendicular to the dislocation. Next, we further reduce the problem to a one-dimensional one by treating only the dynamics of the atoms on the twin line, and assuming that the surrounding atoms not on the twin line create a substrate potential for this row of atoms. The substrate potential as a function of the displacement of an atom on the twin line is shown in Figure 4-5. It has to be noted that the substrate potential is periodic with the periodicity of the lattice parameter d and we have shown the structure within one period. Also it is notable that the energy barriers to twinning is lower the barrier to slip. Therefore these materials are susceptible to twinning rather than slip. The plot we have shown is a calculation performed using

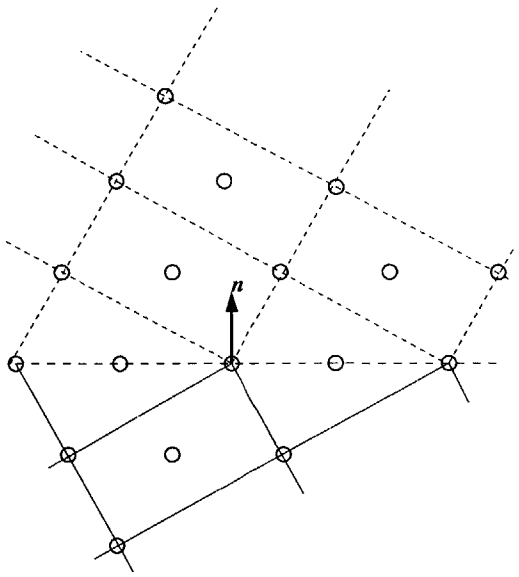

Figure 4-3: A schematic of a twin boundary without dislocations.

a Lenard-Jones interaction potential for atoms arranged in orthorhombic compound twin configuration. The details of this calculation are described in Chapter 6. A qualitatively similar plot has been obtained by Paxton [57] using a quantum mechanical first principles calculation. Due to the presence of the dislocation on the twin boundary atoms on the twin line move relative to each other. However, in twinning, the relative displacements are small compared to the lattice spacing d and so we model the interactions using a linear force law. To summarize, the mechanical analog consists of a chain of point masses connected by linear springs in a periodic substrate potential of period d shown in Figure 4-5. There is one atom in each of the intervals $(nd, nd + d)$, $n = \ldots, -1, 0, 1, \ldots$. If all the atoms are separated by d and located in the left well of the substrate potential, the lattice structure is that of the first variant. If all the atoms are located in the the right well, the lattice is of the second variant. If all the atoms start in the left well at the beginning of a particular motion and end in the right well at the end of the motion, the twin boundary is considered to have advanced by one layer of atoms.

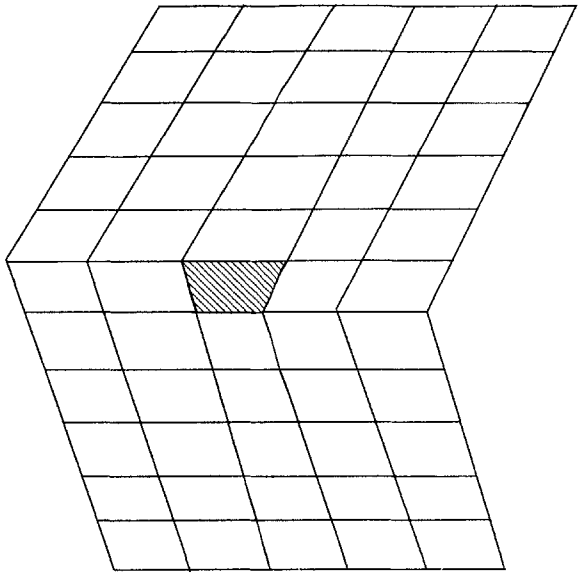

Figure 4-4: A schematic of a twin boundary with a dislocation.

4.4 Mechanical model for interface motion: Description and Analysis

4.4.1 Description and formulation

Consider a substrate $z = \widehat{W}(y)$ which, on the average, is is parallel to the y-axis. Suppose that it is periodic with period d in the y-direction:

$$\widehat{W}(y) = W(y) = W(y+d) \quad \text{for} \quad -\infty < y < \infty. \tag{4.8}$$

The local minima of W are located at $y = i(d-b)/2$ and $y = i(d+b)/2$, $i = 0, \pm 1, \pm 2, \pm 3, ...$ The interval

$$id \ < \ y \ < \ (i+1/2)d, \qquad i = 0, \pm 1, \pm 2, ..., \tag{4.9}$$

represents the *ith left energy-well* of W and $y = i(d-b)/2$ denotes the bottom of this energy-well. The interval

$$(i+1/2)d \ < \ y \ < \ (i+1)d, \qquad i = 0, \pm 1, \pm 2, ..., \tag{4.10}$$

represents the *ith right energy-well* of W and $y = i(d+b)/2$ denotes the bottom of this energy-well.

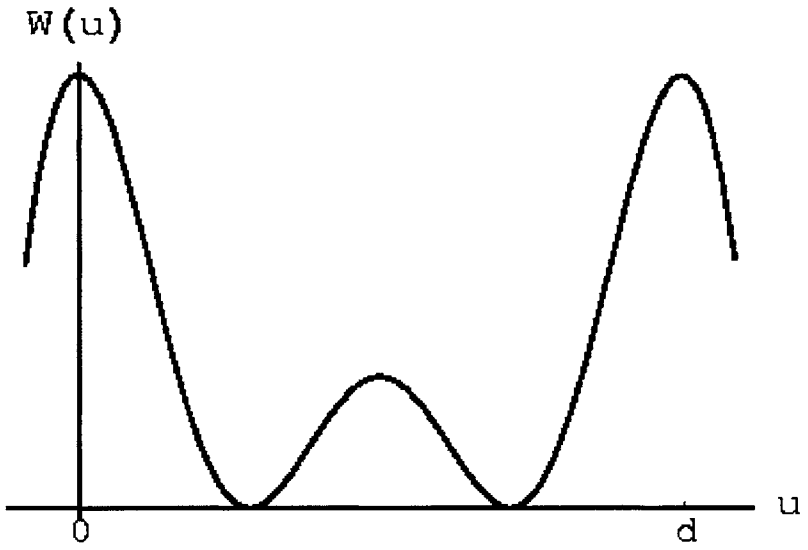

Figure 4-5: Substrate potential

Now consider an infinite chain of particles which lie in equilibrium at the bottom of all the *left* energy-wells. Each particle has mass m and interacts with its two immediate neighbors through a central-force potential $\phi(r)$ where r is the distance between a pair of particles. The associated force is $-\phi'(r)$. In this equilibrium configuration, the spacing between any pair of particles is b and the corresponding force between them is $T = -\phi'(d)$. It is convenient to set $s = T/d$ so that s has the dimensions of stiffness.

Suppose now that a constant force $f > 0$ is applied to each particle in the y-direction and assume that the particles are constrained so that they can only move in the y-direction. If $y = y_n(t)$ denotes the position of the nth particle at time t, the force applied to that particle by its two adjacent particles is $-\phi'(d)\ (y_{n+1} - y_n - d)/d\ +\ \phi'(d)\ (y_n - y_{n-1} - d)/d$. Therefore the equation of motion of the nth particle is

$$m\ddot{y}_n = s(y_{n+1} - 2y_n + y_{n-1})\ -\ W'(y_n)\ + f, \qquad n = 0, \pm 1, \pm 2, \ldots . \tag{4.11}$$

The nth particle is *not* of course restricted to being located in any particular energy-well and is free to move between energy-wells.

It is more convenient to study these equations in terms of the displacement u_n of the nth particle from the bottom of the nth left energy well. Then

$$u_n = y_n - nd, \qquad n = 0, \pm 1, \pm 2, \ldots . \tag{4.12}$$

Then the equations of motion can be written in terms of u_n as (using the periodicity of W)

$$m\ddot{u}_n = s(u_{n+1} - 2u_n + u_{n-1}) \; - \; W'(u_n) \; + f, \qquad n = 0, \pm 1, \pm 2, \ldots \; . \tag{4.13}$$

In this mechanical analog, the row of particles represents the "atoms" along a propagating front. The periodic potential W represents the effect of the rest of the crystal on these particles. The particle spacing d represents the interatomic distance; the forces f represent the shear stress applied on the crystal, and $\mu = W''(0)$ represents the infinitesimal shear modulus of the material. For twinning, the atoms have to move only a fraction of the atomic spacing b to go into the twinned state. Thus it is convenient to set

$$\sigma = f/d^2, \quad G = \mu/d, \quad \rho = m/d^3, \quad \lambda = d/b, \quad c_s = \sqrt{G/\rho}, \quad \text{and} \quad \Omega = \sqrt{\mu/s}, \tag{4.14}$$

so that σ represents the shear stress, G the shear modulus, ρ the mass density and c_s the shear wave velocity. Weiner and Sanders state that the ratio Ω^2 between the two stiffnesses μ and s represents the ratio of noncentral to central forces, see [82].

The applied forces $f(> 0)$ tend to cause the *ith* particle to move forward from the *ith* left energy-well to the *ith* right energy-well. Suppose that this occurs by the steady motion of a *kink* to the right, i.e. suppose that each particle remains in the left energy-well until the kink reaches it, at which time it moves over into the right energy-well. Thus, the chain advances in a steady pattern "one particle at a time". More specifically, suppose that the *nth* particle remains in the *nth* left energy-well for all times less than a certain critical instant $n\tau$, and that at $t = n\tau$ it moves into the *nth* right energy-well, and remains there for all subsequent times. This motion continues steadily with the $(n+1)th$ particle moving into the $(n+1)$ right energy-well at time $t = (n+1)\tau$ and so on. If c denotes the speed with which the kink propagates to the right, and v is its non-dimensionalization with respect to the shear wave speed, then

$$c \; = \; d/\tau, \qquad v = c/c_s. \tag{4.15}$$

Note that at the instant $t = n\tau$, all of the particles to the left of the *nth* one lie in the right energy-well, while all of the particles to its right lie in the left energy-well. The *nth*

particle itself is located at the boundary between the two energy-wells. Thus, for each n,

$$u_n(t) \begin{cases} \in \left(0,\ \frac{1}{2}d\right) & \text{for } -\infty < t < n\tau, \\ = \frac{d}{2} & \text{for } t = n\tau, \\ \in \left(\frac{d}{2}, d\right) & \text{for } n\tau < t < \infty. \end{cases} \tag{4.16}$$

Since we are limiting attention to *steady* motions of the preceding type, the displacement of the nth particle at time t must equal the displacement of the $(n+m)th$ particle at time $t + m\tau$:

$$u_n(t) = u_{n+m}(t + m\tau) \tag{4.17}$$

for all integers n and m.

In *summary* the steady motion of a kink is characterized by the solutions $u_n(t)$ of the set of differential-difference equations (4.13) subject to the range requirement (4.16) and the periodicity requirement (4.17). Our interest here is primarily in determining the propagation speed v.

Frenkel-Kontorova models of this type have been studied extensively in the context of dislocation motion, see for example, [10, 82, 58]. In contrast to most of these studies, our interest here is in the continuum implications of the discrete model.

4.4.2 Analysis of kink motion: a continuum model

In order to analyze the preceding discrete problem it is natural to consider replacing it by an appropriate continuum approximation. Let $u(x,t)$ be defined for $-\infty < x < \infty$, $-\infty < t < \infty$ and be such that

$$u(nb, t) = u_n(t), \qquad n = 0, \pm 1, \pm 2, ... \tag{4.18}$$

Then it is natural to replace the system of ordinary differential-difference equations (4.13) by the single partial differential equation

$$m\frac{\partial^2 u}{\partial t^2} = sb^2\frac{\partial^2 u}{\partial x^2} - W'(u) + f. \tag{4.19}$$

In order to study the steady motion of a kink, the periodicity requirement (4.17) suggests that we seek traveling wave type solutions of the form

$$u(x,t) = \hat{u}(\xi), \qquad \xi = x - ct. \tag{4.20}$$

The range condition (4.16) requires that

$$\hat{u}(\xi) \quad \begin{cases} \in \left(0, \frac{d}{2}\right) & \text{for } \xi > 0, \\ = \frac{d}{2}, & \text{for } \xi = 0, \\ \in \left(\frac{d}{2}, d\right) & \text{for } \xi < 0. \end{cases} \tag{4.21}$$

The discrete problem (4.13), (4.16), (4.17) has now been replaced by the continuous problem (4.19)—(4.21).

In order to obtain an explicit solution, consider the *piecewise parabolic energy*

$$W(u) = \begin{cases} \frac{\mu}{2}\left(u - \frac{(d-b)}{2}\right)^2 & \text{for } 0 < u < d/2, \\ \frac{\mu}{2}\left(u - \frac{(d+b)}{2}\right)^2 & \text{for } d/2 < u < d, \end{cases} \qquad n = 0, \pm 1, \pm 2, \ldots \tag{4.22}$$

Because of (4.20)—(4.22), (4.14) and (4.15), the differential equation (4.19) can be written explicitly as

$$\frac{d}{\Omega^2}\,(v^2\Omega^2 - 1)\hat{u}'' \;+\; \frac{\hat{u}}{d} \;=\; \begin{cases} \frac{\sigma}{G} + \frac{\lambda - 1}{2\lambda} & \text{for} \quad \xi > 0, \\ \frac{\sigma}{G} + \frac{\lambda + 1}{2\lambda} & \text{for} \quad \xi < 0. \end{cases} \tag{4.23}$$

There are three cases to consider: *(i)* $1 - v^2\Omega^2 > 0$, *(ii)* $1 - v^2\Omega^2 < 0$ and *(iii)* $1 - v^2\Omega^2 = 0$. Note first that if a solution involves a shock, i.e. a discontinuity in $\hat{u}'$, the shock propagation speed must equal the wave speed associated with (4.19): $c = (sd^2/m)^{1/2}$ or equivalently $v = 1/\Omega$. Therefore in cases (i) and (ii) one only needs to consider C^1 solutions.

On solving (4.23) in case (i) and enforcing the range conditions (4.21) and the continuity of $\hat{u}$ and $\hat{u}'$ at $\xi = 0$, one finds that necessarily $\sigma = 0$ and that then v can take any value less than $1/\Omega$.

In case (ii), the solution of (4.23) involves waves that propagate with a group velocity that is less than c. If we assume that such waves cannot be present ahead of the kink (whose speed is c), the terms which describe these waves must be omitted on the upstream side

$\xi > 0$. Enforcing the requisite smoothness and the requirement $(4.21)_2$ leads to a function $\hat{u}$ which violates $(4.21)_3$. Thus there is no solution in this case.

In case (iii), (4.23) shows immediately that $\hat{u}$ itself is necessarily discontinuous.

Therefore we are led to the conclusion that the continuous problem (4.19)–(4.22) has a (C^1 or piecewise C^1) solution only if $\sigma = 0$ and that in this case the propagation speed $v(< 1/\Omega)$ is arbitrary.

4.4.3 Analysis of kink motion: the discrete model

Since the preceding continuous problem is not very informative, we now return to the discrete problem. The periodicity condition (4.17) requires the displacement $u_n(t)$ to have the traveling wave form $u_n(t) = \bar{u}(\xi)$, $\xi = nd - ct$. The discrete problem (4.13), (4.16), (4.17), (4.22) can be solved explicitly using Fourier transforms, see [10], leading eventually to the following relation between the stress σ and the propagation speed v:

$$\sigma = G\lambda\Omega^2 \sum_{j=1}^{M} \frac{1}{r_j |D'(r_j)|}, \tag{4.24}$$

$$D(k) = -v^2\Omega^2 d^2\, k^2 + \Omega^2 + 4\sin^2(dk/2), \tag{4.25}$$

and the $2M$ real roots of the equation $D(k) = 0$ have been denoted by $k = \pm r_1, \pm r_2, , \ldots \pm r_M$ with $r_i > 0$.

Our interest is in the implications of this propagation law at the continuum level. The only waves which are "visible" at the continuum scale are those which have a long wavelength compared to the lattice dimension d, i.e. those with $kd << 1$. Thus the propagation law at the continuum scale is obtained from (14) by retaining only the roots r_j relevant to the case $kd << 1$.

Thus we approximate $D(k)$, for small kd, by

$$D = \Omega^2 + (1 - v^2\Omega^2)(kd)^2 - \frac{1}{12}(kd)^4 + O((kd)^6). \tag{4.26}$$

If one formally replaces (15) with (16) in (14) one obtains the following explicit continuum-scale propagation law (kinetic law)

$$\sigma = \frac{G\lambda}{4}\left\{1 - \frac{1 - v^2\Omega^2}{\sqrt{(1 - v^2\Omega^2)^2 + \Omega^2/3}}\right\}, \tag{4.27}$$

which relates the applied stress σ to the kink propagation speed v.

4.4.4 Analysis of kink motion: an improved continuum model

The discrete model of the preceding section led to a kinetic law characterizing kink propagation whereas the previous continuum model did not. This points to the inadequacy of the continuum model rather than the absence of a kinetic law. On plotting a graph of the solution $\bar{u}(\xi)$ of the discrete problem one finds that $\bar{u}(\xi)$ undergoes rapid variations near $\xi = 0$, suggesting that the continuum approximation (4.19) may not be sufficiently accurate in the vicinity of the kink.

This suggests that we consider replacing the set of ordinary differential equations (4.13) by the partial differential equation

$$m\frac{\partial^2 u}{\partial t^2} = sd^2\frac{\partial^2 u}{\partial x^2} + \frac{sd^4}{12}\frac{\partial^4 u}{\partial x^4} - W'(u) + f, \tag{4.28}$$

where we have now kept a higher-order derivative when approximating $u_{n+1} - 2u_n + u_{n-1}$, cf. (4.19). It is expected that the term involving the coefficient d^4 will be very small except in regions where u varies rapidly. The solution of (4.28), (4.20) for the piecewise parabolic energy (4.22) can be readily shown to be

$$\frac{\hat{u}(\xi)}{b} = \begin{cases} \dfrac{r^2}{2(r^2+b^2)}\, e^{-b\xi/b} + \dfrac{\sigma}{G} & \text{for } \xi > 0, \\ -\dfrac{r^2}{2(r^2+b^2)}\, e^{b\xi/b} - \dfrac{b^2}{r^2+b^2}\cos\dfrac{r\xi}{b} + \dfrac{\sigma}{G} + 1 & \text{for } \xi < 0, \end{cases} \tag{4.29}$$

where

$$\left.\begin{aligned} r &= \left[6(1-v^2\Omega^2) + \sqrt{36(1-v^2\Omega^2)^2 + 12\Omega^2}\right]^{1/2} && > 0, \\ b &= \left[-6(1-v^2\Omega^2) + \sqrt{36(1-v^2\Omega^2)^2 + 12\Omega^2}\right]^{1/2} && > 0. \end{aligned}\right\} \tag{4.30}$$

The range condition (4.21) requires that

$$\sigma = \frac{G\lambda}{4}\left\{1 - \frac{1-v^2\Omega^2}{\sqrt{(1-v^2\Omega^2)^2 + \Omega^2/3}}\right\}, \tag{4.31}$$

and $\sigma < G\lambda/6$, the former being the same relationship between the applied stress σ and the kink propagation speed v that we found in Section 4.4.3 from the continuum limit of

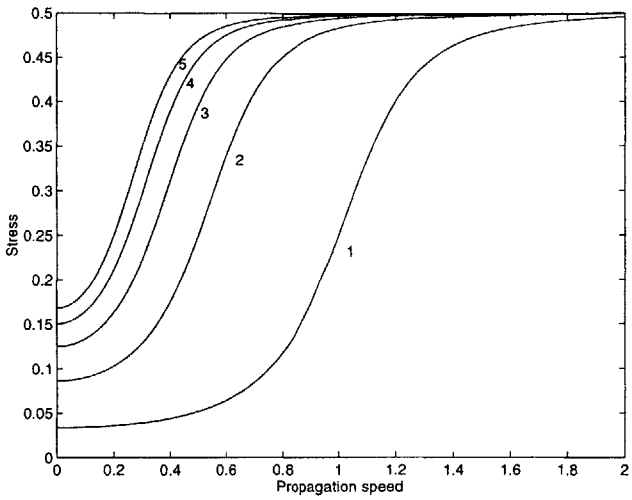

Figure 4-6: The kinetic relation. A graph of stress σ/G versus propagation speed v according to equation (4.31) for $\Omega = 1, 2, 3, 4$ and 5.

the discrete problem.

Remark. The improved continuum model that was described in this Section can be shown to be the same as the *quasicontinuum* model of Pouget [64, 65].

4.4.5 Discussion of kinetic relation

Figure 4-6 shows a plot of the kinetic relation (4.31). Observe that $\sigma \to \sigma_{cr}$ as $v \to 0$ where

$$\sigma_{cr} \;=\; (G\lambda/4)\;\left\{1 \;-\; (1+\Omega^2/3)^{-1/2}\right\}. \tag{4.32}$$

Consider the *equilibrium* of a chain of particles straddling two energy-wells, as characterized by the solution of the equilibrium version of (4.17) subject to $0 < u_n < d/2$ for $n \geq 0$ and $d/2 < u_n < d$ for $n < 0$. This discrete problem can be readily solved to find the displacements u_n. One finds from the range conditions that an equilibrium solution exists only if the stress σ does not exceed the critical value σ_{st} given by

$$\sigma_{st} \;=\; (G/2)\;\Omega\;(\Omega^2+4)^{-1/2}. \tag{4.33}$$

If $\sigma > \sigma_{st}$ the kink must move. If $\sigma < \sigma_{cr}$ the kink cannot move. Note that $\sigma_{st} > \sigma_{cr}$.

Chapter 5

Kinetics of twin boundaries

5.1 Introduction

The dominant mode of deformation in materials with low symmetry crystal structure is twinning. Twin boundaries propagate under relatively low stresses. But experimental observations indicate differences in the mobility of different kinds of twin boundaries (Ichinose et al [38], Chu [17]). In this chapter we examine the mobility of twin boundaries motivated by the micromechanical model of the previous chapter.

During twinning, the atoms on one side of a particular plane (called the twin plane) undergo a shear displacement in a direction parallel to this plane in such a way that the lattice on one side is a rotation of the lattice on the other side; the two lattices are said to the be associated with two variants of martensite. Depending on the two particular variants involved, a twin boundary maybe of one of three types: if both the twin plane and twin normal are rational the twin is said to be a Compound twin, whereas if only the twin plane or the twin normal are rational the twin is said to be either Type I or Type II respectively. Equivalently, for a type I twin the lattice on one side can be obtained by rotating the lattice on the other side by 180° about the twin plane normal; for a type II twin the two lattices are related by a 180° rotation about a vector in the twin plane; for a compound twin the lattices are related in both of these ways. The kinetic relation we derive for twin boundaries should be consistent with these observations.

The basic model is as follows: when the plane of atoms ahead of a twin boundary undergoes a shear displacement u, one can calculate the associated energy $W(u)$ by considering the work done by interatomic forces. This calculation depends on the detailed crystallog-

raphy of the variants, but can be readily carried out for a given material, say CuAlNi. One finds the resulting energy $W(u)$ has a "period-2 wiggly form" as shown schematically in Figure 4-5, i.e. W is periodic and involves two distinct families of barriers (S and T) which separate a sequence of local minima; an examination of the lattice shows that can interpret S and T as corresponding to energy barriers to slip and twinning respectively. In the case of martensitic CuAlNi one finds that the energy W has T barriers which are lower than the slip barriers, which is consistent with the fact that this material twins much more easily than it slips. The twin boundary advances from one plane of atoms to the next when the next plane of atoms move from the energy-well in which they are located to the next one passing over the intermediate T energy barrier.

In fact, the motion of this atoms does not occur simultaneously because this would be energetically difficult in view of the fact that all of the atoms would have to simultaneously cross over the energy-barrier. Instead, it has been observed that during twinning the atoms move over the barrier sequentially, one after the other. This is often described by saying that a "ledge" propagates transversely along the twin boundary, e.g. Klassen-Neklyudova [42], Frank [28]. By studying the dynamics of this sequential motion in the energy field W we can determine the propagation law for the transverse motion of the ledge, and hence for the forward motion of the twin.

This approach is clearly related to, and motivated by, the Frenkel-Kontorova model used to study slip in crystals, where the energy in this case is "period-1" because it has one family of (S-type) energy-barriers, e.g. [10]. Here, the kinetics of dislocation motion is deduced by studying the motion of a ledge through the appropriate energy field.

As described in Chapter 4, the kinetic relation provides a means to resolve the non-uniqueness in the continuum theory. So any equation we derive must be applicable to the continuum. We therefore start by considering a continuum layer in the material undergoing a shear deformation which converts one variant to another. This process models twin boundary propagation. We incorporate a ledge at the continuum level and derive the governing equation of motion. But when this proves inadequate we resort to a modified governing equation which we motivate based on the micromechanical model described above and in Chapter 4. The modified governing equation has higher gradient terms but differs from typical higher gradient theories of phase transformations.

5.2 Twinning deformation

Consider two piecewise homogeneous configurations $\mathcal{B}_1$ and $\mathcal{B}_2$ of a twinned martensitic body as illustrated schematically in Figure 5-1. The first of these involves a twin plane at $\boldsymbol{x}\cdot\hat{\boldsymbol{m}} = 0$, while in the second, the twin plane is at $\boldsymbol{x}\cdot\hat{\boldsymbol{m}} = h$; here $\hat{\boldsymbol{m}}$ denotes a unit vector which is normal to both twin planes. Our goal is to model, and analyze, the dynamics associated with the motion of this interface as it propagates from the former location to the latter.

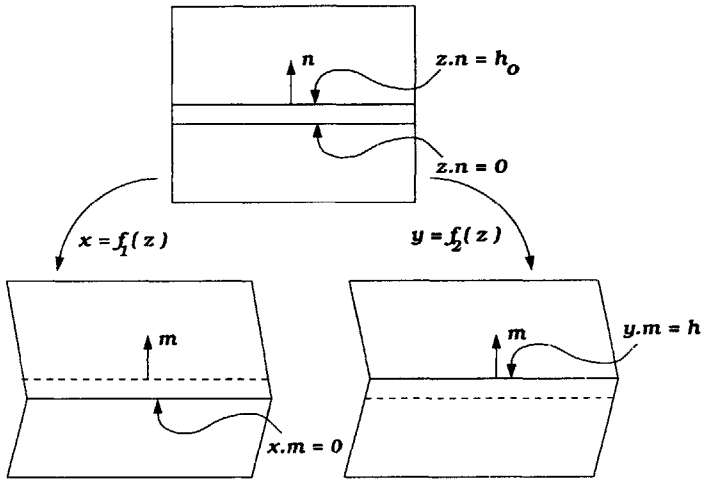

Figure 5-1: The deformations connecting configurations $\mathcal{B}_0$ to $\mathcal{B}_1$ and $\mathcal{B}_2$.

Let $\mathcal{B}_0$ denote some convenient reference configuration (say, one associated with unstressed austenite). Let $\boldsymbol{z}$, $\boldsymbol{x}$ and $\boldsymbol{y}$ denote the respective positions of a particle in $\mathcal{B}_0$, $\mathcal{B}_1$ and $\mathcal{B}_2$, and suppose that $\mathcal{B}_1$ and $\mathcal{B}_2$ can be described with respect to $\mathcal{B}_0$ by the piecewise homogeneous deformations

$$\begin{aligned}
\mathcal{B}_0 \to \mathcal{B}_1: \quad \boldsymbol{x} = \boldsymbol{x}(\boldsymbol{z}) &= \begin{cases} \overset{+}{\boldsymbol{F}}\,\boldsymbol{z} & \text{for } \boldsymbol{z}\cdot\hat{\boldsymbol{n}} \le 0, \\ \overset{-}{\boldsymbol{F}}\,\boldsymbol{z} & \text{for } \boldsymbol{z}\cdot\hat{\boldsymbol{n}} \ge 0, \end{cases} \\
\mathcal{B}_0 \to \mathcal{B}_2: \quad \boldsymbol{y} = \boldsymbol{y}(\boldsymbol{z}) &= \begin{cases} \overset{+}{\boldsymbol{F}}\,\boldsymbol{z} & \text{for } \boldsymbol{z}\cdot\hat{\boldsymbol{n}} \le h_0, \\ \overset{-}{\boldsymbol{F}}\,\boldsymbol{z} + \boldsymbol{c} & \text{for } \boldsymbol{z}\cdot\hat{\boldsymbol{n}} \ge h_0, \end{cases}
\end{aligned} \tag{5.1}$$

In the reference configuration, $\mathcal{B}_0$, the images of the twin planes are described by $\boldsymbol{z}\cdot\hat{\boldsymbol{n}} = 0$, and $\boldsymbol{z}\cdot\hat{\boldsymbol{n}} = h_0$, $\hat{\boldsymbol{n}}$ being the associated unit normal. The material on each side of a twin plane is associated with a distinct "variant" of martensite. The notion of a variant was described more fully and illustrated in Section 2.2; for the present, it is sufficient to know

that when and $\overset{+}{\boldsymbol{F}}$ and $\overset{-}{\boldsymbol{F}}$ correspond to two different variants of the material, then $\overset{+}{\boldsymbol{F}} \neq \overset{-}{\boldsymbol{F}}$ but there are two rotations $\boldsymbol{R}_1$ and $\boldsymbol{R}_2$ such that $\overset{+}{\boldsymbol{F}} = \boldsymbol{R}_1 \overset{-}{\boldsymbol{F}} \boldsymbol{R}_2$. Note in particular that necessarily $\det \overset{+}{\boldsymbol{F}} = \det \overset{-}{\boldsymbol{F}}$.

Continuity of the deformations $\boldsymbol{x}(\boldsymbol{z})$ and $\boldsymbol{y}(\boldsymbol{z})$ across their respective twin planes require that

$$\begin{aligned} \overset{+}{\boldsymbol{F}} - \overset{-}{\boldsymbol{F}} &= \boldsymbol{a} \otimes \boldsymbol{n}, \\ \boldsymbol{c} &= h_0 \boldsymbol{a}, \end{aligned} \tag{5.2}$$

for some vector $\boldsymbol{a}$.

It is illustrative to write the condition in the equivalent form or alternatively,

$$\overset{+}{\boldsymbol{F}} = (\boldsymbol{1} + b\hat{\boldsymbol{a}} \otimes \boldsymbol{m}) \overset{-}{\boldsymbol{F}} \tag{5.3}$$

where

$$\begin{aligned} \hat{\boldsymbol{a}} &= \boldsymbol{a}/|\boldsymbol{a}|, \\ b &= |\boldsymbol{a}||(\overset{-}{\boldsymbol{F}})^{-\mathrm{T}} \boldsymbol{n}|. \end{aligned} \tag{5.4}$$

Since $\det \overset{+}{\boldsymbol{F}} = \det \overset{-}{\boldsymbol{F}}$ it follows from (5.3) that $\hat{\boldsymbol{a}} \cdot \hat{\boldsymbol{m}} = 0$. Thus, the deformation gradient $\overset{+}{\boldsymbol{F}}$ is seen to be equivalent to the deformation gradient $\overset{-}{\boldsymbol{F}}$ followed by a simple shear whose magnitude is b, shear direction $\hat{\boldsymbol{a}}$ and shear normal is $\hat{\boldsymbol{m}}$.

For our present purposes it is more convenient to use $\mathcal{B}_1$ as the reference configuration rather that $\mathcal{B}_0$. By (5.1) and (5.3), the deformation which takes $\mathcal{B}_1 \to \mathcal{B}_2$ (Figure 5-2) can be written as

$$\boldsymbol{y}(\boldsymbol{x}) = \begin{cases} \boldsymbol{x}, & \boldsymbol{x} \cdot \boldsymbol{m} \leq 0, \\ (\boldsymbol{1} + b\hat{\boldsymbol{a}} \otimes \boldsymbol{m})\boldsymbol{x}, & 0 \leq \boldsymbol{x} \cdot \boldsymbol{m} \leq h, \\ \boldsymbol{x} + \boldsymbol{c}, & \boldsymbol{x} \cdot \boldsymbol{m} \geq h. \end{cases} \tag{5.5}$$

Observe that in this deformation, the region below the plane $\boldsymbol{x} \cdot \hat{\boldsymbol{m}} = 0$ remains rigidly in place, the layer $0 \leq \boldsymbol{x} \cdot \hat{\boldsymbol{m}} \leq h$ undergoes simple shear, and the region above the plane $\boldsymbol{x} \cdot \hat{\boldsymbol{m}} = h$ undergoes rigid translation.

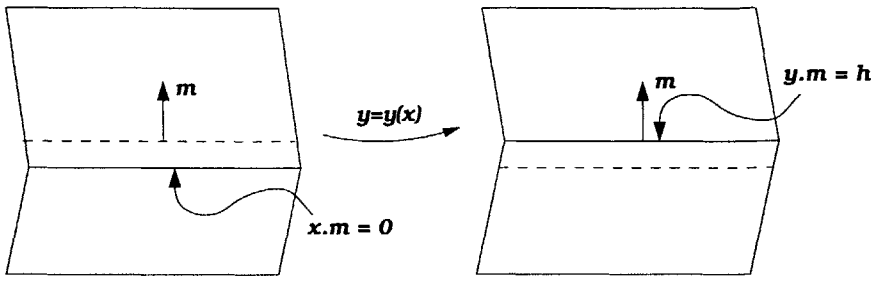

Figure 5-2: The deformation connecting configurations $\mathcal{B}_1$ and $\mathcal{B}_2$.

Now consider the *motion*

$$\boldsymbol{y}(\boldsymbol{x},t) = \begin{cases} \boldsymbol{x}, & \boldsymbol{x}\cdot\boldsymbol{m} \leq 0, \\ (1+\gamma(x,t)\hat{\boldsymbol{a}}\otimes\boldsymbol{m})\boldsymbol{x}, & 0 \leq \boldsymbol{x}\cdot\boldsymbol{m} \leq h, \\ \boldsymbol{x}+\boldsymbol{c}(x,t), & \boldsymbol{x}\cdot\boldsymbol{m} \geq h. \end{cases} \tag{5.6}$$

on some time interval $[t_1, t_2]$. Here we have set $x = \boldsymbol{x}\cdot\hat{\boldsymbol{a}}$, and by continuity $\boldsymbol{c}(x,t) = \gamma(x,t)h\hat{\boldsymbol{a}}$. We take $\gamma(x,t)$ to be a smooth function of x,t with $\gamma(x,t_1) = 0, \gamma(x,t_2) = b$. Thus the motion (5.6) commences from $\mathcal{B}_1$ at time t_1 and terminates at $\mathcal{B}_2$ at time t_2.

5.3 Discussion of motion (5.6).

Based on the form of the deformation (5.5), it seems natural to consider a motion of the form (5.6). Note, however, that even though the motion (5.6) involves a twin plane at $\boldsymbol{x}\cdot\hat{\boldsymbol{m}} = 0$ at time t_1 and a twin plane at $\boldsymbol{x}\cdot\hat{\boldsymbol{m}} = h$ at time t_2, it does not describe continuous propagation of a twin plane from the former location to the latter. Instead, at a typical instant $t \in (t_1, t_2)$ during the motion (5.6), the planes $\boldsymbol{x}\cdot\hat{\boldsymbol{m}} = 0$ and $\boldsymbol{x}\cdot\hat{\boldsymbol{m}} = h$ both carry discontinuities in the deformation gradient.

The motivation for considering the motion (5.6) comes from a lattice analog of the present problem. Figure 5-3 shows a lattice involving a twin plane $\mathcal{T}$. The plane of atoms immediately above this twin plane has been denoted by $\mathcal{P}$. If the atoms on and below $\mathcal{T}$ are held fixed, while those on and above $\mathcal{P}$ are rigidly translated to the right until the atoms on

$\mathcal{P}$ reach the dotted positions shown in the figure, one sees that $\mathcal{P}$ becomes the twin plane instead of $\mathcal{T}$. This describes the advance of the twin plane from $\mathcal{T}$ to $\mathcal{P}$. During this motion the only "bonds" (i.e. the lines connecting dots in the Figure 5-3) which change length are those in the layer between $\mathcal{T}$ and $\mathcal{P}$. This suggests a motion of the form (5.6) with $\gamma = \gamma(t)$ and h representing the distance between $\mathcal{T}$ and $\mathcal{P}$.

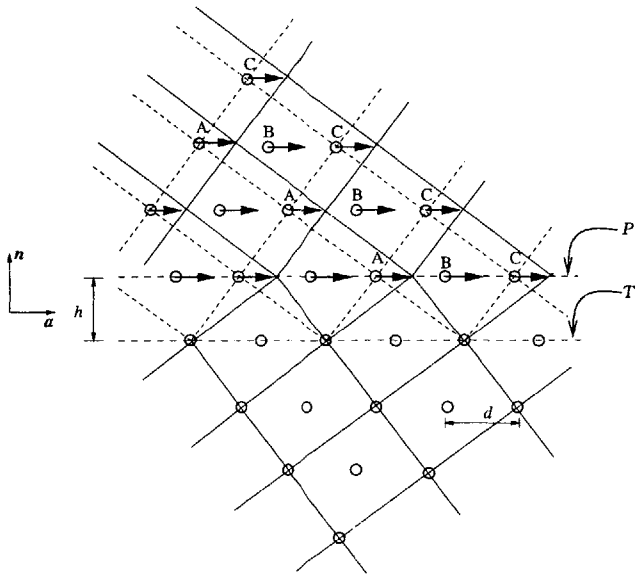

Figure 5-3: Schematic of compound twin in orthorhombic lattice undergoing shear. The solid lines connect atoms at initial positions and the dotted lines connect atoms at a generic instant $t \in (t_1, t_2)$.

By allowing γ in (5.6) to depend on x as well as t, we are retaining the ability to describe a motion in which, at the lattice scale, the atoms do not move in unison. For example, the atoms on $\mathcal{P}$ might prefer to move to their new locations sequentially, one at a time, and this would be described in the continuum theory by a traveling wave. The need to allow for spatially non-uniform shearing shearing can be motivated by examining how the energy varies during various motions. Even though the initial and final configurations, $\mathcal{B}_1$ and $\mathcal{B}_2$, both involve homogeneous strain fields within the layer, one can show that the energetically most favorable path which connects $\mathcal{B}_1$ to $\mathcal{B}_2$ does not involve homogeneous strains.

In order to demonstrate this we first calculate the total potential energy of the layer. Note from (5.6) that the deformation gradient tensor within the layer is given by

$$\boldsymbol{F}(x,t) = \tilde{\boldsymbol{F}}(\gamma(x,t), \epsilon(x,t)) \qquad \text{where} \quad \epsilon = \gamma_x \boldsymbol{x} \cdot \hat{\boldsymbol{m}},$$

where the matrix of components of $\tilde{\boldsymbol{F}}(\gamma(x,t),\epsilon(x,t))$ in the basis $\{\hat{\boldsymbol{a}},\hat{\boldsymbol{m}},\hat{\boldsymbol{a}}\times\hat{\boldsymbol{m}}\}$ is

$$[\tilde{\boldsymbol{F}}(\gamma,\epsilon)] = \begin{pmatrix} 1+\epsilon & \gamma & 0 \\ \gamma & 1 & 0 \\ 0 & 0 & 1 \end{pmatrix}. \tag{5.7}$$

Observe that in addition to a simple shear, the layer also undergoes a uniaxial strain ϵ in the shear direction $\hat{\boldsymbol{a}}$.

Let $\phi(\boldsymbol{F})$ denote the Helmholtz free-energy potential of the material. Then the restriction of the free-energy to deformations of the type we are considering is $\tilde{\Phi}(\gamma,\epsilon) = \phi(\tilde{\boldsymbol{F}}(\gamma,\epsilon))$. We have obtained a free–energy for homogeneous material in Chapter 3. We therefore assume the free–energy for this inhomogeneous deformation to take the separable form

$$\tilde{\Phi}(\gamma,\epsilon) = \phi(\tilde{\boldsymbol{F}}(\gamma,\epsilon)) = \Phi(\gamma) + \frac{1}{2}\mu_0\epsilon^2, \tag{5.8}$$

where $\Phi(\gamma)$ is the free–energy of the homogeneous material and $\frac{1}{2}\mu_0\epsilon^2$ is the contribution to the energy by the kink in the layer. The material constant μ_0 represents the elastic modulus associated with an infinitesimal uniaxial strain in the direction $\hat{\boldsymbol{a}}$ superposed on the reference configuration. Note that ϕ has local minima at $\boldsymbol{F} = \overset{+}{\boldsymbol{F}}$ and since these correspond to two variants of the material one also has $\phi(\overset{+}{\boldsymbol{F}}) = \phi(\overset{-}{\boldsymbol{F}})$. It follows that $\Phi(\gamma)$ has local minima at $\gamma = 0$ and b and that $\Phi(0) = \Phi(b)$.

Turning next to the potential energy of the layer, recall first that its lower surface $\boldsymbol{x}\cdot\hat{\boldsymbol{m}} = h$. The potential energy PE of the strip can be readily shown to be given by

$$PE = h\int_{-L/2}^{L/2}\{\Phi(\gamma) - \sigma\gamma + \frac{1}{2}\lambda_1\gamma_x^2\}dx \qquad \text{where} \qquad \lambda_1 = \frac{1}{3}\mu_0 h^2. \tag{5.9}$$

Observe that the strain-gradient term γ_x^2 here arises automatically due to the inhomogeneous nature of the deformation.

We can now demonstrate why shear strain γ has been allowed to depend on x. Consider the motion (5.6) with

$$\gamma(x,t) = \frac{\gamma_2(t)e^{-\beta(x-x_0(t))/L} + \gamma_1(t)e^{-\beta(x-x_0(t))/L}}{e^{-\beta(x-x_0(t))/L} + e^{-\beta(x-x_0(t))/L}}, \quad \beta > 0. \tag{5.10}$$

In the special case $\gamma_1(t) = \gamma_2(t) = \gamma(t)$ this describes a homogeneous shearing motion. In general, for sufficiently large values of $\beta >> 0$, (5.6) implies that $\gamma(x,t) \approx \gamma_1(t)$ for $-L/2 < x < x_0(t)$ and $\gamma(x,t) \approx \gamma_2(t)$ for $x_0(t) < x < L/2$. Thus in general (5.6) describes an evolving strain field which, at each instant t, is more-or-less piecewise constant (with respect to x).

First consider the choice $x_0(t) = 0$ and suppose $\gamma_1(t)$ and $\gamma_2(t)$ each increase monotonically from 0 to b. Evaluating the potential energy (5.6) at the motion (5.6) leads to an expression of the form $PE(t) = PE(\gamma_1(t), \gamma_2(t))$. Figure 5-4 shows a contour map of $PE(\gamma_1, \gamma_2)$. Observe the energy-wells at $(0,0)$ and (b,b) correspond to the two martensite variants. The figure also shows four paths $(\gamma_1(t), \gamma_2(t))$ connecting $(0,0)$ and (b,b) where the paths have been parameterized by t. Note that $\gamma_1(t) = \gamma_2(t)$ along path-1 and so this corresponds to a motion in which the strip deforms homogeneously. On the other hand, along path-4 observe that $\gamma_1(t)$ increases first while $\gamma_2(t)$ remains constant and subsequently $\gamma_2(t)$ increases at constant $\gamma_1(t)$ - this describes a motion in which the left half of the strip deforms first and the right half deforms thereafter. Figure 5-5 shows how the potential barrier $PE(t)$ varies with t along each of these paths. Observe that the path energy barrier associated with path-1 is not the energetically favored path. The results depend critically on the values chosen for the various parameters (for this calculation we have chosen the material data for CuAlNi); for a different choice of parameter values path-1 may, of course, be the energetically favorable path.

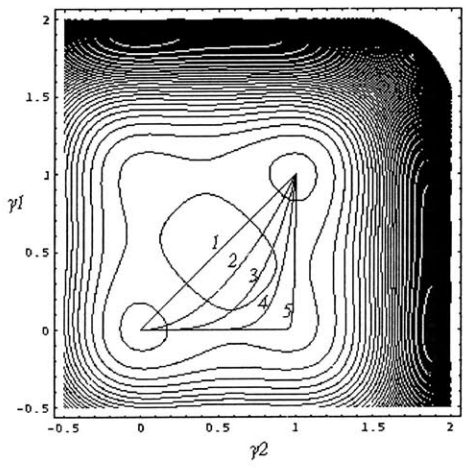

Figure 5-4: Contours of the potential energy for $\sigma = 0$ and γ/b given by (5.10).

As as a second special case of (5.6), consider the choice $\gamma_1(t) = 0, \gamma_2(t) = b$ and let

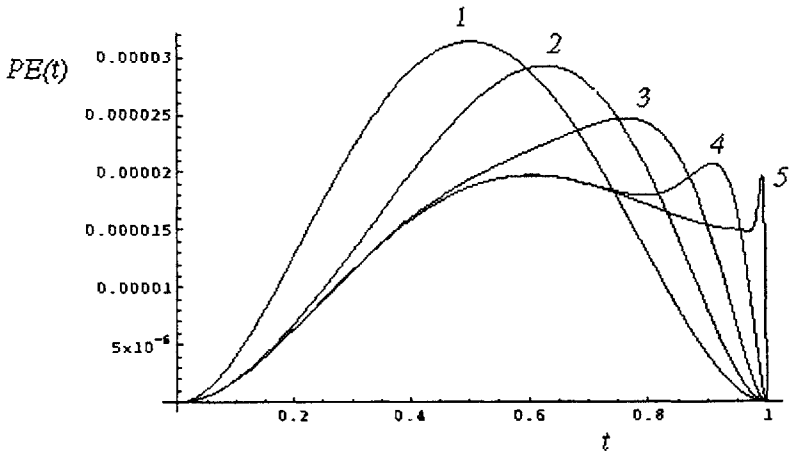

Figure 5-5: Slices of the energy along the four paths indicated in Figure 5-4.

$x_0(t)$ increase monotonically from $-L/2$ to $L/2$. For a sufficiently large value of $\beta >> 0$, (5.6) implies that $\gamma(x,t) \approx 0$ for $-L/2 < x < x_0(t)$; these two segments of the strip are therefore associated with the two martensitic variants and there is a narrow transition zone at $x_0(t)$. As $x_0(t)$ increases from $-L/2$ to $L/2$ the strain field (5.10) now describes a smooth traveling wave transforms the material from the variant $\gamma = 0$ to the variant $\gamma = b$. Figure 5-6 shows how the potential $PE(t)$ varies with t during such a motion. Observe that the energy remains essentially constant except from short transient at the beginning and the end. This is due to the fact that most of the energy is contained in the narrow transition zone is contained within the strip. Note that the energy barrier associated with this motion, is even smaller than that associated with path-4 considered previously.

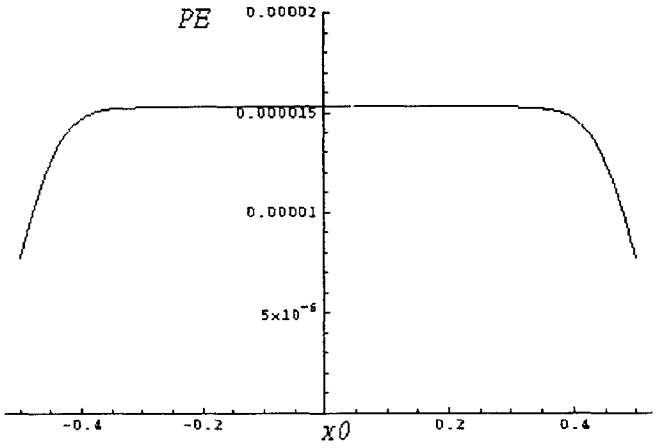

Figure 5-6: Energy of the layer as a function of the position of the kink x_0

While we have not found the energetically optimum path we have demonstrated that it does not correspond to a uniform shear. Of the paths we have examined, the traveling wave is the energetically most favorable one.

5.4 Equation of motion and kinetic law

5.4.1 Kinetic law from equation of motion

In attempting to model the propagation of the twin boundary from $\boldsymbol{x}\hat{\boldsymbol{m}} = 0$ and $\boldsymbol{x}\hat{\boldsymbol{m}} = h$ we have now been led us to study the progressive lateral transformation of the layer $0 < \boldsymbol{x}\hat{\boldsymbol{m}} < h$ from one variant to the other. The kinetic energy, KE, associated with the motion (5.6) can be readily found to be

$$KE = h\int_{-L/2}^{L/2} \frac{1}{2} m\gamma_t^2 dx \qquad \text{where} \qquad m = \frac{1}{3}\rho h^2. \tag{5.11}$$

It follows from (5.9) and (5.11), for example using Hamilton's principle, that the associated equation of motion is

$$m\gamma_{tt} = -\Phi'(\gamma) + \sigma + \lambda_1\gamma_{xx} \tag{5.12}$$

Recall, as described below (5.8), that the two well energy $\Phi(\gamma)$ has local minima of equal height at $\gamma = 0, b$: $\Phi(0) = \Phi(b), \Phi'(0) = \Phi'(b) = 0, \Phi''(0) > 0, \Phi''(b) > 0$. Furthermore, we shall assume that Φ is convex on two semi-infinite intervals which contain $\gamma = 0$ and $\gamma = b$ respectively, and that it is concave on the intermediate interval.

Let $\gamma(x,t) = \overset{+}{\gamma}$ and $\gamma(x,t) = \bar{\gamma}$ denote the equilibrium solutions of (5.12) with the properties

$$\sigma = \Phi'(\overset{+}{\gamma}) = \Phi'(\bar{\gamma}), \qquad \Phi''(\overset{+}{\gamma}) > 0, \quad \Phi''(\bar{\gamma}) > 0, \quad \overset{+}{\gamma} > \bar{\gamma}, \tag{5.13}$$

see Figure 5-7; they correspond to the two (stressed) variants of the material. We now seek a steady solution of (5.12) which describes the transformation from $\overset{+}{\gamma}$ to $\bar{\gamma}$, i.e. we seek a traveling wave solution of the form

$$\gamma(x,t) = \hat{\gamma}(\xi), \qquad \xi = x - vt, \tag{5.14}$$

$$\gamma(\xi) \to \bar{\gamma} \text{ as } \xi \to +\infty, \qquad \gamma(\xi) \to \overset{+}{\gamma} \text{ as } \xi \to -\infty. \tag{5.15}$$

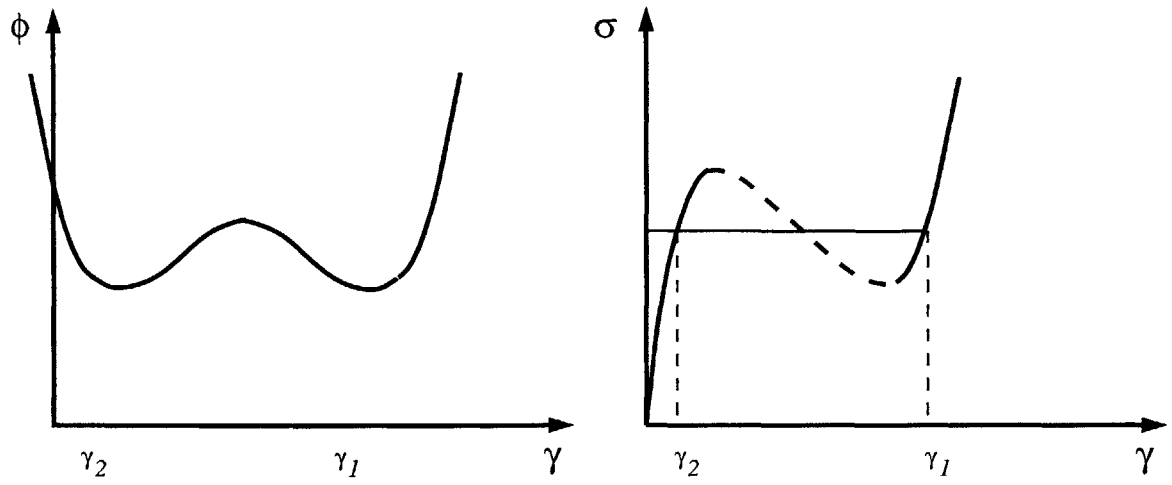

Figure 5-7: Equilibrium solutions of (5.12)

Substituting (5.14) into (5.12) leads to the ordinary differential equation

$$(\lambda_1 - mv^2)\gamma''(\xi) - \Phi'(\gamma(\xi)) + \sigma = 0, \qquad -\infty < \xi < +\infty, \tag{5.16}$$

and we seek a solution $\gamma = \gamma(\xi)$ of (5.16) subject to (5.15). Note that (5.16) can be viewed as the equation governing the dissipationless motion of mass $(\lambda_1 - mv^2) > 0$ (or $(mv^2 - \lambda_1) > 0$) in a potential field $-\Phi(\gamma) + \sigma\gamma$ (or $\Phi(\gamma) - \sigma\gamma$ respectively) where Φ has the properties listed in (5.13). Note that in both cases, $(\lambda_1 - mv^2) > 0$ and $(mv^2 - \lambda_1) > 0$, the corresponding potential energy has local extrema at $\gamma = \overset{\pm}{\gamma}$. By (5.15), the motion of interest is one in which the particle is released from rest at "time" $\xi = -\infty$ from $\gamma = \overset{+}{\gamma}$ and is to reach $\gamma = \bar{\gamma}$ at time $\xi = +\infty$ with zero speed. This problem can be solved using the phase plane method or by direct solution as outlined in Section 4.4. We conclude that according to the existing continuum model the propagation law is $\sigma = 0$ and the propagation speed is limited by $v < \sqrt{\lambda_1/m}$.

5.4.2 Kinetic law from an improved model

The differential equation (5.12) which formed the basis for the preceding model is effectively the averaged equation of motion corresponding to the kinematic ansatz (5.6). It is not equivalent to the general three dimensional equations of motion of continuum mechanics. In order to improve this model one approach would be to generalize the assumed form of the motion (5.6) and then carry out the analysis similar to the above. However, since the

propagation law that we are seeking is the vehicle by which the continuum theory inherits dynamical information from the lattice theory, it seems more natural to adopt an approach which considers the lattice, even if in some rough way.

Accordingly, we return to the lattice version of the problem as depicted in Figure 5-3. Suppose that the atoms on the plane $\mathcal{P}$ are labeled by the indices $i = \ldots, -1, 0, 1, \ldots$, and that the interatomic forces between atoms in this plane are approximated, to leading order, by linear springs. Then, if $w_n(t)$ denotes the horizontal displacement of the *nth* atom in the shearing direction $\hat{\boldsymbol{a}}$, the *force on the nth atom* due to its neighboring atoms on $\mathcal{P}$ is

$$k[w_{n+1}(t) - w_n(t)] + k[w_{n-1}(t) - w_n(t)]. \tag{5.17}$$

Let $w(x,t)$ be a smooth interpolating function which is defined for all x and t and is such that $w_n(t) = w(nd,t)$; here d is the distance between the atoms on plane $\mathcal{P}$. We can now express the force on the *nth* atom as $k[w(nd+d,t) - w(nd,t)] + k[w(nd-d,t) - w(nd,t)]$. By formally expanding this in a Taylor series about $x = nd$ we find that (5.17) can be approximated as

$$\kappa_1 w_{xx}(nd,t) + \kappa_2 w_{xxxx}(nd,t) + \ldots \tag{5.18}$$

where

$$\kappa_1 = kd^2 > 0, \qquad \kappa_2 = \frac{1}{12} kd^4 > 0. \tag{5.19}$$

This has been called the *quasi-continuum approximation* of the interatomic force by Pouget [64, 65].

Returning to the continuum theory, recall from (5.8) that the term $\lambda_1 \gamma_{xx}$ in (5.12) arose due to the uniaxial deformation of strip in the shearing direction, thus suggesting that we can identify this term being related to the force on an atom considered above. This in turn suggests that the natural generalization of the equation of motion (5.12) is

$$m\gamma_{tt} = -\Phi'(\gamma) + \sigma + \lambda_1 \gamma_{xx} + \lambda_2 xxxx, \tag{5.20}$$

where by $(5.9)_2$ and (5.19)

$$\lambda_1 = \frac{1}{3}\mu_0 h^2 > 0, \quad \lambda_2 = \frac{\kappa_2}{\kappa_1}\lambda_1 > 0; \tag{5.21}$$

the term $-\Phi'(\gamma)$ in (5.20) may be thought of as representing the force on an atom due to the atoms *not* on the plane $\mathcal{T}$. Since it may appear that we have simply added a higher-order strain-gradient term to the original equation (5.12), it is worth pointing out that had this been the case, we would have used the opposite sign in front of λ_2 (as for example in the beam equation). The potential energy corresponding to (5.20) (other than for the term associated with σ) is

$$PE = h \int_{L/2}^{L/2} [\Phi(\gamma) + \frac{1}{2}\lambda_1 \gamma_x^2 - \frac{1}{2}\lambda_2 \gamma_{xx}^2] dx \tag{5.22}$$

and this is *not* positive definite. The usual strain-gradient formalism we would have started from (5.22) with the opposite sign in front of λ_2. The non-positive definiteness of (5.22) can potentially have important implications regarding the stability of the solution that we will find. Finally, it is worth noting that one can readily derive, from (5.20), the following balance between the rate of work and energy:

$$\int_{L/2}^{L/2} \sigma \gamma_t h dx = \frac{d}{dt}[PE + KE] \tag{5.23}$$

where the potential energy and kinetic energy are given by (5.22) and (5.11) respectively.

5.5 Evaluating the kinetic law for martensitic twins in CuAlNi.

We now use the generalized equation of motion (5.20) to determine the kinetic relation for the two types of twins with rational twin boundaries, viz. compound twins and type-I twins in the shape memory alloy CuAlNi. The micromechanical model proposed in the previous sections is not applicable to type II twins since they have irrational boundaries and are thought to have a quasi–continuous distributions of coherency dislocations. Zhang et al [88] remark that type II twin boundaries are gradually and randomly curved. We therefore perform our calculations only for the compound and type I twin boundaries.

In order to examine the kinetics of the various twin interfaces in this material, we set $\overset{-}{\boldsymbol{F}} = \boldsymbol{U}_J$ and $\overset{+}{\boldsymbol{F}} = \boldsymbol{Q}\boldsymbol{U}_I$, $I \neq J$, in the calculations of the Section 5.2, with $\boldsymbol{Q}$ being a suitable rotation. The twinning equation (2.7), now reads $\boldsymbol{Q}\boldsymbol{U}_J - \boldsymbol{U}_I = \boldsymbol{a} \otimes \hat{\boldsymbol{n}}$. For each choice of I and J, $I \neq J$, this has two solutions $\{\boldsymbol{a}, \hat{\boldsymbol{n}}, \boldsymbol{Q}\}$ which can be determined using the formulae given in [11]. The value of the corresponding twinning shear b can then be calculated from:

	Compound twins	Type I twins
$\{\hat{\boldsymbol{a}}\}$	$\{0.0186, 0.9998, 0\}$	$\{0.0186, 0.9998, 0\}$
$\{\hat{\boldsymbol{n}}\}$	$\{-1, 0, 0\}$	$\{0, 1/\sqrt{2}, -1/\sqrt{2}\}$
$\{\hat{\boldsymbol{m}}\}$	$\{-0.9998, 0.0186, 0\}$	$\{-0.0123, 0.6609, -0.7504\}$
b	0.0745	0.261

Table 5.1: Compound and Type I solutions of the twinning equation in the cubic austenite basis $\{\boldsymbol{c}_1, \boldsymbol{c}_2, \boldsymbol{c}_3\}$.

	Compound twins	Type I twins
h/a_0	1.0420	0.6887
d/a_0	1.0427	1.3641
h/d	0.9993	0.5049

Table 5.2: Height of the layer and interatomic spacing from lattice calculation.

$b = |\boldsymbol{a}||\boldsymbol{U}_I^{-1}\hat{\boldsymbol{n}}|$.

In view of symmetry, there are only two essential cases to consider: twins associated with $\{\boldsymbol{U}_1, \boldsymbol{U}_2\}$ and those associated with $\{\boldsymbol{U}_1, \boldsymbol{U}_3\}$. Observe from (2.1) that $\boldsymbol{U}_1$ and $\boldsymbol{U}_2$ are subjected to the same stretch in the $\boldsymbol{c}_3$ direction; thus the twinning motion (5.6) involving these two stretches involves no distortion in the $\boldsymbol{c}_3$ direction. These two variants are therefore "easy" to combine in a compatible manner and the deformation is two dimensional. In contrast, a twin which connects $\boldsymbol{U}_1$ to $\boldsymbol{U}_3$ involves fully three-dimensional kinematics. The solutions of $\boldsymbol{Q}\boldsymbol{U}_2 - \boldsymbol{U}_1 = \boldsymbol{a} \otimes \hat{\boldsymbol{n}}$ are said to describe compound twins: for such a twin, the twin plane (defined by $\hat{\boldsymbol{n}}$) is a plane of atoms and the twinning direction (defined by $\hat{\boldsymbol{a}}$) coincides with a row of atoms. On the other hand the two solutions of $\boldsymbol{Q}\boldsymbol{U}_3 - \boldsymbol{U}_1 = \boldsymbol{a} \otimes \hat{\boldsymbol{n}}$ describe a *type-I twin* and a *type-II twin*: for a type-I twin, $\hat{\boldsymbol{n}}$ is the normal to a plane of atoms but $\hat{\boldsymbol{a}}$ does not coincide with a row of atoms; for a type-II twin, the plane normal to $\hat{\boldsymbol{n}}$ is not a plane of atoms but $\hat{\boldsymbol{a}}$ does coincide with a row of atoms.

Explicit formulae for the solutions of the twinning equation have been given by [11]. Specializing their result to $\boldsymbol{Q}\boldsymbol{U}_J - \boldsymbol{U}_1 = \boldsymbol{a} \otimes \hat{\boldsymbol{n}}$, $J = 2, 3$ and making use of (2.9) and (2.10) with lattice parameters given by (2.2) leads to the solution of the twinning equation listed in Table 5.1.

The height of the layer h and the interatomic spacing along the twin boundary can be calculated from the lattice parameters. They are listed in Table 5.2. The moduli of the orthorhombic phase are obtained from Yasunaga et al [85, 86] and are listed in Table 3.2.

Since the equation (5.20) is obtained from a lattice calculation, we calculate the parame-

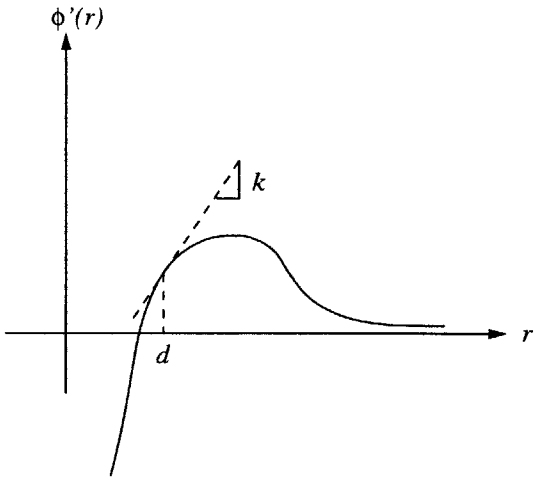

Figure 5-8: k from the slope of the Lenard–Jones force curve at an interatomic spacing d.

ter k and the function $\Phi'(\gamma)$ from an atomistic calculation using a Lenard–Jones interatomic potential. The details of the calculation are given in the next chapter. The spring constant k is obtained as the slope of the interatomic force curve at the interatomic lattice spacing d along the twin boundary as shown in Figure 5-8.

The equation (5.20) is then solved for both compound and type I twins using a finite difference method with an initial conditions given by

$$\begin{aligned} \gamma(x,0) &= (\overset{+}{\gamma} - \bar{\gamma})H(x - x_0) + \bar{\gamma}, \\ \gamma_t(x,0) &= 0, \end{aligned} \tag{5.24}$$

where $H(x)$ is the Heaviside function and $x_0 \in (0, L)$.

The boundary conditions are fixed at the equilibrium solution

$$\begin{aligned} \gamma(0,t) &= \bar{\gamma}, \qquad \gamma(L,t) = \overset{+}{\gamma} \\ \gamma_x(0,t) &= 0, \qquad \gamma_x(L,t) = 0. \end{aligned} \tag{5.25}$$

The equation is solved at particular values of σ and the kink velocity is tracked. The steady state kink velocity is obtained for each σ. A plot of σ vs the steady state kink velocity is shown in Figure 5-9 for compound and type I twins. Figures 5-10 and 5-11 show the displacement of the layer at two different instants of time. Note that the atoms behind the kink are in vibration but the atoms ahead of the kink are stationary. This is the same

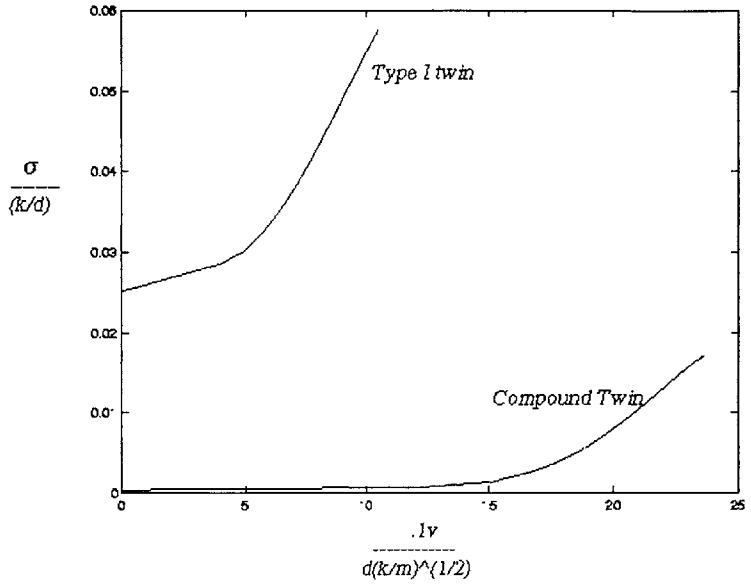

Figure 5-9: Kinetic relation for compound and type I twins relating $\{\boldsymbol{U}_1, \boldsymbol{U}_2\}$ and $\{\boldsymbol{U}_1, \boldsymbol{U}_3\}$ respectively.

behavior observed in the analytic solution in Chaper 4.

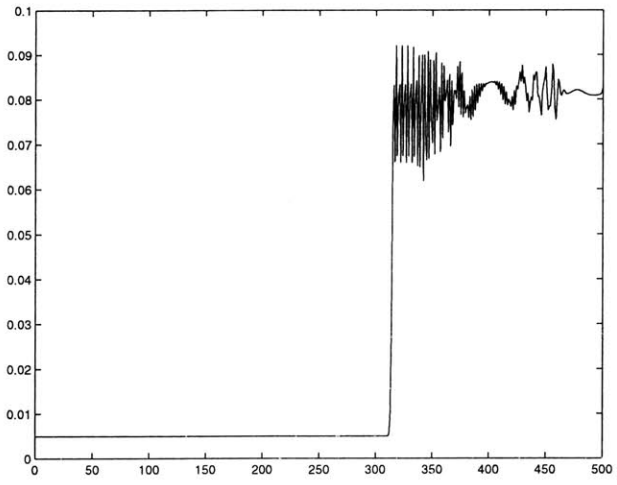

Figure 5-10: Displacement of atoms on the twin boundary at a time $t = t_1$.

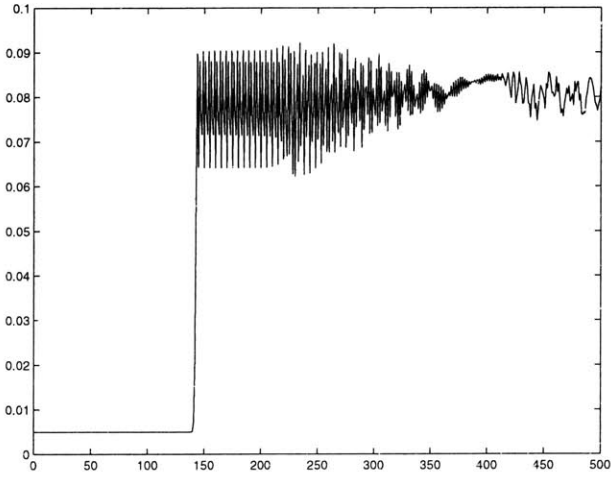

Figure 5-11: Displacement of atoms on the twin boundary at a time $t = t_2 > t_1$.

Chapter 6

Comparison of polynomial free energy with molecular statics

6.1 Introduction

The polynomial free energy obtained for cubic-orthorhombic crystals in Chapter 3 has been fitted to: (1) the symmetry of the cubic crystal, (2) location of the extrema of the function (the wells), (3) the curvature of the function at the extrema, and, (4) the relative heights of the wells. The barrier between the energy wells has not been fitted to experimental data. In fact, no experimental data of the barrier height is available since the material is unstable in that region. We therefore would like to make an independent calculation of the barrier height and compare with that obtained from the polynomial free energy.

We do this calculation in the particular case of simple shear of a martensite variant. We perform a molecular statics calculation of the energy barrier to shear of a martensite variant in a particular direction and plane of atoms determined through crystallography theory. Each martensite variant can be transformed to another through a simple shear as described in Chapter 5. We use a Lenard-Jones pair potential for the atoms and fit the Lenard-Jones parameters to the elastic moduli and the lattice parameter of CuAlNi.

This calculation may conceivably be performed using a first principles quantum mechanical calculation for greater reliability of results. Such a calculation has been performed by Paxton [57] for the case of twinning in Ni-Al. For simplicity, we have restricted our comparison to a calculation using a Lenard-Jones pair potentials.

In Section 6.2 we calculate the energy for a shear deformation that transforms variant 1 of martensite to variant 2. These lattices are compound twins related. We also calculate the energy for the shear deformations that take variant 1 into variant 3. There are two such shear deformations depending on whether the lattices are type I or type II related to each other. In Section 6.3, we describe the molecular statics calculation and calculate the energy associated with deformations between variants 1 and 2 and variants 1 and 3. Finally, we compare the energy of twinning shear deformation calculated from the lattice based pair potentials and the polynomial free energy.

6.2 Specialization of polynomial free energy

In the last chapter, the continuum description of twinning involved a particular motion of a layer between the two variants. The motion was a time dependent homogeneous shear deformation on a particular plane with normal $\hat{\boldsymbol{m}}$ and in a particular shear direction $\hat{\boldsymbol{a}}$ given by equation (5.6). We can calculate the potential energy of the layer as it undergoes this special deformation and the resulting energy will be a slice of the three dimensional free energy. In particular, we calculate the potential energy of the layer for a deformation that takes variant 1 to variant 2 (compound twin solution of the twinning equation) and the deformations that transform variant 1 to variant 3 (type I and type II solutions of the twinning equation). The variant numbering follows (2.1).

From (5.6), the deformation gradient for the layer is

$$\boldsymbol{F}(\gamma) = \boldsymbol{U}_1 + \gamma \hat{\boldsymbol{a}} \otimes \boldsymbol{m} \tag{6.1}$$

where $\boldsymbol{U}_1$ is the stretch tensor associated with variant 1.

The Lagrangian strain tensor is then

$$\boldsymbol{E}(\gamma) = \frac{1}{2}\left(\boldsymbol{F}(\gamma)^T \boldsymbol{F}(\gamma) - \mathbf{1}\right). \tag{6.2}$$

Using this in the polynomial free energy (3.14) we obtain the free energy of the layer

$$\Phi(\gamma) = \hat{\Psi}(\boldsymbol{E}(\gamma)) \tag{6.3}$$

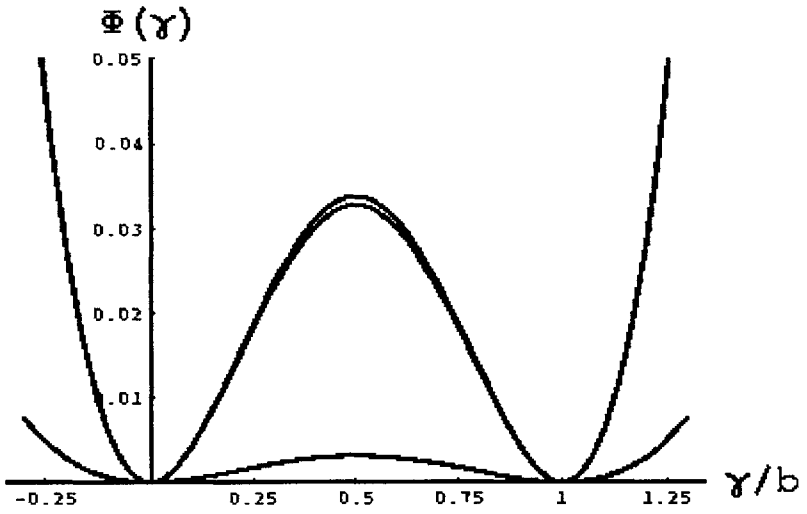

Figure 6-1: The energy $\Phi(\gamma)$ from the polynomial free energy for compound, type I and type II twins.

The plots for compound, type I and type II twins are shown in Figure 6-1.

6.3 Molecular statics calculation

In the previous section we calculated the energy of a layer as it undergoes a shear deformation that takes it from one martensite variant to another. But, as was pointed out in Section 4.3, twin boundaries are sharp even up to atomic level. Since we would like to use this energy in a twin boundary model, we must calculate the energy from a molecular statics calculation. For convenience, we prefer to use cubic austenite as the reference configuration even though the austenite phase is not involved in any of these calculations.

Consider a crystal lattice with a twin plane and which has piecewise constant deformation gradients such that they are rank-one connected by the twinning equation (2.7). Let $\boldsymbol{r}_i^c$ denote the position vector of the atoms of this body in the reference configuration. The position vectors of the atoms in the current configuration are $\boldsymbol{r}_i^o = \boldsymbol{U}_1 \boldsymbol{r}_i^c$ for $\boldsymbol{r}_i^c \cdot \hat{\boldsymbol{m}} \leq 0$ and $\boldsymbol{r}_i^o = \boldsymbol{U}_2 \boldsymbol{r}_i^c$ for $\boldsymbol{r}_i^c \cdot \hat{\boldsymbol{m}} \geq 0$.

Now, assume that the atoms on and ahead of the interface are displaced in tandem by an amount u and in the direction of the shear vector $\boldsymbol{a}$ (see Figure 5-3). Then

$$\boldsymbol{u} = u \frac{\boldsymbol{a}}{|\boldsymbol{a}|} \tag{6.4}$$

is the displacement of the atoms ahead of the twin plane.

The current position vectors of the atoms ahead of the interface are

$$\boldsymbol{r}_i = \boldsymbol{r}_i^o - \boldsymbol{u}. \tag{6.5}$$

The energy of interaction of an atom on the twin plane $\mathcal{P}$ is given by

$$W(u) = \sum \phi(|\boldsymbol{r}_i|), \tag{6.6}$$

where the sum is over all the neighboring atoms and $\phi(\rho)$ is a pair potential which depends only on the interatomic distance ρ. Since the twin boundary is in equilibrium at zero stress we require $W(u)$ to have minima at $u = 0$ and $u = b$. From symmetry, when one of the minima is enforced the other is automatic.

For the pair potential we choose the Lenard–Jones form

$$\phi(\rho) = \frac{A}{\rho^{12}} - \frac{B}{\rho^6}. \tag{6.7}$$

We fit the two Lenard–Jones parameters A and B to the minimum condition on $W(u)$ and the elastic modulus of the CuAlNi alloy in the shear direction $\boldsymbol{a}$ and on the twin plane with normal $\hat{\boldsymbol{m}}$.

Note that the assumption of pair potential energy of interaction is weak on several counts. The Lenard–Jones interatomic energy does not account for the different atoms present in the alloy. Also, the Lenard–Jones potential is not considered suitable for describing metallic bonds. We therefore use the Lenard–Jones function only in this specific deformation for which it has been fitted and not for more general calculations.

The energy during the atomic displacement converting variant 1 to variant 2 and variant 3 is calculated and displayed in Figure 6-2.

We can see that the lattice energy and the polynomial free energy compare very well for the twinning shear deformation. Figures 6-3, 6-4, and 6-5 compare respectively the compound, type I and type II twin energies.

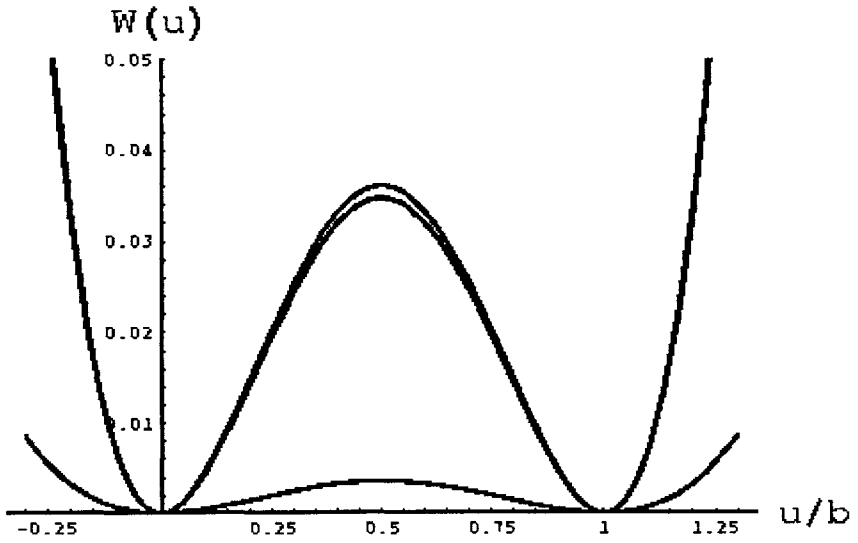

Figure 6-2: The energy $W(u)$ from lattice calculation for compound, type I and type II twins.

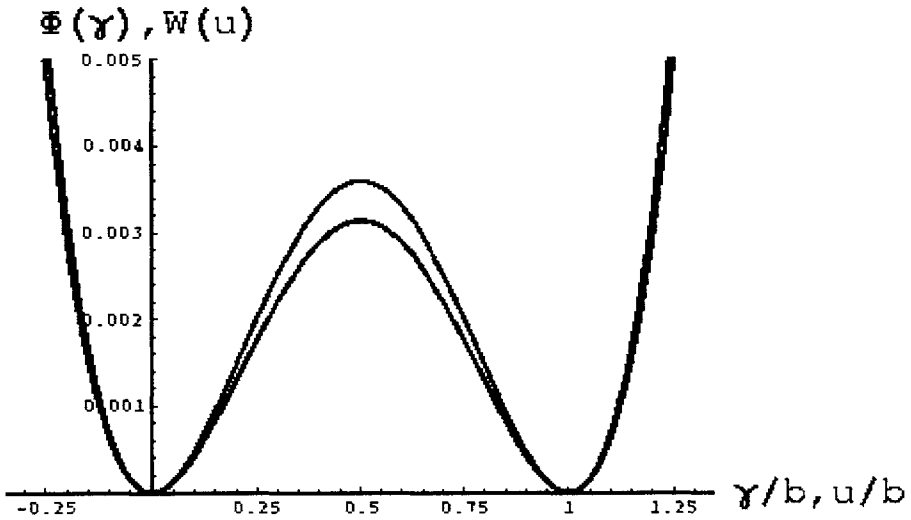

Figure 6-3: The polynomial free energy (a) $\Phi(\gamma)$ and lattice energy (b) $W(u)$ for compound twins.

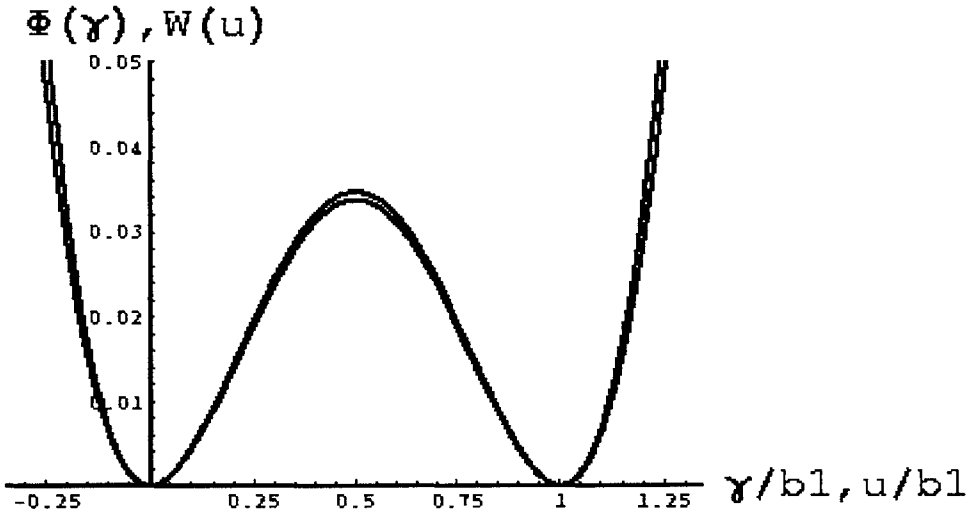

Figure 6-4: The polynomial free energy (a) $\Phi(\gamma)$ and lattice energy (b) $W(u)$ for type I twins.

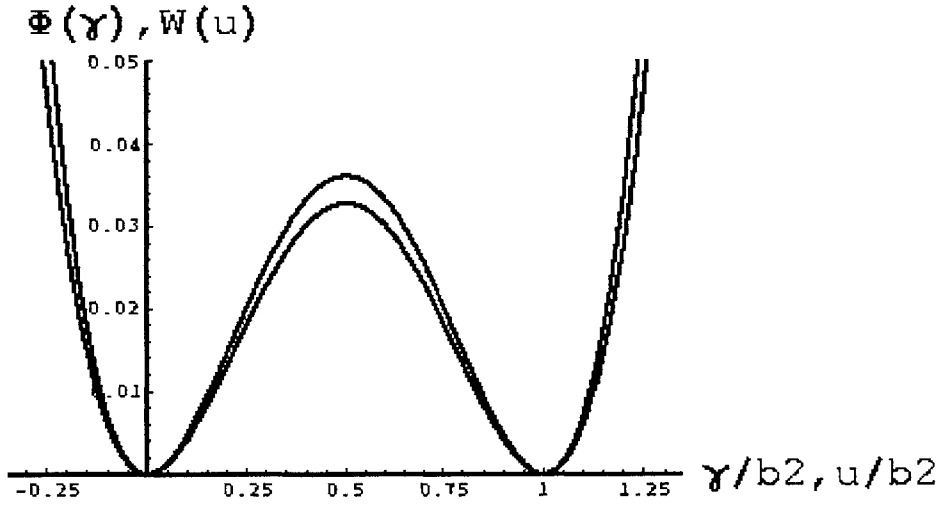

Figure 6-5: The polynomial free energy (a) $\Phi(\gamma)$ and lattice energy (b) $W(u)$ for type II twins.

Chapter 7

Kinetics of phase boundaries

7.1 Introduction

The shape memory effect, as described in Chapter 1 is caused in part by the motion of phase boundaries in solids. The kinetics of these phase boundaries control the rate of transformation of the alloys. Compatible interfaces cannot exist between cubic austenite and orthorhombic martensite for the lattice parameters of Cu-Al-Ni (see Section 2.2). There are several possible types of phase boundaries between austenite and twinned martensite depending on the geometry of the twins as well as the orientation of the interface. The mobility of a phase boundary is dependent on the microstructure of the twins and, in particular, the phase boundary orientation. Shield [69] has examined the mobility of these interfaces from the point of view of the resolved shear stress on the interfaces. Our focus is on the effect of the microstructure on the mobility. For this we study a model of phase boundary motion that is analogous to the twin boundary motion studied in Chapter 5. We calculate the energy for deformations which connect austenite to various types of twinned martensite using the energy developed in Chapter 3. This introduces an orientation effect into the model. Also, another feature of the model is the presence of a transversely propagating ledge on the interface. Ledges have been widely observed in experiments as a mechanism by which phase boundaries propagate (e.g. Porter and Easterling [63], Hirth et al [36]). We have not come across any experimental literature which reports observations of ledges in Cu-Al-Ni interfaces. Nevertheless, we believe that ledges would provide an energetically more favorable means of phase boundary propagation and hence we include them in our model. Our model is two dimensional in scope but is reduced to one dimension by the

introduction of the ledges.

In Section 7.2 we reprise the crystallography and continuum theory of the phase boundary. In Section 7.3 we present the physical model of a propagating phase boundary and in Section 7.4 we present the calculation and the results. In Section 7.5 we present the calculated macroscopic response of a uniaxial specimen based on the mathematical model proposed in this chapter.

7.2 Description of phase boundaries

As described in Section 2.2 the austenite phase in Cu-Al-Ni cannot form a coherent interface with a single variant of martensite. However, the austenite phase does form interfaces with finely twinned martensite. In such cases, the interface is only coherent in an average sense. If austenite is taken as the reference configuration and the martensite variants have deformation gradients $\boldsymbol{F}_I$ and $\boldsymbol{F}_J$ the compatibility of the interface may be expressed mathematically by the rank-one connection

$$(\lambda \boldsymbol{F}_I + (1-\lambda)\boldsymbol{F}_J) - \mathbf{1} = \boldsymbol{s} \otimes \boldsymbol{\nu}, \tag{7.1}$$

where $\boldsymbol{\nu}$ is the normal to the interface and $\lambda \in (0,1)$ is a scalar. Note that the deformation gradients of the martensite variants are still related through the twinning equation

$$\boldsymbol{F}_I - \boldsymbol{F}_J = \boldsymbol{a} \otimes \boldsymbol{n}. \tag{7.2}$$

Thus, for compatibility, the deformation gradient of martensite has to be $\lambda \boldsymbol{F}_I + (1-\lambda)\boldsymbol{F}_J$ which is not on the energy wells. Away from the interfaces the material is in the form of twinned martensite so the deformation gradient alternates between $\boldsymbol{F}_I$ and $\boldsymbol{F}_J$ which minimizes the energy and near the interface the material takes a deformation gradient $\lambda \boldsymbol{F}_I + (1-\lambda)\boldsymbol{F}_J$ in a transition layer (Figure 7-1). The twins end in needle-like shapes or cusps (see Tsai [87]) in the transition layer. A detailed examination of sequences of deformations which minimize the energy as well as provide compatibility may be found in Ball and James [11].

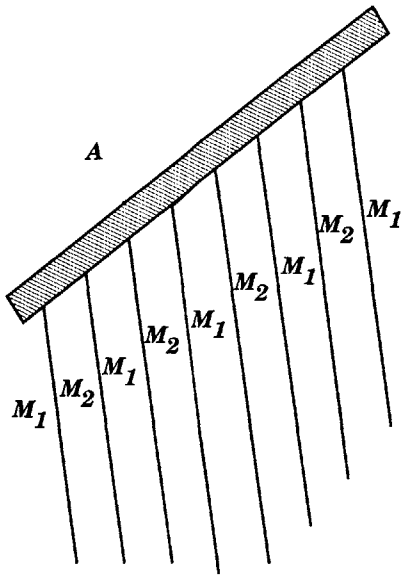

Figure 7-1: A body composed austenite and twinned martensite separated by a transition region.

7.3 Micromechanical model

We would like to consider the propagation of such a phase boundary under applied loading and for the purposes of our model we assume that the transition layer is absent and that the twins end on the interface as shown in Figure 7-2. Thus in our model compatibility suffers. However, if the thickness of twins is made small then the interface can be considered to be compatible on the average. Further, following an analogy to twin boundary propagation we assume that the phase boundary propagation is achieved by the localized deformation of a thin layer of material. As this layer undergoes a suitable motion from a specified initial position to a final position, the interface may be considered to have propagated to a new location. For the purpose of our model we assume that each block of austenite of thickness w ahead of the interface transforms to a block of twinned martensite of thickness λw of variant I and $(1-\lambda)w$ of variant J as depicted in figure 7-2. Thus the region under consideration is the smallest which, when subjected to an appropriate deformation, would transform to a pair of variants of martensite in accordance with the bulk martensite structure.

Consider the intermediate layer to be subdivided into a row of regions of thickness w. Each of these regions is capable of being deformed into a pair of twins. We number these regions $0, \pm 1, \pm 2, \pm 3, ...$ starting from an arbitrary region and assigning the positive numbers to the regions on the right and negative numbers to the regions on the left. The

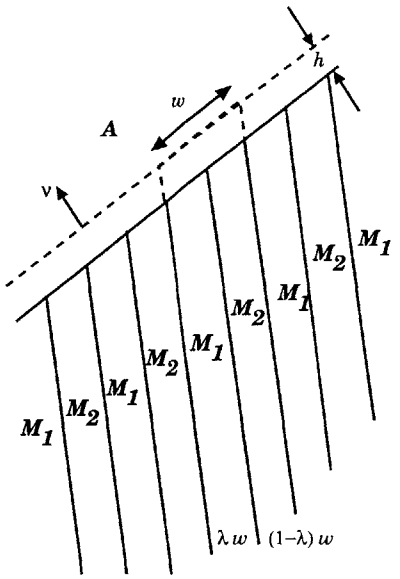

Figure 7-2: Austenite-martensite interface with a transforming layer.

nth such region extends from $nw < \boldsymbol{x}_l \cdot \boldsymbol{s} < (n+1)w$ where $\boldsymbol{x}_l \in \{\boldsymbol{x} : 0 < \boldsymbol{x} \cdot \boldsymbol{\nu} < h\}$. We assume that, in the process of phase transformation, the following motion occurs in the layer:

$$\boldsymbol{y}_l(u(t)) = (\mathbf{1} + u(t)\boldsymbol{s} \otimes \boldsymbol{\nu})\boldsymbol{x}_l \tag{7.3}$$

where, as $u(t)$ goes from 0 to 1, the layer transforms from austenite to twinned martensite. We allow each region $nw < \boldsymbol{x}_l \cdot \boldsymbol{s} < (n+1)w$ to undergo this motion separately and the deformation of the nth region is parameterized with $u_n(t)$. If the Helmholtz free–energy of this material is given by $\psi(\boldsymbol{F})$ then the energy density of the transforming layer is given by

$$W(u) = \lambda\psi\left((1-u)\boldsymbol{I} + u\boldsymbol{F}_I\right) + (1-\lambda)\psi\left((1-u)\boldsymbol{I} + u\boldsymbol{F}_J\right) \tag{7.4}$$

In terms of the free–energy for Cu-Al-Ni obtained in Chapter 3 the energy is given by

$$W(u) = \lambda\hat{\Psi}\left(\boldsymbol{E}_I(u)\right) + (1-\lambda)\hat{\Psi}\left(\boldsymbol{E}_J(u)\right) \tag{7.5}$$

where $\boldsymbol{E}_I(u) = \frac{1}{2}\{[(1-u)\boldsymbol{I} + u\boldsymbol{F}_I]^T[(1-u)\boldsymbol{I} + u\boldsymbol{F}_I] - \mathbf{1}\}$ and $\boldsymbol{E}_J(u)$ is obtained by replacing I with J in the previous expression. This energy density is a "double-well" potential shown in Figure 7-4. The first well is associated with austenite and the second well is associated with twinned martensite.

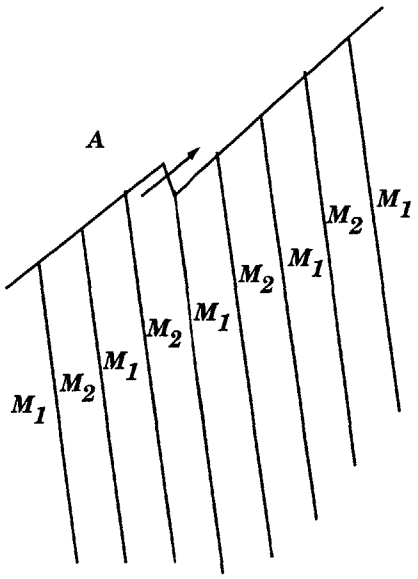

Figure 7-3: Ledges in austenite-twinned martensite phase boundaries.

The free-energy of the nth region is given by $W(u_n)$. Now if we allow that the adjacent regions experience deformations $\boldsymbol{y}_l(u_{n-1}(t))$ and $\boldsymbol{y}_l(u_{n-1}(t))$ and exert a force on the nth region, the simplest model the force on the nth region exerted by the nearest neighbors is a linear interaction

$$s(u_{n+1}(t) - u_n(t)) - s(u_n(t) - u_{n-1}(t)) \tag{7.6}$$

where s is a force constant.

The equation of motion of the nth region can then be written as

$$m\ddot{u}_n(t) = \sigma + s(u_{n+1}(t) - u_n(t)) - s(u_n(t) - u_{n-1}(t)) - W'(u_n(t)) \tag{7.7}$$

Here, σ is the contribution of the applied macroscopic resolved shear stress on the interface and the force $-W'(u_n)$ arises from the energy barrier to the motion of the region. The applied force σ drives each of the regions to the martensite well. We are interested in the case where all the regions are initially located in the austenite energy well and eventually end up in the martensite energy well.

We let $u(x,t)$ be a smooth interpolating function which is defined on all x and t such that $u_n(t) = u(nw,t)$. By expanding the nearest neighbor interaction in a Taylor's series

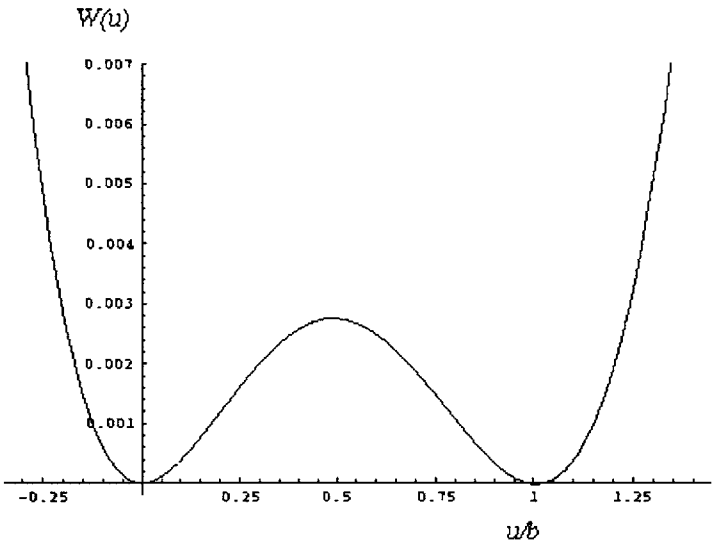

Figure 7-4: Energy density of the transforming layer.

about $x = nw$, we find that (7.6) may be approximated by

$$\mu_1 u_{xx}(nw,t) + \mu_2 u_{xxxx}(nw,t) + \ldots \tag{7.8}$$

Substituting the above terms into the micromechanical equation of motion (7.7) we obtain a continuum version

$$m\ddot{u}(x,t) = \sigma + \mu_1 u_{xx}(x,t) + \mu_2 u_{xxxx}(x,t) - W'(u(x,t)) \tag{7.9}$$

7.4 Kinetic law

We solve (7.9) for two types of austenite–martensite interfaces with the martensite twinned between variants $\{\boldsymbol{U}_1, \boldsymbol{U}_3\}$. There are four solutions (2.13) and (2.14) of the phase boundary equation with $I = 1$ and $J = 3$. We plot the energy of the deforming layer for the four solutions in Figure 7-5.

To solve (7.9) we use an implicit finite difference method with a central differencing scheme and initial conditions given by

$$\begin{aligned} u(x,0) &= (\overset{+}{u} - \bar{u})H(x - x_0) + \bar{u}, \\ u_t(x,0) &= 0, \end{aligned} \tag{7.10}$$

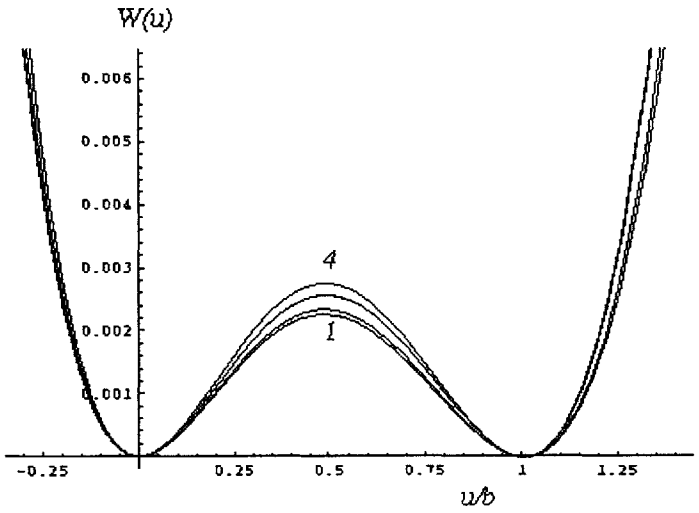

Figure 7-5: Energy density of the transforming layer for four solutions of austenite– martensite interfaces.

where $H(x)$ is the Heaviside function and $x_0 \in (0, L)$. The boundary conditions are fixed at the equilibrium solution

$$\begin{aligned} u(0,t) &= \bar{u}, \qquad u(L,t) = \overset{+}{u} \\ u_x(0,t) &= 0, \qquad u_x(L,t) = 0. \end{aligned} \tag{7.11}$$

The equilibrium values $\bar{u}$ and $\overset{+}{u}$ are the solutions of the equation $\sigma = W'(\bar{u}) = W'(\overset{+}{u})$ as shown in Figure 5-7. The kinetic relation for two types of twin solutions are given in Figure (7-6).

7.5 Isothermal response of strips under uniaxial loading

The kinetic relation obtained in the last section exhibits certain features of interest. In this section we utilize this kinetic relation in a constitutive model to predict the uniaxial response of uniform strip of Cu-Al-Ni. Our constitutive model allows us to examine the isothermal displacement controlled response of a strip of material with the austenite crystallographic axes oriented at various angles to the loading axis. We also examine the response when the orientation is held fixed and a constant displacement rate is applied at various temperatures.

Consider a strip initially unstressed and of length L and composed entirely of austenite.

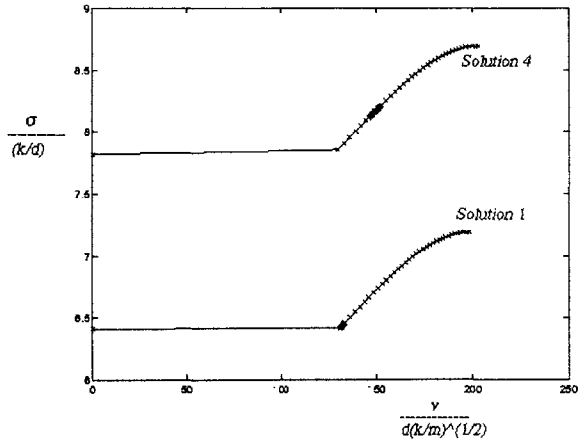

Figure 7-6: The kinetic relation for two different austenite-martensite interface solutions.

As the strip is loaded at a constant displacement rate $\dot{\delta}(t)$, the strip initially elongates purely elastically and the stress $\sigma(t)$ is given by

$$\sigma(t)/E_a = \dot{\delta}(t)/L. \tag{7.12}$$

At a certain stress, martensite nucleates. We assume that martensite nucleates at a stress level such that the calculated driving traction $\sigma = \sigma_{cr}^m$ (the ordinate on the kinetic relation at zero velocity). The subsequent elongation of the strip is due to the motion of a phase boundary which transforms austenite to twinned martensite. The displacement is now related to the stress by

$$\delta(t) = s(t)[\tau(t)/E_{tm} + \gamma_T] + [L - s(t)][\tau(t)/E_a]. \tag{7.13}$$

This equation can be solved for the stress $\tau(t)$ simultaneously with the kinetic relation obtained numerically in the previous section. In the above equation E_a, E_{tm} and γ_T are the elastic modulus of austenite, elastic modulus of twinned martensite and the transformation strain respectively.

After the entire strip is transformed to martensite, we begin to unload. The unloading process takes place elastically until the stress reaches a value such that the driving traction $\sigma = \sigma_{cr}^a$ (the ordinate at zero velocity in the reverse transformation). At that value of the stress austenite nucleates and the reverse transformation takes place. The subsequent stress level is obtained by solving (7.13) with the kinetic relation of the reverse transformation.

At the transformation temperature the kinetic relation for the reverse transformation is symmetric but at other temperatures it is required to be calculated.

Chapter 8

Conclusions and Future Work

8.1 Conclusions and discussion

In this thesis we have provided a constitutive model for the phase transforming shape memory alloy Cu-Al-Ni. In particular, the constitutive model for such materials requires specification of a free–energy function as well as kinetic relations for the various kinds of mobile interfaces that exist in the material. In Chapter 3 we presented a free–energy function that had the material symmetry properties of this material as well as wells corresponding to each of the phases. This free–energy was systematically constructed to closely match the material properties of the material such as the elastic moduli, latent heat and transformation temperature and strains. The result is very useful in deducing fully three-dimensional stress-strain relations for this material in a range of temperatures about the transformation temperature. The free-energy by itself is useful in describing homogeneous single–phase materials. However, for multiphase crystals this free energy has to be used in conjunction with the balance laws of continuum mechanics such as the balance of linear and angular momenta, and energy. In multiphase crystals moving interfaces require a kinetic law to be imposed.

The kinetic law connects the microscale structure of the material with the macroscopic theories. Determining this law requires homogenizing the microscale information such that the continuum scale law retains the appropriate microstructural data. In Chapter 4, we studied this process in detail for a mechanical analog of interface motion by a kink or ledge mechanism. We were able to derive a model of twin boundary motion based on the Cauchy–Born hypothesis regarding the atomic positions and macroscopic deformation

gradients. A discrete one–dimensional model was obtained by separately considering atoms on the interface and atoms away from the interface. The forces due to the atoms away from the interface contributed a non–linear term and brought in the microstructure of the boundary. Analysis of the discrete model and continuum approximations indicated that simplistic approximations prove insufficient to capture important features of the discrete model. An improved continuum model was derived by retaining higher order terms in a Taylor's series expansion of the discrete terms. The improved continuum model is analogous to the *quasicontinuum approximation* of Pouget [64, 65]. The kinetic relation obtained from this mechanical model has the desirable feature that below a critical driving force the interfaces do not propagate (see Abeyaratne, Chu and James [1]).

The kinetic relations for various types of interfaces were explicitly obtained next. In Chapter 5, the kinetic relation was obtained for twin boundaries using the method detailed in Chapter 4. The various features of the model were explicitly calculated using the geometry of the twins as determined from crystallography and interface compatibility conditions. A Lenard–Jones energy was used in a calculation to determine the force contribution of the atoms away from the interface and on the interface. The Lenard–Jones parameters were fitted to the appropriate elastic moduli and the lattice parameters. In Chapter 6, this Lenard–Jones calculation was compared with an appropriate slice of the bulk free–energy and the energies were found to match closely. It remains to be investigated whether this matching is serendipitous. The kinetic relations obtained for compound and Type I twins using the model shows strong dependence on the microstructure. A quantitative estimate of the stress required to move the twin boundaries at low speeds for compound and Type I twins shows that the stresses required for Type I twins are about 40 times that required to move compound twins, in close agreement with values reported by Chu [17], and Ichinose et al [38].

Phase boundaries in Cu-Al-Ni separate austenite phase from twinned martensite. In the interests of compatibility with austenite the martensite twins taper into needles close to the interface. The martensite twins can only be of Type I or Type II. The transition zone in which the martensite twins taper off into needle–like structures is very small to minimize energy. In our model of the austenite–martensite phase boundary we neglect the transition zone and consider an interface between austenite and twinned martensite. Using a similar one–dimensional discrete model for a ledge propagating along the phase

boundary kinetic relations were calculated for the propagating phase boundary. There exist several kinds of possible phase interfaces separating austenite from either Type I or Type II twinned martensite. Calculation of the kinetic relation for two different microstructures shows the dependence of the kinetic relation on the microstructure. We have not found relevant experimental data for either qualitative or quantitative comparison of this result. The kinetic relation has the property that the width of the hysteresis loops do not go to zero with decreasing loading rate as has been observed by some experimenters Chu [17]. The kinetic relation is also qualitatively similar to that obtained by Abeyaratne, Chu and James [1].

8.2 Future work

Finally, we discuss some open problems for future work. In our thesis, we have studied the constitutive modeling of phase transforming materials. We have provided a method for the calculation of the free–energy for cubic–orthorhombic materials. The method is quite general and may be adapted easily to other materials. In particular, TiNi is an industrially important alloy which undergoes cubic–monoclinic transformations and for which a general three–dimensional free–energy will prove invaluable.

While the free–energy was valid for a small range of temperatures around the transformation temperature, the mechanical analog model used to derive the kinetic relation in case of twin boundary and phase boundary motion is valid only for low temperatures. It is important to incorporate thermal effects into the kinetic relation for it to be applicable to room temperature problems. Due to the Cauchy–Born hypothesis, the notion of deformation gradients is carried up to the atomic level. However, temperature poses more subtle problems. At the microscale, temperature is viewed in terms of atomic vibration. For example, the waves emanating from the kink (see Chapter 4) may be viewed as conduction of the latent heat of transformation. The atomic vibration around the kink should be averaged in an appropriate fashion to obtain the temperature. The problem of homogenization in case of finite temperature problems is a delicate one.

An important condition in phase transformations that we have not considered in our thesis is a nucleation criterion. Our constitutive modeling has been restricted to situations with a preexisting twin or phase boundaries. Nucleation is also a microscale effect which

influences the macroscale behavior. A consistent means of incorporating the nucleation criterion is important.

The mechanical analog that we considered introduces the effect of the atoms off the twin plane by means of a substrate potential. We assume a very restrictive motion for the atoms away from the twin plane. Rather than such as rigid motion as envisaged in our model, perhaps a more realistic approach to modeling atoms away from the twin plane would be to move them by differing amounts as we move away from the twin plane. This would provide a different substrate potential. Some authors have introduced an *elastic* substrate to model the relaxation of the motion of atoms away from the twin plane. Also atoms are believed to shuffle (i.e. not follow the exact path of the continuum deformation but choose more complicated motions) during interface motion. Incorporating atomic shuffles into the micromechanical model and then homogenizing might prove a useful approach to studying their influence on interface motion kinetics.

Appendix A

Symmetry transformations

A cubic material contains five classes with different symmetries. The complete listing of all crystal classes may be found in Green and Adkins [33]. Here we restrict attention to crystal system with the point group of $4/m\ \bar{3}\ 2/m$ which is the gyroidal system according to the terminology of Dana and Hurlbut [21].

We list the symmetry transformations which leave the gyroidal cubic crystal form-invariant.

$$\boldsymbol{I}: \quad x_1' = x_1, \quad x_2' = x_2, \quad x_3' = x_3; \quad e_{ij}' = e_{ij}. \tag{A.1}$$

$$\boldsymbol{C}: \quad x_1' = -x_1, \quad x_2' = -x_2, \quad x_3' = -x_3; \quad e_{ij}' = e_{ij}. \tag{A.2}$$

$$\boldsymbol{R}_1: \quad \left.\begin{array}{lll} x_1' = -x_1, & x_2' = x_2, & x_3' = x_3 \\ e_{11}' = e_{11}, & e_{22}' = e_{22}, & e_{33}' = e_{33} \\ e_{12}' = -e_{12}, & e_{23}' = e_{23}, & e_{31}' = -e_{31} \end{array}\right\} \tag{A.3}$$

$$\boldsymbol{R}_2: \quad \left.\begin{array}{lll} x_1' = x_1, & x_2' = -x_2, & x_3' = x_3 \\ e_{11}' = e_{11}, & e_{22}' = e_{22}, & e_{33}' = e_{33} \\ e_{12}' = -e_{12}, & e_{23}' = -e_{23}, & e_{31}' = e_{31} \end{array}\right\} \tag{A.4}$$

$$\boldsymbol{R}_3: \quad \left.\begin{array}{lll} x_1' = x_1, & x_2' = x_2, & x_3' = -x_3 \\ e_{11}' = e_{11}, & e_{22}' = e_{22}, & e_{33}' = e_{33} \\ e_{12}' = e_{12}, & e_{23}' = -e_{23}, & e_{31}' = -e_{31} \end{array}\right\} \tag{A.5}$$

$$\boldsymbol{D}_1: \quad \left.\begin{array}{lll} x_1' = x_1, & x_2' = -x_2, & x_3' = -x_3 \\ e_{11}' = e_{11}, & e_{22}' = e_{22}, & e_{33}' = e_{33} \\ e_{12}' = -e_{12}, & e_{23}' = e_{23}, & e_{31}' = -e_{31} \end{array}\right\} \tag{A.6}$$

$$\boldsymbol{D}_2: \quad \left.\begin{array}{lll} x_1' = -x_1, & x_2' = x_2, & x_3' = -x_3 \\ e_{11}' = e_{11}, & e_{22}' = e_{22}, & e_{33}' = e_{33} \\ e_{12}' = -e_{12}, & e_{23}' = -e_{23}, & e_{31}' = e_{31} \end{array}\right\} \tag{A.7}$$

$$\boldsymbol{D}_3: \quad \left.\begin{array}{lll} x_1' = -x_1, & x_2' = -x_2, & x_3' = x_3 \\ e_{11}' = e_{11}, & e_{22}' = e_{22}, & e_{33}' = e_{33} \\ e_{12}' = e_{12}, & e_{23}' = -e_{23}, & e_{31}' = -e_{31} \end{array}\right\} \tag{A.8}$$

$$\boldsymbol{T}_1: \quad \left.\begin{array}{lll} x_1' = x_1, & x_2' = x_3, & x_3' = x_2 \\ e_{11}' = e_{11}, & e_{22}' = e_{33}, & e_{33}' = e_{22} \\ e_{12}' = e_{13}, & e_{23}' = e_{23}, & e_{31}' = e_{12} \end{array}\right\} \tag{A.9}$$

$$\boldsymbol{T}_2: \quad \left.\begin{array}{lll} x_1' = x_3, & x_2' = x_2, & x_3' = x_1 \\ e_{11}' = e_{33}, & e_{22}' = e_{22}, & e_{33}' = e_{11} \\ e_{12}' = e_{23}, & e_{23}' = e_{12}, & e_{31}' = e_{31} \end{array}\right\} \tag{A.10}$$

$$\boldsymbol{T}_3: \quad \left.\begin{array}{lll} x_1' = x_2, & x_2' = x_1, & x_3' = x_3 \\ e_{11}' = e_{22}, & e_{22}' = e_{11}, & e_{33}' = e_{33} \\ e_{12}' = e_{12}, & e_{23}' = e_{31}, & e_{31}' = -e_{23} \end{array}\right\} \tag{A.11}$$

$$\boldsymbol{M}_1: \quad \left.\begin{array}{lll} x_1' = x_2, & x_2' = x_3, & x_3' = x_1 \\ e_{11}' = e_{22}, & e_{22}' = e_{33}, & e_{33}' = e_{11} \\ e_{12}' = e_{23}, & e_{23}' = e_{31}, & e_{31}' = e_{12} \end{array}\right\} \tag{A.12}$$

$$\left.\begin{array}{rlll} & x_1' = x_3, & x_2' = x_1, & x_3' = x_2 \\ \boldsymbol{M}_2: & e_{11}' = e_{33}, & e_{22}' = e_{11}, & e_{33}' = e_{22} \\ & e_{12}' = e_{13}, & e_{23}' = e_{12}, & e_{31}' = e_{23} \end{array}\right\} \tag{A.13}$$

Here the transformation $\boldsymbol{I}$ is the identity transformation and $\boldsymbol{C}$ is central inversion. $\boldsymbol{R}_i$ are reflections in planes normal to x_i-axes, $i = 1, 2, 3$ and $\boldsymbol{D}_i$ are the rotations through 180° of the coordinate system about the x_i- axes respectively, $i = 1, 2, 3$. The transformation $\boldsymbol{T}_1$ is a reflection in the plane through the x_1-axis and the line bisecting the angle between the x_2- and x_3-axes. The transformation $\boldsymbol{T}_2$ is a reflection on the plane passing through the x_2-axis and the line bisecting the angle between the x_1- and x_3-axes and the transformation $\boldsymbol{T}_3$ is the reflection on the plane passing through the x_3-axis and the line bisecting the angle between the x_1- and x_2-axes. Finally, the transformations $\boldsymbol{M}_1$ and $\boldsymbol{M}_2$ are rotations of the axes through 120° and 240° respectively about a line passing through the origin and the point $(1, 1, 1)$.

The gyroidal cubic crystal has the following symmetry transformations characterizing it (these are the 24 rotations described in Section 2.2):

$$\left.\begin{array}{c} \boldsymbol{I}, \\ \boldsymbol{D}_1,\ \boldsymbol{D}_2,\ \boldsymbol{D}_3,\ \boldsymbol{R}_2\boldsymbol{T}_1,\ \boldsymbol{R}_3\boldsymbol{T}_1,\ \boldsymbol{R}_1\boldsymbol{T}_2,\ \boldsymbol{R}_3\boldsymbol{T}_2,\ \boldsymbol{R}_1\boldsymbol{T}_3,\ \boldsymbol{R}_2\boldsymbol{T}_3, \\ \boldsymbol{M}_1,\ \boldsymbol{D}_1\boldsymbol{M}_1,\ \boldsymbol{D}_2\boldsymbol{M}_1,\ \boldsymbol{D}_3\boldsymbol{M}_1,\ \boldsymbol{M}_2,\ \boldsymbol{D}_1\boldsymbol{M}_2,\ \boldsymbol{D}_2\boldsymbol{M}_2,\ \boldsymbol{D}_3\boldsymbol{M}_2 \\ \boldsymbol{C}\boldsymbol{T}_1,\ \boldsymbol{R}_1\boldsymbol{T}_1,\ \boldsymbol{C}\boldsymbol{T}_2,\ \boldsymbol{R}_2\boldsymbol{T}_2,\ \boldsymbol{C}\boldsymbol{T}_3,\ \boldsymbol{R}_3\boldsymbol{T}_3. \end{array}\right\} \tag{A.14}$$

We now state without proof three relevant theorems on invariants (see Weyl [83]) which can be applied to the free energy function $\hat{\Psi}(E_{11}, E_{22}, E_{33}, E_{12}, E_{23}, E_{13})$ to obtain its polynomial basis.

Theorem 1 *A polynomial basis for polynomials which are symmetric in the two sets of variables* $(y_1, y_2, \ldots, y_n)$ *and* $(z_1, z_2, \ldots, z_n)$ *is formed by the quantities*

$$\left.\begin{array}{ll} K_j = \frac{1}{2}(y_j + z_j) & j = 1, 2, \ldots, n \\ K_{jk} = \frac{1}{2}(y_j z_k + y_k z_j) & j, k = 1, 2, \ldots, n \end{array}\right\} \tag{A.15}$$

Theorem 2 *A polynomial basis for polynomials which are symmetric in three pairs of vari-*

ables (y_1, z_1) *and* (y_2, z_2) *and* (y_3, z_3) *is formed by the quantities*

$$\left.\begin{aligned} &L_1 = y_1 + y_2 + y_3, \qquad L_2 = y_2y_3 + y_3y_1 + y_1y_2, \qquad L_3 = y_1y_2y_3 \\ &L_4 = z_1 + z_2 + z_3, \qquad L_5 = z_2z_3 + z_3z_1 + z_1z_2, \qquad L_6 = z_1z_2z_3 \\ &L_7 = y_2z_3 + y_3z_2 + y_3z_1 + y_1z_3 + y_1z_2 + y_2z_1, \\ &L_8 = y_1z_2z_3 + y_2z_3z_1 + y_3z_1z_2, \\ &L_9 = z_1y_2y_3 + z_2y_3y_1 + z_3y_1y_2. \end{aligned}\right\} \tag{A.16}$$

Theorem 3 *A polynomial basis for a polynomial in the variables* $y_1, y_2, \ldots, z_n, N_1, \ldots, N_k$, *which is form invariant under the group of transformations under which group* $N_1, \ldots, N_k$ *are invariant is formed by adjoining to the quantities* $N_1, \ldots, N_k$ *the polynomial basis for the polynomials in the variables* $y_1, y_2, \ldots, z_n$ *which are form invariant under the given group of transformations.*

First $\boldsymbol{D}_1$ leads to the restriction that the form of [1]

$$\hat{\Psi}(E_{11}, E_{22}, E_{33}, E_{12}, E_{23}, E_{13}) = \hat{\Psi}(E_{11}, E_{22}, E_{33}, -E_{12}, E_{23}, -E_{13}) \tag{A.17}$$

Taking

$$(y_1, y_2) = (E_{12}, E_{13}), \quad (z_1, z_2) = (-E_{12}, -E_{13}), \tag{A.18}$$

$$(N_1, N_2, N_3, N_4) = (E_{11}, E_{22}, E_{33}, E_{23}) \tag{A.19}$$

in Theorems 1 and 3 we find that $\hat{\Psi}$ must be expressible as a polynomial in the seven quantities $E_{11}, E_{22}, E_{33}, E_{23}, E_{12}^2, E_{13}^2, E_{12}E_{13}$.

Next the transformations $\boldsymbol{D}_2$ and $\boldsymbol{D}_3$ lead to

$$\hat{\Psi}(E_{11}, E_{22}, E_{33}, E_{23}, E_{12}^2, E_{13}^2, E_{12}E_{13}) = \hat{\Psi}(E_{11}, E_{22}, E_{33}, -E_{23}, E_{12}^2, E_{13}^2, -E_{12}E_{13}) \tag{A.20}$$

Again, taking

$$(N_1, N_2, N_3, N_4, N_5) = (E_{11}, E_{22}, E_{33}, E_{12}^2, E_{13}^2) \tag{A.21}$$

[1]The functional form for $\hat{\Psi}$ changes with each additional restriction but we retain the symbol $\hat{\Psi}$ for convenience.

$$(y_1, y_2) = (E_{23}, E_{12}E_{13}), \quad (z_1, z_2) = (-E_{23}, -E_{12}E_{13}) \tag{A.22}$$

in Theorems 1 and 3, we find that $\hat{\Psi}$ must be expressible as a polynomial in $E_{11}, E_{22}, E_{33}, E_{12}^2, E_{23}^2, E_{13}^2, E_{12}E_{23}E_{13}$.

Finally the remaining transformations lead to the following limitations on $\hat{\Psi}$:

$$\begin{aligned}
\hat{\Psi}(E_{11}, E_{22}, E_{33}, E_{12}^2, E_{23}^2, E_{13}^2, E_{12}E_{23}E_{13}) &= \hat{\Psi}(E_{11}, E_{33}, E_{22}, E_{13}^2, E_{23}^2, E_{12}^2, E_{12}E_{23}E_{13}) \\
&= \hat{\Psi}(E_{22}, E_{11}, E_{33}, E_{12}^2, E_{13}^2, E_{23}^2, E_{12}E_{23}E_{13}) \\
&= \hat{\Psi}(E_{33}, E_{22}, E_{11}, E_{23}^2, E_{12}^2, E_{13}^2, E_{12}E_{23}E_{13}) \\
&= \hat{\Psi}(E_{22}, E_{33}, E_{11}, E_{23}^2, E_{13}^2, E_{12}^2, E_{12}E_{23}E_{13}) \\
&= \hat{\Psi}(E_{33}, E_{11}, E_{22}, E_{13}^2, E_{12}^2, E_{23}^2, E_{12}E_{23}E_{13})
\end{aligned}$$

Taking

$$(y_1, z_1) = (E_{11}, E_{23}^2), \quad (y_2, z_2) = (E_{22}, E_{13}^2), \quad (y_3, z_3) = (E_{33}, E_{12}^2) \tag{A.23}$$

$$N_1 = E_{12}E_{23}E_{13} \tag{A.24}$$

in Theorems 2 and 3 we obtain that the free energy $\hat{\Psi}$ is a function of the nine polynomials $P_1, \ldots, P_9$ listed in Equation (3.9).

Appendix B

Calculation of the elastic moduli from the free energy

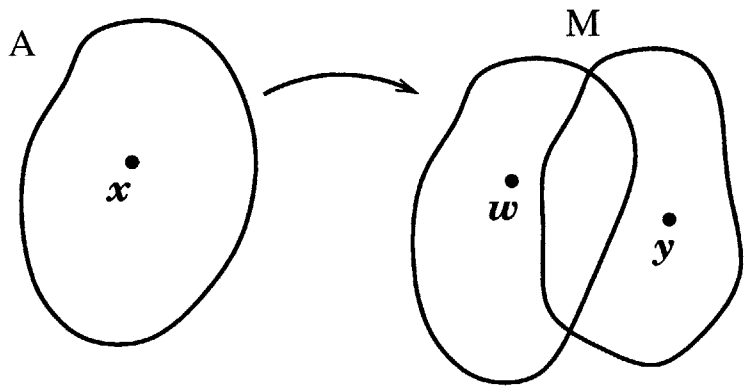

Figure B-1: Infinitesimal deformations from martensite state

Since our reference configuration is cubic austenite, the elastic moduli of the austenite phase is simply obtained from the free energy function through

$$C^a_{ijkl} = \left.\frac{\partial^2 \tilde{\Psi}}{\partial E_{ij} \partial E_{kl}}\right|_{\boldsymbol{E}=\boldsymbol{0}}. \tag{B.1}$$

In the case of the martensite, a little more care is required in calculating the elastic moduli. Consider a body $\mathcal{B}$ in the reference configuration. Let points $\boldsymbol{x}$ be mapped into points $\boldsymbol{w}$ in unstressed martensite. Then $\boldsymbol{w} = \boldsymbol{U}\boldsymbol{x}$ where $\boldsymbol{U}$ is a Bain stretch tensor corresponding to one of the variants of martensite. Now let the body be deformed further from the unstressed

martensite by $\boldsymbol{u}(\boldsymbol{x}) = \boldsymbol{u}(\boldsymbol{w}(\boldsymbol{x}))$. Then the deformation gradient is

$$F_{ij} = U_{ij} + \frac{\partial u_i}{\partial x_j}, \tag{B.2}$$

and the Lagrangian strain tensor is

$$E_{ij} = \frac{1}{2}(F_{ki}F_{kj} - \delta_{ij}) = \frac{1}{2}(U_{ik}U_{kj} + U_{kj}\frac{\partial u_k}{\partial x_i} + U_{ki}\frac{\partial u_k}{\partial x_j} - \delta_{ij}). \tag{B.3}$$

Since,

$$\frac{\partial u_k}{\partial x_i} = U_{pi}\frac{\partial u_k}{\partial w_p}, \tag{B.4}$$

the strain tensor can also be written as

$$E_{ij} = \frac{1}{2}(U_{ik}U_{kj} - \delta_{ij}) + \frac{1}{2}U_{pi}(\frac{\partial u_q}{\partial w_p} + \frac{\partial u_p}{\partial w_q})U_{qj}. \tag{B.5}$$

If we denote the strain from the unstressed martensite variant by $\epsilon_{pq} = \frac{1}{2}(\frac{\partial u_q}{\partial w_p} + \frac{\partial u_p}{\partial w_q})$ then the elastic moduli of the martensite phase are given by

$$C^m_{ijkl} = \left.\frac{\partial^2 \tilde{\Psi}}{\partial \epsilon_{ij}\partial \epsilon_{kl}}\right|_{\epsilon_{mn}=0} = \left.\frac{\partial^2 \tilde{\Psi}}{\partial E_{ab}\partial E_{cd}}\right|_{\boldsymbol{E}=\boldsymbol{E}_m} U_{ai}U_{bj}U_{ck}U_{dl}. \tag{B.6}$$

Bibliography

[1] R. Abeyaratne, C. Chu, and R.D. James. Kinetics of materials with wiggly energies: theory and application to the evolution of twinning microstructures in a Cu-Al-Ni shape memory alloy. *Phil Mag A-Physics of Condensed Matter Defects and Mechanical Properties*, 73(2):457–97, 1996.

[2] R. Abeyaratne and J.K Knowles. On the dissipative response to discontinuous strains in bars of unstable elastic material. *Int. J. Solids Structures*, 24:1021–1044, 1988.

[3] R. Abeyaratne and J.K Knowles. On the driving traction acting on a surface of strain discontinuity in a continuum. *J. Mech. Phys. Solids*, 38:345–360, 1990.

[4] R. Abeyaratne and J.K Knowles. Implications of viscosity and strain-gradient effects for the kinetics of propagating phase boundaries in solids. *SIAM J. Appl. Math.*, 51:1205–1221, 1991.

[5] R. Abeyaratne and J.K Knowles. Kinetic relations and propagation of phase boundaries in solids. *Arch. Rational Mech. Anal.*, 114:119–154, 1991.

[6] R. Abeyaratne and J.K Knowles. A continuum model of a thermoelastic solid capable of undergoing phase transitions. *J. Mech. Phys. Solids*, 41:541–571, 1993.

[7] R. Abeyaratne and S. Vedantam. Propagation of a front by kink motion: From a discrete model to a continuum model. In P. Argoul, M. Fremond, and Q.S. Nguyen, editors, *IUTAM Symposium on Variations of Domains and Free-Boundary Problems in Solid Mechanics*. Kluwer Academic Publishers, 1997.

[8] R. Abeyaratne and S. Vedantam. Kinetics of twin boundaries. forthcoming, 2000.

[9] A. Askar. *Lattice Dynamical Foundations of Continuum Theories.* World Scientific, 1985.

[10] W. Atkinson and N. Cabrera. Motion of a frenkel-kontorowa dislocation in a one–dimensional crystal. *Physical Review*, 138:A763–766, 1965.

[11] J.M Ball and R.D. James. Fine phase mixtures as minimizers of energy. *Arch. Rational Mech. Anal.*, 100(1):13–52, 1987.

[12] A. Bekker, L.C. Brinson, and K. Issen. Localized and diffuse thermoinduced phase transformation in 1-D shape memory alloys. *Journal of Intelligent Material Systems and Structures*, 9(5):355–65, 1998.

[13] K. Bhattacharya. Wedge-like microstructure in martensites. *Acta metall. mater.*, 39(10):2431–444, 1991.

[14] K. Bhattacharya and R.D. James. A theory of thin films of martensitic materials with applications to microactuators. *J. Mech. Phys. Solids*, 47(3):531-76, 1999.

[15] J.S. Bowles and J.K. Mackenzie. The crystallography of martensitic transformations I,II. *Acta Metall.*, 2:129–147, 1954.

[16] J.W. Christian. *The theory of transformations of metals and alloys.* Pergamon Press, Oxford, 1975.

[17] C. Chu. *Hysteresis and microstructures: a study of biaxial loading of compound twins of Cu-Al-Ni single crystals.* PhD thesis, University of Minnesota, Minneapolis, MN, 1993.

[18] C. Collins and M. Luskin. The computation of austenitic-martensitic phase transitions. In M. Rascle, D. Serre, and M. Slemrod, editors, *PDEs and continuum models of phase transitions : proceedings of an NSF-CNRS joint seminar held in Nice, France, January 18-22, 1988*, pages 34–50. Springer-Verslag, 1988.

[19] J.A. Combs and S. Yip. Single–kink dynamics in a one–dimensional atomic chain: A nonlinear atomistic theory and numerical simulation. *Physical Review B*, 28(12):6873–6885, 1983.

[20] J.F. Currie, S.E. Trullinger, A.R. Bishop, and J.A. Krumhansl. Numerical simulation of sine-gordon soliton dynamics in the presence of perturbations. *Physical Review B*, 15(12):5567–5580, 1977.

[21] J.D. Dana and C.S. Hurlbut. *Dana's Manual of Mineralogy.* Wiley Chapman and Hall, New York, 1959.

[22] D.Rönnpagel, Th. Streit, and Th. Pretorius. Including thermal activation in simulations calculations of dislocation glide. *Phys. stat. sol.*, 135:445–454, 1993.

[23] Y.Y. Earmme and J.H. Weiner. Loss–free dislocation motion in a lattice model. *Physical Review Letters*, 33(26):1550–1552, 1974.

[24] J.L. Ericksen. The Cauchy and Born hypotheses for crystals. In M.E. Gurtin, editor, *Phase transformations and materials instabilites in solids*, pages 61–77. Academic Press, 1984.

[25] J.L. Ericksen. Constitutive theory for some constrained elastic crystals. *Int. J. Solids Structures*, 22(9):951–64, 1986.

[26] J.D. Eshelby. The continuum theory of lattice defects. In F. Seitz and D. Turnbull, editors, *Solid State Physics*, volume 3, pages 79–144. Academic Press, New York, 1956.

[27] F. Falk and P. Konopka. Three-dimensional Landau theory describing the martenstitic phase transformation of shape-memory alloys. *J. Phys: Condens. Matter*, 2:61–77, 1990.

[28] F.C Frank. Crystal dislocation: elementary concepts and definitions. *Phil. Mag.*, 42(362):809–819, 1951.

[29] J. Frenkel and T. Kontotova. On the theory of plastic deformation and twinning. *Phys. Z. Sowjet Union*, 13:1, 1938.

[30] E. Fried and M. Gurtin. Dynamic solid–solid transitions with phase characterized by an order parameter. *Physica D*, 72(4):287–308, 1994.

[31] J.J. Gilman. *Micromechanics of Flow in Solids.* McGraw-Hill, 1969.

[32] P.F. Gobin and G. Guenin. Martensitic transformation: An approach to the martensite nucleation problem. In *Solid State Phase Transformations in Metals and Alloys*, pages 573–629. Orsay : Les éditions de physique, 1978.

[33] A.E. Green and J.E. Adkins. *Large Elastic Deformations*, chapter 1. Clarendon Press, Oxford, 1970.

[34] M.E. Gurtin. Two-phase deformation of elastic solids. *Arch. Rational Mech. Anal.*, 84(1):1–29, 1983.

[35] K.F. Hane and T.W. Shield. Symmetry and microstructure in martensites. *Philosophical Magazine A*, 78(6):1215–1252, 1998.

[36] J.P. Hirth, R.G. Hoagland, and R.J. Kurtz. The motion of multiple height ledges and disconnections in phase transformations. *Minerals, Metals and Mater. Soc. and ASM Int. Metallurgical and Materials Transactions A-Physical Metallurgy and Materials Science,*, 29A(8):2033–8, 1998.

[37] J.P. Hirth and J. Lothe. *Theory of Dislocations.* Krieger, Florida, 1982.

[38] S. Ichinose, Y. Funatsu, N. Otani, T. Ichikawa, S. Miyazaki, and K. Otsuka. Deformation modes of 2H type martensite single crystals in a $(Cu, Ni)_3$ Al alloy. In *Proc. Int. Symposium Intermetallic Compounds*, pages 263–266, Sendai, Japan, 1991.

[39] R.D. James. Finite deformation by mechanical twinning. *Arch. Rational Mech. Anal.*, 82:143–176, 1981.

[40] R.D. James. Displacive phase transformations in solids. *J. Mech. Phys. Solids*, 34(4):143–176, 1986.

[41] M.A. Jaswon and D.B. Dove. The crystallography of deformation twinning. *Acta Crystallographica*, 13:232–240, 1960.

[42] M.V. Klassen-Neklyudova. *Mechanical twinning of crystals.* Consultants Bureau, New York, 1964.

[43] Y. Koyoma and O. Nittono. Structural phase transformations in the indium-rich solid solutions. *J. Physique Coll.*, 43(C–4):145–50, 1982.

[44] A.I. Landau. The dynamics of dislocation (kink) in the frenkel–kontorova model in the case of a nonzero environment temperature. *Phys. stat. sol.*, 191:67–75, 1995.

[45] C. Liang and C.A. Rogers. One-dimensional thermomechanical constitutive relations for shape memory materials. *Journal of Intelligent Material Systems and Structures*, 8(4):285–302, 1997.

[46] O. Nittono and Y. Koyoma. Phenomenological considerations of phase transformations in indium-rich alloys. *Japan J. Appl. Phys*, 21(5):680–8, 1982.

[47] K. Otsuka, K. Nakai, and K. Shimizu. Structure dependence of superelasticity in Cu-Al-Ni alloy. *Scripta Metallurgica*, 8(8):913–918, 1974.

[48] K. Otsuka, H. Sakamoto, and K. Shimizu. A new type of pseudoelasticity in single variant twinned martensites. *Scripta Metallurgica*, 11(1):41–46, 1977.

[49] K. Otsuka, H. Sakamoto, and K. Shimizu. The characteristics of a metastable 2H type phase in a quenched β_1 Cu-Al-Ni alloy. *Transactions of the Japan Institute of Metals,*, 20(5):244–254, 1979.

[50] K. Otsuka, H. Sakamoto, and K. Shimizu. Successive stress-induced martensitic transformations and associated transformation pseudoelasticity in Cu-Al-Ni alloys. *Acta Metallurgica*, 27(4):585–601, 1979.

[51] K. Otsuka and K. Shimuzu. Morphology and crystallography of thermoelastic γ' Cu-Al-Ni martensite. *Japan J. Appl. Phys*, 8(10):1696–1704, 1969.

[52] K. Otsuka and K. Shimuzu. Morphology and crystallography of thermoelastic Cu-Al-Ni martensite analyzed by the phenomenological theory. *Trans. JIM*, 15:103–108, 1974.

[53] K. Otsuka, M. Takahashi, and K Shimizu. Single interface martensitic transformation in Cu-Al-Ni alloy. *Metallurgical Transactions A-Physical Metallurgy and Materials Science*, 4(8):2003–2006, 1973.

[54] K. Otsuka, C.M. Wayman, K. Nakai, H. Sakamoto, and Shimizu K. Superelasticity effects and stress-induced martensitic transformations in Cu-Al-Ni alloys. *Acta Metallurgica*, 24(3):207–26, 1976.

[55] G.P. Parry. On the elasticity of monatomic crystals. *Math. Proc. Camb. Phil. Soc.*, 80(1):189–211, 1976.

[56] Y. Partom. The drag force on a moving dislocation. I. Zero temperature (lattice drag force). *J. Appl. Phys.*, 1979.

[57] A.T. Paxton. Theoretical strength, twinning, antitwinning and pseudotwinning—A quantum mechanical approach. In *Twinning in advanced materials : proceedings of a symposium sponsored by the Chemistry and Physics of Materials Committee and the Alloy Phases Committee of TMS Technical Divisions (EMPMD and SMD) at the 1993 Materials Week, October 18-20, 1993, Pittsburgh, Pennsylvania*, pages 27–41, 1994.

[58] D. Perchak and J.H. Weiner. Local–mode approximations in the Frenkel–Kontorova or Sine–Gordon chain. *Physical Review B*, 22:2683–2692, 1980.

[59] A.M. Pettinger. *A regularized couple stress theory and its implications on nucleation and kinetics of phase transformations in anti-plane shear.* PhD thesis, Massachusetts Institute of Technology, Cambridge, MA, 1998.

[60] M. Peyrard and M. Remoissenet. Solitonlike excitations in a one–dimensional atomic chain with a nonlinear deformable substrate potential. *Physical Review B*, 26(6):2886–2899, 1982.

[61] A.C. Pipkin and A.S. Wineman. Material symmetry restrictions on non-polynomial constitutive equation. *Arch. Rational Mech. Anal.*, 12:252–268, 1963.

[62] M. Pitteri. Reconciliation of local and global symmetries of crystals. *Journal of Elasticity*, 14(2):175–190, 1984.

[63] D.A. Porter and K.E. Easterling. *Phase transformations in Metals and Alloys.* van Nostrand-Reinhold, New York, 1981.

[64] J. Pouget. Dynamics of patterns in ferroelastic–martensitic transformations. I. Lattice model. *Physical Review B*, 43(4):3575–3581, 1991.

[65] J. Pouget. Dynamics of patterns in ferroelastic-martensitic transformations. II. Quasicontinuum model. *Physical Review B*, 43(4):3582–3592, 1991.

[66] J.R. Rice. Inelastic constitutive relations for solids: an internal-variable theory and its application to metal plasticity. *J. Mech. Phys. Solids*, 19(6):433–455, 1971.

[67] H. Sakamoto, K. Otsuka, and K. Shimizu. Rubber-like behavior in a Cu-Al-Ni alloy. *Scripta Metallurgica*, 11(7):607–611, 1977.

[68] J.A. Shaw and S. Kyriakides. Thermomechanical aspects of NiTi. *J. Mech Phys Solids*, 38:345–360, 1995.

[69] T.W. Shield. Orientation dependence of the pseudoelastic behaviour of single crystals of Cu-Al-Ni in tension. *J. Mech. Phys. Solids*, 43(6):869–895, 1996.

[70] K. Shimizu, H. Sakamoto, and K. Otsuka. Phase diagram associated with stress-induced martensitic transformations in a Cu-Al-Ni alloy. *Scripta Metallurgica*, 12(9):771–776, 1978.

[71] K. Shimuzu and K. Otsuka. Optical and electron microscope observations of transformation and deformation characterisitics in CuAlNi Marmem alloys. In J. Perkins, editor, *Shape memory effect in alloys*, New York, 1975. Plenum Press.

[72] G.F. Smith. Further results on the strain energy function for anistropic elastic materials. *Arch. Rational Mech. Anal.*, 10:108–110, 1962.

[73] G.F. Smith and R.S. Rivlin. The strain energy function for anisotropic elastic materials. *Trans. Am. Math. Soc.*, 88:175–193, 1958.

[74] M. Suezawa and K. Sumino. Behaviour of elastic constants in Cu-Al-Ni alloy in the close vicinity of Ms–point. *Scripta Metall.*, 10:789–792, 1976.

[75] C. Truesdell and W. Noll. The non–linear field theories of mechanics. In S. Flügge, editor, *Encyclopaedia of Physics*, volume 3/3. Springer-Verlag, Berlin, 1965.

[76] L. Truskinovsky. Structure of an isothermal phase discontinuity. *Soviet Physics Doklady*, 30:945–948, 1985.

[77] G. van Tandeloo and S. Amelinckx. Group-theoretical considerations concerning domain formation in ordered alloys. *Acta Crystall.*, A30(3):431–40, 1974.

[78] P. Villars and L.D. Calvert. *Pearson's handbook of crystallographic data for intermetallic phases.* American Society for Metals, Metals Park, OH, 1985.

[79] C. M. Wayman. *Introduction to the crystallography of martensitic transformations.* Macmillan, New York, 1964.

[80] J.H. Weiner. Dislocation velocities in a linear chain. *Physical Review*, 136:A863–868, 1964.

[81] J.H. Weiner. Thermal effects on dislocation velocities in a linear chain. *Physical Review*, 139(2A):A442–A450, 1965.

[82] J.H. Weiner and W.T. Sanders. Peierls stress and creep of a linear chain. *Physical Review*, 134:A1007–1015, 1964.

[83] H. Weyl. *The classical theory of groups*, pages 36, 53, 276. Princeton University Press, 1946.

[84] A.S. Wineman and A.C. Pipkin. Material symmetry restrictions on constitutive equations. *Arch. Rational Mech. Anal.*, 17:184–214, 1964.

[85] M. Yasunaga, Y. Funatsu, S. Kojima, K. Otsuka, and T. Suzuki. Ultrasonic velocity near the martensitic transformation temperature. *J. Physique Coll.*, 43(C-4):603–608, 1982.

[86] M. Yasunaga, Y. Funatsu, S. Kojima, K. Otsuka, and T. Suzuki. Measurement of elastic constants. *Scr. Metall.*, 17(9):1091–1094, 1983.

[87] Hung yu Tsai. *Mechanics of Deformation Twinning.* PhD thesis, Cornell University, 1994.

[88] J. Zhang, W. Cai, Y. Zheng, and L. Zhao. Type II twins and their deformation characteristics in 18 R martensite in a Cu-Zn-Al alloy. *Materials Letters*, 34(3-6):351–355, 1998.